Title	Research on Wearable Sensor system for 3D lower limb kinematics analysis
Author(s)	LIU, Kun
Citation	高知工科大学, 博士論文.
Date of issue	2010-09
URL	http://hdl.handle.net/10173/604
Rights	
Text version	author

Research on Wearable Sensor system for 3D lower limb kinematics analysis

Liu Kun

A dissertation submitted to
Kochi University of Technology
in partial fulfillment of the requirements
for the degree of

Doctor of Philosophy

Special Course for International Students
Graduate School of Engineering
Kochi University of Technology
Kochi, Japan

August 2010

Abstract

Kinematics analysis of lower limb can provide a deeply and quantitatively understanding of motion mechanism and assessment of motion abilities, which is fundamental for rehabilitating and clinical applications. However, human motion data are commonly obtained by means of traditional laboratory-restricted bulky equipments, such as force plate and optical camera system. Therefore, cheaper and more comfortable human kinematic and kinetic analysis devices with compact biomedical sensor combinations are in urgent necessity for visual and quantitative gait phase analysis and human kinematics and kinetics analysis.

In this dissertation, some methods for lower limb kinematics analysis were provided, and relevant prototypes of wearable sensor systems were developed and tested for ambulatory and unobtrusive motion measurement of lower limb in daily activities instead of the traditional ones. First，a novel method using a double-sensor difference based algorithm for analyzing rigid segment rotational angles in 2 directions was presented and discussed, To verify the method qualitatively, a prototype of a wearable sensor system only using one kind of inertial sensor (accelerometer) was developed. The prototype was first test on a board which performed a one-freedom of rotation in sagital plane, then was tested on the thigh of a volunteer to obtain the pitch and yaw angles for the lower limb segment orientation when the thigh swung in the original place without translation. To promote the double-sensor difference based algorithm to analyze human segment rotational angles in two directions when the subject walked in a straight line, a wearable sensor system based only on triaxial accelerometers was developed to obtain the pitch and yaw angles of thigh segment. To evaluate the method, the system was first tested on a two degrees of freedom (DOF) mechanical arm assembled out of rigid segments and encoders. Then, to estimate the human segmental orientation, the wearable sensor system was tested on the thighs of eight volunteer subjects, who walked in a straight forward line in the work space of an optical motion analysis system at three

self-selected speeds: slow, normal and fast.

However, just the lower limb segment orientation is not enough to estimate the gait posture. To visually and quantitatively confirm lower limb posture, except the double-sensor difference based algorithm, a virtual-sensor difference based algorithm was proposed for analyzing the knee joint and hip joint angles. Using accelerometers and gyroscopes, flexion/extension (FE) and abduction/adduction (AA) hip joint angles and FE knee joint angle were estimated for orientations of the lower limb segments; knee and ankle joint trajectories were obtained with the segmental orientations and lengths for the positions of lower limb joints. As a further research of the physical-sensor difference based algorithm and virtual-sensor difference based algorithm, an original approach based on accelerometers and magnetometers for ambulatory estimation of 3D knee joint kinematics in anatomical coordinate system was presented. The FE, AA and inversion/extension (IE) rotation angles of the knee joint in the anatomical joint coordinate system were estimated. Then, to visually and quantitatively confirm the 3D lower limb posture, combine all the method above, a wearable sensor system was developed and tested on the lower limb.

Finally, some research challenges and future directions are discussed for developing a new biomechanical analysis technique.

Contents

Abstract 2

Chapter 1 6
Introduction 6
1.1 Project Motivation 6
1.2 Research Background 6
1.3 Project Description 9
1.4 Project Objectives and Contributions 10
Reference 11

Chapter 2 13
Biomechanics of the lower limb joints 13
2.1. Introduction 13
2.2 Lower limb joints 13
2.2.1 Articular anatomy and joint types 13
2.2.2 The Hip joint 16
2.2.3 The Knee joint 17
2.2.4 The foot structure; the Ankle Joint. 17
2.3 Kinematics of joints 18
2.3.1 Reviews: 18
2.3.2 Analytical methods 19
2.4 Kinetics of joints 24
Reference 25

Chapter 3 27
Method for Segment Orientation analysis Using Triaxial Accelerometers 27
3.1 Introduction 27
3.2 Materials and methods 28
3.2.1 Double-sensor difference based algorithm for analyzing the orientation of a rotational rigid body in 2D frame 29
3.2.2 Analysis of the orientation of a rotational rigid body in 3D frame 30
3.2.3. Simulation and analysis 32
3.2.4. Experiment 36
3.3 Results 37
3.4 Discussion 38
3.5 Conclusion 40
References 40

Chapter 4 42
Approach to Ambulatory Assessment of Human Segmental Orientation on a Wearable Sensor System 42
4.1 Introduction 42
4.2. Methods and Materials 44
4.2.1 Calculation of the under limb segmental orientation 44
4.2.2 Experiment design 46
4.3. Results 49
4.4. Discussion 50
4.5. Conclusion 53
References 53

Chapter 5 55
Estimation of Lower Limb Gait Posture using Accelerometers and Gyroscopes 55
5.1 Introduction 55

5.2. Materials and methods 57
5.2.1 Virtual-sensor difference based algorithm for the calculation of knee joint angle . 57
5.2.2 Gait posture analysis of the lower limb 58
5.3 Experiment using the developed wearable sensor system 60
5.4 Results 62
5.5 Discussion 65
5.6 Conclusion 66
References 67

Chapter 6 68
Visual and quantitative estimation of lower limb 3D gait posture using accelerometers and magnetometers 68
6.1 Introduction 68
6.2 Method 69
6.2.1 Estimation of the hip joint angles using physical-sensor difference based algorithm 69
6.2.2 Calculation of the knee joint angles using the virtual-sensor difference based algorithm 72
6.2.3 Definition of anatomical coordinate system for lower limb motion analysis 74
6.2.4 3D Knee joint kinematics in Anatomical coordinate system 77
6.2.5 3D Gait posture analysis of the lower limb 79
6.3 Experiments 81
6.4 Results 84
6.4.1 Results for the knee joint 3D kinematics in Anatomical coordinate system 84
6.4.2 Results for 3D the lower limb gait posture analysis. 86
6.5 Discussion and Conclusion 87
References 90

Chapter 7 92
Conclusion 92

Appendix A 94
Abbreviations and Symbols 94
Appendix B 95
Terminology in gait phase analysis 95
Appendix C 97
Drawings, Schematics and PCB Layouts 97
Appendix D 99
MATLAB Code (Offline analysis) 99

Acknowledgements 102

List of Publications 103
Academic Journal Papers 103
International Conference Proceedings 103

Chapter 1

Introduction

1.1 Project Motivation

Gait analysis is a subject that has interested researchers for many years. Recently, it has been examined for the purposes of biometrics and rehabilitation, such as clinical evaluation of human gait and development of lower-limb prostheses. Ambulatory assessment of gait posture is a promising clinical tool to diagnose walking disabilities. Three-dimensional (3D) quantitative information of the lower limb gait posture is essential for the clinical evaluation and therapeutic treatment comparisons in the orthopedic and rehabilitation fields [(1)]. Besides, the main function of lower-limb prostheses is restoration of ambulation (walking or running). Advances in the fields of materials science and engineering in the past several decades have greatly enhanced the ability of prosthetic devices to restore this function to the patient. Especially to develop intelligent lower-limb prostheses for the amputation patient, proper alignment - the correct spatial relationship between the prosthesis socket and residual limb, the cooperation between the health lower limb and the lower-limb prostheses - is paramount to enabling an efficient, comfortable and natural gait [(2)(3)]. Clinically, alignment is obtained through a dynamic procedure using subjective assessments of the gait pattern by the prosthetist, and the cooperation also needs the subjective feedback from the healthy lower limb for the prosthesis posture control. Therefore, the kinetics analysis of the lower limb joints, the human lower limb posture estimation and motion analysis is the first important subject to research.

1.2 Research Background

In the lab, the typical system for human motion analysis is the camera-based optical motion system for kinematic data combined with force platforms for kinetic data [(4)]. However, since the system is bulky, expensive and complex, it restricts the user to a constrained environment where cameras are installed and therefore not applicable for out-lab ambulatory measurement of lower limb posture in ordinary life.

As far as estimation of lower limb posture is concerned, segment orientation angles have been estimated using accelerometers and/or gyroscopes. However, when accelerometers were used to measure the accelerations of human lower limb segments, the measured signal along each sensitive axis was a resultant acceleration composed of gravitational, translational and rotational accelerations and noise, which cannot be separated [(4)]. Hence, the actual resultant acceleration couldn't be simply integrated as angular acceleration alone to predict the rotational angular velocity and displacement for segmental orientation, since it was composed of translational and gravitational acceleration components and noise at any time when the subject moved at any speed, which would lead in integral errors [(5)]. If the angular displacement of the rotational segment is calculated using the equation $\theta=(180/\pi \arcsin(a_z /g)$, where a_z is the measured vertical acceleration, the measured subject must remain still, or the linear acceleration component must be neglected. Hooman et al. [(6)] obtained the angular displacement of the rotational segment by numerically integrating the angular velocity captured by a gyroscope, but the integrated result was distorted by offsets and drifts. Luinge et al. [(7)] presented another method, but the gyroscope offset had to be continuously recalibrated and the orientation had to be continuously corrected. Hooman et al. [(8)] presented a method to solve the contradiction, obtaining the angular displacement with both accelerometer and gyroscope, and switching between the two sensors according to the wave frequency of the body segment. However, it proved difficult to achieve an accurate switching frequency. Karol et al. [(9)] presented a methodology for joint angle measurement, but it combined three kinds of sensors (gyroscope, accelerometer and magnetometer) and the study was limited to a static system (no global rotational or linear acceleration existed).

In motion analysis of the lower limb motion, the 3D knee joint kinematics is also crucial. J. Faver et al. [(10)] [(11)] developed an ambulatory system to measure the 3D knee angles by filtering and integrating the gyroscope signals from the thigh and shank, the f/e and a/a rotational angles were obtained. However, the data derived by integration of angular acceleration or angular velocity was distorted by offset and angle drift, and a proper calibration was not given. H. Dejnabadi et al. [(6)] gave a new approach to

estimate sagittal kinematics of lower limbs without accumulation of errors. Virtual accelerometers were fixed in the knee joint center and ankle to measure the joint rotational angles using external skin-mounted accelerometer and gyroscope, but only the f/e joint angle in the sagittal plane was estimated. K. O'Donovan [12] presented a technique which used a combination of rate gyroscope, accelerometer and magnetometer to measure 3D inter-segment joint angles, but the investigation of the performance of the technique was limited to a static system, and there was no evaluation for dynamic system. R. Takeda proposed a novel method for measuring human gait posture using tri-axial accelerometers and gyroscopes [13], in which the optimization algorithm used for estimating gravitational acceleration gave an optimal lower limb gait posture. However, since the algorithm involved searching for large number of combinations, it was not suitable for small computing devices. Willemsen et al. gave a method using only accelerometers to estimate the rotational angles of lower extremities without integration [14], but the movements of the lower limb joints were only analyzed in the sagittal plane and thus two-dimensional.

Therefore, cheaper and more comfortable wearable sensor system comprised of inertial sensors, such as accelerometers, gyroscopes and magnetometers, was developed and appear to be promising for measuring human movement. Various methods using inertial sensors were available for assessing 3D human posture in motion [15]. Also many ambulatory systems for various clinical applications have been developed to monitor physical activities, for example, are ambulatory systems for the quantitative and qualitative analysis of gait and posture in chronic pain patients treated [16] or for joint angle measurement [17]. To estimate body segment orientation, integrating angular velocity of the body segments measured by gyroscopes was a common method [18], but the results were distorted by offsets and drifts in the data. Another method to estimate the hip and knee joint angles and positions for the 3D lower limb posture using the gravitational acceleration along the anterior axis of the segment was proposed [19]. However, the result was insensitive to the complex geomagnetic field distortions. An inertial sensor-based method for estimating knee joint FE angle using segmental acceleration and angular velocity data was described

[20]. Although the method did not make use of the earth's magnetic field so that it was insensitive to the complex geomagnetic field distortions, it was only used for analyzing the knee joint FE angle but not the lower limb posture. A method for ambulatory measurement of three-dimensional (3D) knee joint angle with a combination of gyroscopes and accelerometers was presented [21] [22]. It was expandable to other joints for limb posture analysis. Another method for gait posture estimation using accelerometers and gyroscopes was present [23], but the experiments were conducted at fairly low velocity (88 steps/min) and the result showed that it was better for qualitative analysis than quantitative analysis. Besides, the algorithm involved searching for large number of combinations so that it was not suitable for small computing devices.. Dejnabadi et al. also proposed a method to estimate sagittal kinematics of lower limbs using body-fixed accelerometers and gyroscopes [8], but there was no detailed application for the lower limb posture analysis.

1.3 Project Description

The project outlined in this dissertation is rooted in the above discussion. The project's contribution is in the development of a wearable motion capture system that is portable and effective in its results for visual and quantitative estimation of the 3D human gait posture. Advances in sensor technology in the past decades have made possible the concept of a wearable measurement system consisting of multiple sensors and a data logging system capable of accurate motion capture. There have been many attempts at the creation of motion capture systems that make use of this technology. Section 1.2 above has shown a comprehensive review of such devices. The majority of these systems have been applied directly to humans and not to prosthetic device design. Uncontrollable errors are introduced for a variety of reasons when sensors are attached directly to human subjects, including, but not limited to sensor placement repeatability error, movement between externally attached sensors and the skin, and relative subcutaneous movement between the musculature and dermis.

Motion capture of a prosthetic limb's motion while walking has many advantages over the motion capture of a healthy limb due to the nature of the device. A prosthetic

device is a rigid mechanism thus; sensors can be firmly mounted - via screws or other mounting methods securely to it. This eliminates many of the errors introduced by attachment of sensors to the human body and skin. The rigid nature of the device also simplifies the mathematical analysis needed to capture motion from the sensor signals and provides a known reference frame with a known center of mass.

1.4 Project Objectives and Contributions

Therefore, there is a need for a system that should be accurate, ambulatory, and easy to use in routine practice, and could visually and quantitatively confirm the lower limb posture. The aim of our work is to propose a practical approach and develop an ambulatory system to analyze lower limb gait posture under normal life conditions, without using gravitational acceleration and integration of angular velocity. The posture detection allows the assessment of the hip joint and the knee joint kinematics, the joint angles, positions and other temporal gait parameters (i.e. swing and stance).

In this paper, an approach using a physical-sensor difference and virtual-sensor difference based algorithm to visually and quantitatively confirm lower limb posture was proposed. It was first used for ambulatory estimation of real time orientation of certain lower limb segment with fewer types and numbers of sensors (only accelerometers) and without integration of accelerations or angular velocities. As a further research, accelerations and angular velocities exerted on lower limb segments by accelerometers and gyroscopes were used to estimate the hip and knee joint angles, and the knee joint and ankle joint positions. Then, for a further application of the double-sensor difference based algorithm to estimate 3D lower limb joint kinematics, an original approach based on accelerometers and magnetometers for ambulatory estimation and analysis of 3D knee joint kinematics was presented. At last, to improve on the method employed in all the previous works, we present a technique for visually and quantitatively analyzing the 3D lower limb posture for gait analysis in the geomagnetic field employing only accelerometers and magnetometers, but no gyroscopes.

The project involved the design and fabrication of a prototype measurement system

consisting of micro-electro-mechanical sensors (MEMS) mounted on a rigid bar. The placement and configuration of the sensors on a bar, which represented a lower-limb prosthetic device, was used to allow study of the effect of sensor placement. Features of the developed system include the ability to track lower limb motions and analyze human gait using only small, lightweight sensors at a cost of less.

The algorithm in this dissertation was developed for analysis of collected data with the purpose of reconstructing the kinematics of the gait cycle (movement of the prototype system). The system itself has been briefly tested for feasibility in low frequency motion capture similar to that of a walking cycle. With the continuously decreasing of costs and miniaturization of the inertial sensors, we are working for realization of sensor assemblies in a single chip to measure two groups of 3D angular accelerations and one group of 3D magnetic field data simultaneously for joint kinematic analysis, then promote it to develop wearable systems for clinical applications, such as ambulatory measurement and analysis of lower limb gait in the daily life for patients or health persons.

Reference

(1) Asla RJ, Kozanek M., Wan L., Rubash HE., Li G., 2006. Six DOF in vivo kinematics of the ankle joint complex: application of a combined dualorthogonal fluoroscopic and magnetic resonance imaging technique. Journal of Orthopaedic Research 24 (5), 1019–1027

(2) Lannon, N. “Trans-tibial Alignment: Normal Bench Alignment.” *ISPO Ortholetter* 12. (2003) pp. 12-13.

(3) Blumentritt, S., et. al. “Effects of Sagittal Plane Prosthetic Alignment on Standing Transtibial Amputee Knee Loads.” *Prosthetics and Orthotics International.* 23.3 (1999) pp. 231-238.

(4) Kavanagh, J.J., Morrison, S., James, D.A., Barrett, R., 2006. Reliability of segmental accelerations measured using a new wireless gait analysis system. Journal of Biomechanics 39(15), 2863-2872.

(5) Agnes Zijlstra, Jon H.M. Goosen, Cees C.P.M. Verheyen, Wiebren Zijlstra, 2008. A body-fixed-sensor based analysis of compensatory trunk movements during unconstrained walking. Gait and Posture 27(1), 164-167.

(6) Hooman Dejnabadi, Brigitte M. Jolles, Emilio Casanova, Pascal Fua, Kamiar Aminian, 2006. Estimation and Visualization of Sagittal Kinematics of Lower Limbs Orientation Using Body-Fixed Sensors. IEEE Transactions on biomedical Engineering 53(7), 1385-1392.

(7) Luinge H. J., P. H. Veltink, 2005. Measuring orientation of human body segments using miniature gyroscopes and accelerometers. Medical and Biological Engineering and Computing 43(2), 273-282.

(8) Hooman Dejnabadi, B. M. Jolles, and K. Aminian, 2005. A new approach to accurate measurement of uniaxial joint angles based on a combination of accelerometers and gyroscopes. IEEE Transactions on Biomedical Engineering 52(8), 1478-1484.

(9) Karol J. O'Donovan, Roman Kamnik, Derek T. O'Keeffe, Gerard M. Lyons, 2007. An inertial and magnetic sensor based technique for joint angle measurement. Journal of Biomechanics 40(12), 2604-2611.

(10) J.Favre, F.Luthi, B.M.Jolles, O.Siegrist, B.Najafi and K.Aminian, "A new ambulatory system for comparative evaluation of the three-dimensional knee kinematics, applied to anterior cruciate ligament injuries," Knee Surgery Sports Traumatology Arthroscopy, vol. 14, no. 7, pp. 592-604, 2006.

(11) J. Favre, B.M. Jolles, R. Aissaoui, K. Aminian, "Ambulatory measurement of 3D knee joint angle," J. Biomech., vol. 41, no.5, pp. 1029-1035, 2008.

(12) K. O'Donovan, R. Kamnik, D. O'Keeffe, G. Lyons, "An inertial and magnetic sensor based technique for joint angle measurement," J. Biomech., vol. 40, no.12, pp. 2604-2611, 2007.

(13) R. Takeda, S. Tadano, M. Todoh, M. Morikawa, M. Nakayasu, S. Yoshinari, "Gait analysis using gravitational acceleration measured by wearable sensors," J. Biomech., vol. 42, no.3, pp. 223-233, 2009.

(14) T. M. Willemsen, C. Frigo and H. B. K. Boom, "Lower extremity angle measurement with accelerometers-error and sensitivity analysis," IEEE Trans. Biomed. Eng., vol. 38, no. 12, pp. 1186-1193, 1991.

(15) Christine Azevedo , et al., 2005. Rehabilitation of Functional Posture and Walking-Coordination of Healthy and Impaired Limbs. Journal of Automatic Control 15 (Supplement), 11-14.

(16) Padgaonkar A. J., K. W. Krieger, and A. I. King, "Measurement of angular acceleration of a rigid body using linear accelerometers," ASME J. Appl. Mech., vol. 42, pp. 552-556, 1975.

(17) Karol J. O'Donovan, Roman Kamnik, Derek T. O'Keeffe, Gerard M. Lyons, 2007. An inertial and magnetic sensor based technique for joint angle measurement. Journal of Biomechanics 40 (12), 2604-2611.

(18) Dejnabadi, H., Jolles, Brigitte M., Casanova, Emilio, Fua, Pascal, Aminian, Kamiar, 2006. Estimation and visualization of sagittal kinematics of lower limbs orientation using body-fixed sensors. IEEE Transactions on Biomedical Engineering 53 (7), 1385–1392.

(19) Takeda Ryo, Tadano Shigeru, Todoh Masahiro, Morikawa Manabu, Nakayasu Minoru, Yoshinari Satoshi, 2009b. Gait posture estimation using wearable acceleration and gyro sensors. Journal of Biomechanics 42 (15), 2486-2494.

(20) Glen Cooper, Ian Sheret, Louise McMillian, Konstantinos Siliverdis, Ning Sha, Diana Hodgins, Laurence Kenney, David Howard, 2009. Inertial sensor-based knee flexion-extension angle estimation. Journal of Biomechanics 42 (16), 2486-2494.

(21) Favre, J., Aissaoui, R., Jolles, B.M., de Guise, J.A., Aminian, K., 2009. Functional calibration procedure for 3D knee joint angle description using inertial sensors. Journal of Biomechanics 42 (14), 2330-2335

(22) Favre, J., Jolles, B.M., Aissaoui, R., Aminian, K., 2008. Ambulatory measurement of 3D knee joint angle. Journal of Biomechanics 41 (5), 1029–1035.

(23) Takeda Ryo, Tadano Shigeru, Todoh Masahiro, Morikawa Manabu, Nakayasu Minoru, Yoshinari Satoshi, 2009a. Gait analysis using gravitational acceleration measured by wearable sensors. Journal of Biomechanics 42 (3), 223-233.

Chapter 2

Biomechanics of the lower limb joints

2.1. Introduction

The human skeleton is a system of bones joined together to form segments or links. These links are movable and provide for the attachment of muscles, ligaments, tendons etc. to produce movement. The junction of two or more bones is called an articulation. There are a great variety of joints even within the human body and a multitude of types among living organisms that use exo- and endoskeletons to propel. Articulation can be classified according to function, position, structure and degrees of freedom for movement they allow etc. Joint biomechanics is a division of biomechanics that studies the effect of forces on the joints of living organisms.

Development of treatments, devices and exercise regimes for healthy joints, as well as learning from the great variety of naturally existing joints for the purpose of nature-inspired technology, requires a fundamental understanding of the mechanics of joints and joint tissues, and their interaction with the underlying biological mechanisms. At the current state of the art, the definition of joint biomechanics can be broadened to encompass these complex interactions and the relevant technology. It is the purpose of this chapter to introduce a current understanding of joint biomechanics with an emphasis on the structure, kinematics and kinetics of human lower limb joints.

2.2 Lower limb joints

2.2.1 Articular anatomy and joint types

Anatomic and structural classification of joints typically results in three major categories, according to the predominant tissue or design supporting the articular elements together, that is, joints are called *fibrous*, *cartilaginou*s, or *synovial*. In this part, we just introduce the synovial joint which is useful to our lower limb motion analysis.

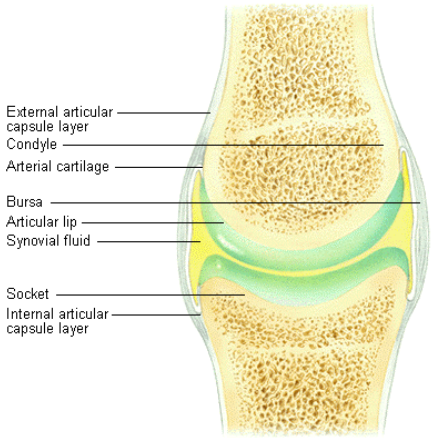

Fig. 1-1 Basic structure and components of a synovial joint (also called diarthroses).

Synovial joints are cavitated. In general two rigid skeletal segments are brought together by a capsule of connective tissue and several other specialized tissues, that form a cavity. The joints of the lower and upper limbs are mainly synovial since these are the most mobile joints. Mobility varies considerably and a number of subcategories are defined based on the specific shape or architecture and topology of the surfaces involved (e.g. planar, saddle, ball and socket) and on the types of movement permitted (e.g. flexion and extension, medial and lateral rotation). Fig. 1-2 shows some kinds of the synovial joints which would be used in our research. Fig. 1-3 shows the lower limb joints. The basic structural characteristics that define a synovial joint can be summarized in four features: a *fibrous capsule* that forms the joint cavity, a specialized *articular cartilage* covering the articular surfaces, a *synovial membrane* lining the inner surface of the capsule which also secretes a special lubricating fluid, the *synovial fluid*. Additional supportive structures in synovial joints include discs, menisci, labra, fat pads, tendons and ligaments.

Ball and socket (Other names: Spheroidal; endarthroses)
Description: Ball-shaped head fits into concave socket
Movement: Widest range of all joints; triaxial
Example: Shoulder and hip joints

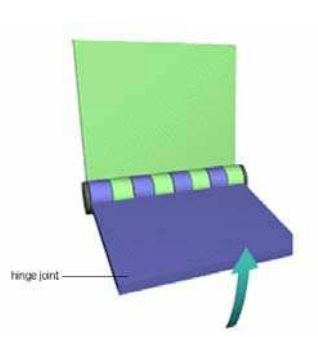


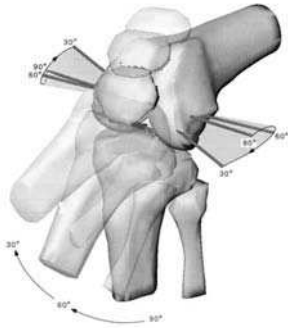

Hinge (Other name: Ginglymus)
Description: Spool-shaped head fits into concave surface
Movement: In one plane about single axis (uniaxial); like hinged-door movement (namely, flexion and extension)
Examples: Elbow, knee, ankle, and interphalangeal joints

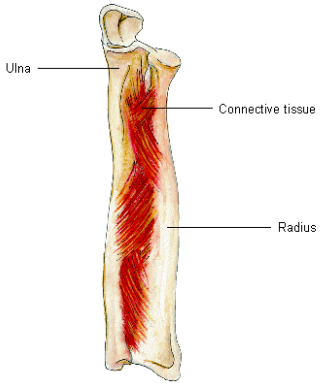

Pivot (Other name: Trochoid)
Description: Arch-shaped surface rotates about rounded or peglike pivot
Movements: Rotation: uniaxial
Example: Between axis and atlas; between radius and ulna

Fig. 1-2 Diarthroses – Synovial Joints

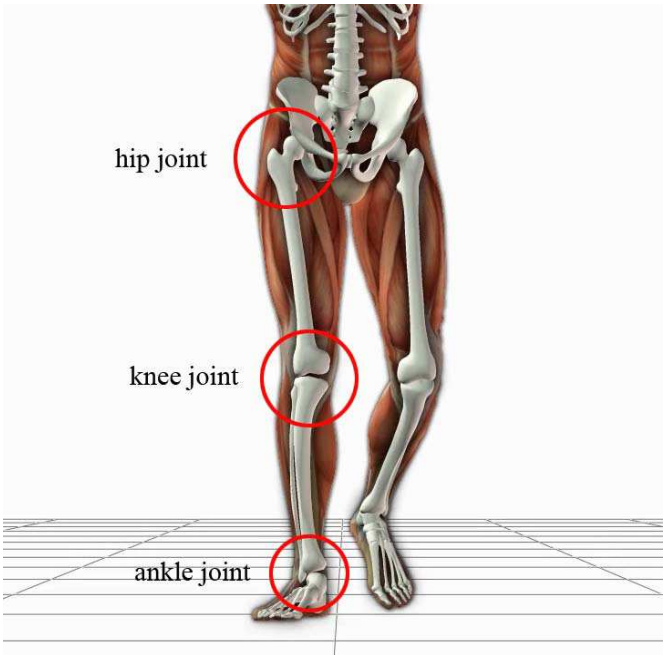

Fig. 1-3 Lower limb joints (Hip joint, knee joint and ankle joint)

Table 1-1 Major joints in the human lower limbs along with the segments-bones that they articulate, their respective type DOF and type/range of motion they provide.

Joint	Bones	Type	DOF	Type of motion	Range of Motion (deg)
Hip	Femur Acetabulum	Diarthrosis (spheroidal)	3	Flexion Extension Abduction Adduction Medial rotation Lateral rotation Circumduction	90-120 10-20 30-45 30 30-40 60 Complete
Knee	Tibia Femur	Diarthrosis (ginglymus)	2	Flexion Extension Medial rotation Lateral rotation	120-140 0 30 40
Ankle	Tibia Fibula alus	Diarthrosis (ginglymus)	1	Flexion Extension	20-30 40-45

2.2.2 The Hip joint

The hip joint is the link of the upper body and the pelvis/trunk with the lower limbs, the main locomotion facility of the body. It is a ball-and-socket joint (Table 1-1) in which the head of the femur resides in the acetabulum of the pelvis, making one of the largest and most stable joints in the body. The surface area and the radius of curvature of the articular surface of the acetabulum closely match that of the articular surface of the femoral head. The femoral ball is embraced by the acetabular socket, allowing rotation to occur with virtually no translation. The cartilage that covers the acetabulum thickens peripherally [(1)]. A plane through the circumference of the acetabulum immediately at its opening would project with the sagittal plane intersections at an angle of 40° (opening posterior) and 60° (opening laterally). During most ambulatory activities, such as normal bipedal locomotion, the lower extremity is positioned anteriorly in the sagittal plane with only small rotations necessary in the other two planes. Hip flexion of at least 120°, abduction of at least 20°, and external rotation of at least 20° are necessary for carrying out normal daily activities. Activities such as descending stairs sitting, rising from a chair, and dressing require greater degrees of flexion and rotation at the hip joint. For example descending stairs requires 36° of motion whereas squatting requires 122° of motion in the sagittal plane [(2)].

2.2.3 The Knee joint

The knee consists of a two joint structure: the femorotibial joint and the patellofemoral joint. The femorotibial joint is the largest joint in the body and is considered to be a modified hinged joint containing the articulating ends of the femur and tibia. The patellofemoral joint consists of the patella, the largest sesamoid bone, and the trochlea of the femur. Taken together, the knee joints function to control the distance between the pelvis and the foot as a control link. Surface motion occurs simultaneously in both sagittal and the transverse plane with the first being the dominant plane of motion [3, 4]. The instant center of rotation, designated primarily by the femoral condyle surface shape, follows a semicircular pathway, and the direction of displacement of the femorotibial contact points is tangential to the surface of the tibia, indicating gliding throughout the range of motion. However, the axis of rotation at the knee does not remain fixed during flexion. Indeed, as the knee flexes the screw axis will sweep out a ruled surface in space, known as the axode (Fig. 1-2). This fluctuation in the screw axis signifies that the knee is not truly a hinge joint, for which the axode would degenerate to a fixed line in space. Usually, the knee is approximated as a hinge joint, a simplification that may be acceptable for flexion angles between 45° and 90° where the moving screw axis remains very close to the line passing through the centers of curvature of the two posterior femoral condyles. The motion at the articular surfaces is not one of pure rolling, but a combination of rolling and sliding as indicated by the screw axis which never lies near the articular surfaces of the tibiofemoral joint.

2.2.4 The foot structure; the Ankle Joint.

The ankle joint can be described as a saddle-shaped lower end structure of a long bone (tibia and fibula). Its inferior transverse ligament encloses the superior aspect of the body of the talus (the trochlea). It is the joint that first receives the transient impact that travels through the tibia in gait or other movement. The subtalar and ankle joint act like a mitered hinge. The tibial surface forming the superior dome of the ankle is concave sagittally, is slightly convex from side to side, and is oriented about 93° from

the long axis of the tibia (it is higher on the lateral than the medial side). The primary motion of the ankle joint is dorsiflexion-plantarflexion. Its axis of rotation is obliquely oriented with respect to all 3 anatomic planes with ankle dorsiflexion and tibial internal rotation being associated with subtalar eversion (pronation) whereas the ankle plantarflexion and tibial external rotation are associated with subtalar inversion (supination). The axis extends from anterior, superior, and medial to inferior, posterior, and lateral as it is passing through the inferior tips of the malleoli. It is at angles of 93° with respect to the long axes of the tibia and about 12° to the joint surface.

2.3 Kinematics of joints

2.3.1 Reviews:

Mechanical analysis can refer to kinetics (forces) and/or kinematics (movement), with kinetics being the cause and kinematics the result. Mechanical analysis can develop models proceeding from forces to movements or vice versa. The simplest and most essential system of mechanical formulations for explaining and describing motion is the Newton's second law. More advanced techniques include the Lagrange, d'Alembert and Hamilton's methods. In general all these methods start by describing equations of motion for a rigid body for translation, rotation or combinations of them for both two and three-dimensional space. If the model assumes that the articulated segments that create the articulation are modeled as rigid bodies the remaining task is to calculate the relative motion between the two segments by applying graphics or joint kinematic analysis.

Kinematics is the study of the movements of rigid structures, independent of the forces that might be involved. Two types of movement, translation (linear displacement) and rotation (angular displacement), occur within 3 orthogonal planes; that is, movement has 6 degrees of freedom (DOF). Each extremity of the humans is composed of articulated skeletal segments, between which, motion occurs at joints. Most joint motion is minimally translational and primarily rotational. For human motion to be effective, not only must a comparatively rigid segment rotate its position relative to an adjacent segment, but many adjacent limb movements must interact as

well.

An important property of pure translation of a rigid body (RB) is that the displacement vectors of all points in the body are identical and are non-zero. In pure rotation of a RB, although points in the body experience nonzero displacements, one point in that body experiences zero displacement. In addition to that rule Euler's theorem shows that in pure rotation all points along a particular line through that undisplaced point also experience zero displacement. This line is also known as the axis of rotational displacement. Chasles Theorem further states that any displacement of a RB can be accomplished by a translation along a line parallel to the axis of rotation that is defined by Euler's theorem plus a rotation about that same parallel axis. Simply that suggests that any displacement in three dimensions (3D) is equivalent to a translation plus a rotation.

2.3.2 Analytical methods

Simple kinematic analysis of pure planar translations and rotation or combinations of the two as well as complicated 3D analysis of a rigid body requires the positional information of a minimum of three noncolinear points to describe this motion uniquely. If the position of three points at two instants is known, the displacement from one position to another may be interpreted as translation, rotation or both. Therefore, the first task is to continually monitor the positions of three points on each rigid body.

2.3.2.1 Coordinate Systems and Transformation

In the analysis of experimental joint mechanics data, the transformation of point coordinates from one coordinate system to another is a frequent task [5, 6]. A typical application of such a transformation would be gait analysis data recorded in a laboratory fixed coordinate system that must be converted to a reference system fixed to the skeleton of the test subject. The laboratory fixed coordinate system may be designated by ***xyz*** and the body reference system by ***abc*** (Fig. 1-4). The location of a point *S(a/b/c)* in the body reference system is defined by the radius vector

$s = a \cdot e_a + b \cdot e_b + c \cdot e_c$. Consider the reference system to be embedded into the laboratory system. Then the radius vector $r_m = x_m \cdot e_x + y_m \cdot e_y + z_m \cdot e_z$ describes the origin of the reference system in the laboratory system. The location of *S(x/y/z)* is now expressed by the coordinates *a, b, c*. The vector equation $r = r_m + s$ gives the radius vector for point S in the laboratory system (Fig. 1-4). Employing the full notation we have:

$$r = (x \cdot e_x + y \cdot e_y + z \cdot e_z) = (x_m \cdot e_x + y_m \cdot e_y + z_m \cdot e_z) + (a \cdot e_a + b \cdot e_b + c \cdot e_c).$$

A set of transformation equations results after some intermediate matrix algebra to describe the coordinates.

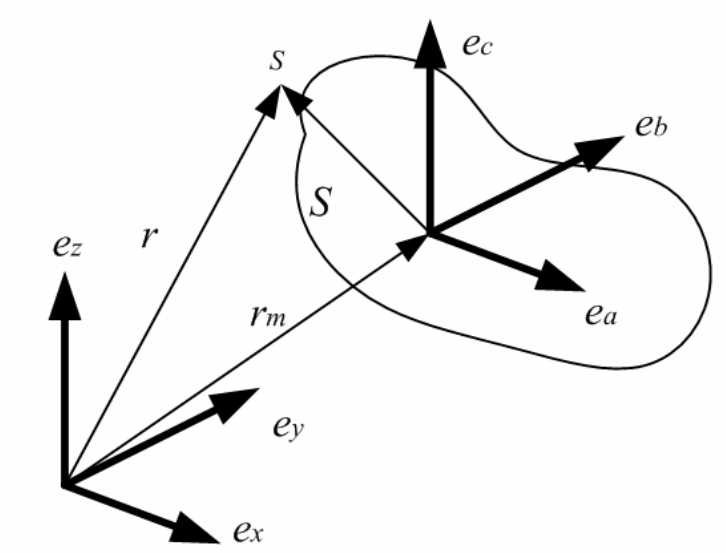

Fig. 1-4. Changing the coordinate systems, transformation of point coordinates from one coordinate system to another.

The scalar products of the unit vectors in the *xyz* and *abc* systems produce a set of nine coefficients $\boldsymbol{C}_{ij}$. The cosine of the angle between the coordinate axes of the two systems corresponds to the value of the scalar products. Three "direction cosines" define the orientation of each unit vector in one system with respect to the three unit vectors of the other system. Due to the inherent properties of orthogonality and unit length of the unit vectors, there are six constraints on the nine direction cosines, which leave only three independent parameters describing the transformation. Employing the matrix notation of the transformation equation we have:

$$\begin{bmatrix} x \\ y \\ z \end{bmatrix} = \begin{bmatrix} x_m \\ y_m \\ z_m \end{bmatrix} + \begin{bmatrix} c_{11} & c_{12} & c_{13} \\ c_{21} & c_{22} & c_{23} \\ c_{31} & c_{32} & c_{33} \end{bmatrix}$$

In coordinate transformations the objects remain unchanged and only their location and orientation are described in a rotated and possibly translated coordinate system. If a measurement provides the relative spatial location and orientation of two coordinate systems the relative translation of the two systems and the nine coefficients $\boldsymbol{C}_{ij}$ can be calculated. The coefficients are adequate to describe the relative rotation between the two coordinate systems.

2.3.2.2 Translation in three-dimensional space

In translation in 3D space the rigid object moves parallel to itself (Fig. 5). Pure translation in 3D space leaves the orientation of the body unchanged as in the case of pure 2D translation.

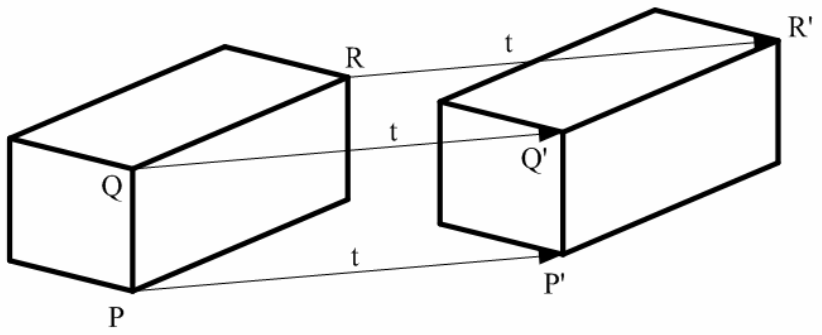

Fig. 1-5. A rigid body (shoebox) moves parallel to itself. The radius vectors from O to P and from O' to P' are designated by r and r', so that r' = r + t, where t is the difference vector.

2.3.2.3 Rotations about the coordinate Axes

A rotation in three-dimensional space is defined by specifying an axis and an angle of rotation (Fig. 1-6). The axis can be described by its 3D orientation and location [7]. A rotation, as does the translation explained earlier, leaves all the points on the axis unchanged; all other points move along circular arcs in planes oriented perpendicular to the axis [8].

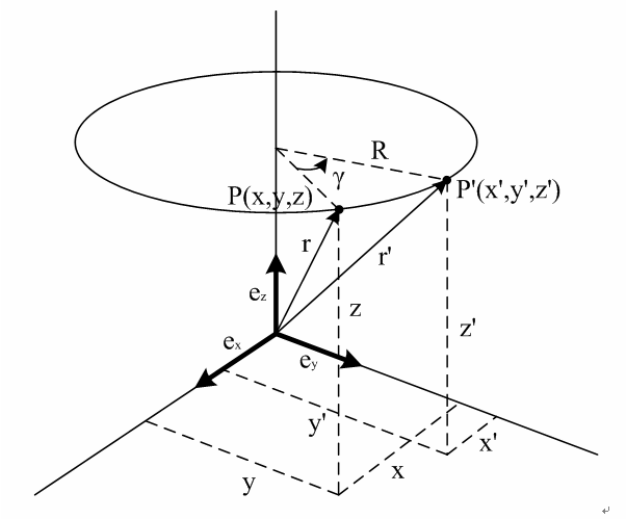

Fig.1- 6. Rotation about the z-axis of the coordinate system.

This rotation moves an arbitrary point *P* to location *P'* with constant distance *z* from the *xy*-plane (*z*=*z'*). This produces the following matrix notation for the respective equations for the rotation that changes *x*- and *y*- coordinates but leaves the *z*- coordinate unchanged.

$$r = \begin{bmatrix} x' \\ y' \\ z' \end{bmatrix} = \begin{bmatrix} \cos\gamma & -\sin\gamma & 0 \\ \sin\gamma & \cos\gamma & 0 \\ 0 & 0 & 1 \end{bmatrix} \cdot \begin{bmatrix} x \\ y \\ z \end{bmatrix} = D_z(\gamma) \cdot r$$

The matrix describing a rotation about the *z*-axis is designated ***Dz(γ)***. The matrices describing a rotation about the *y*-axis through angle β and about *x*-axis through angle α are similar.

$$r = \begin{bmatrix} x' \\ y' \\ z' \end{bmatrix} = \begin{bmatrix} \cos\beta & 0 & \sin\beta \\ 0 & 1 & 0 \\ -\sin\beta & 0 & \cos\beta \end{bmatrix} \cdot \begin{bmatrix} x \\ y \\ z \end{bmatrix} = D_y(\beta) \cdot r \quad r = \begin{bmatrix} x' \\ y' \\ z' \end{bmatrix} = \begin{bmatrix} 1 & 0 & 0 \\ 0 & \cos\alpha & -\sin\alpha \\ 0 & \sin\alpha & \cos\alpha \end{bmatrix} \cdot \begin{bmatrix} x \\ y \\ z \end{bmatrix} = D_x(\alpha) \cdot r$$

Assume that the first rotation of a rigid body occurs about the *z*-axis of a coordinate system. The second rotation occurs supposedly about the x'-axis, i.e., about a body-fixed axis on the body (previously rotated about its z-axis). Matrix intermediate calculation here gives:

$$r'' = D_{z'} * D_{x'} * r$$

In this calculation the sequence of the matrices is very important especially as this sequence differs from what one might expect. First, the matrix of the second partial rotation acts on the vector ***r*** and then, in a second step on the matrix of the first partial

rotation. If the sequence of the two partial rotations is interchanged, the combined rotation is described by

$r'' = D_x * D_{z'} * r$

2.3.2.4 Euler and Bryant-Cardan angles

Any desired orientation of a body can be obtained by performing rotations about three axes in sequence. There are, however, many ways of performing three such rotations. One can do this task at random but for reasons of clarity two conventions are frequently used: the Euler's and Bryant-Cardan's rotations.

In the Euler notation the general rotation is decomposed of three rotations about body-fixed axes in the following manner (Fig. 1-7):

Rotation 1: about the z-axis through the angle φ rotation matrix $\boldsymbol{D_z(\varphi)}$;

Rotation 2: about the x'-axis through the angle θ rotation matrix $\boldsymbol{D_{x'}(\theta)}$;

Rotation 3: about the z''-axis through the angle ψ rotation matrix $\boldsymbol{D_{z''}(\psi)}$;

The matrix describing Euler's combined rotation is given by the matrix product

$\boldsymbol{B} = \boldsymbol{D_z}(\varphi) * \boldsymbol{D_{x'}}(\theta) * \boldsymbol{D_{z''}}(\psi)$ (Euler)

According to the Bryant and Cardan the general rotation is decomposed of three rotations about body-fixed axes in the following manner (Fig. 1-7):

Rotation 1: about the *x*-axis through the angleφ_1 (Pitch angle) rotation matrix $\boldsymbol{D_x(\varphi_1)}$;

Rotation 2: about the *y'*-axis through the angleφ_2 (Roll angle) rotation matrix $\boldsymbol{D_{y'}(\varphi_2)}$;

Rotation 3: about the *z''*-axis through the angleφ_3 (Yaw anle) rotation matrix $\boldsymbol{D_{z''}(\varphi_3)}$;

in which case the matrix of combined rotation is given by:

$\boldsymbol{B} = \boldsymbol{D_x}(\varphi_1) * \boldsymbol{D_{y'}}(\varphi_2) * \boldsymbol{D_{z''}}(\varphi_3)$ (Bryant-Cardan)

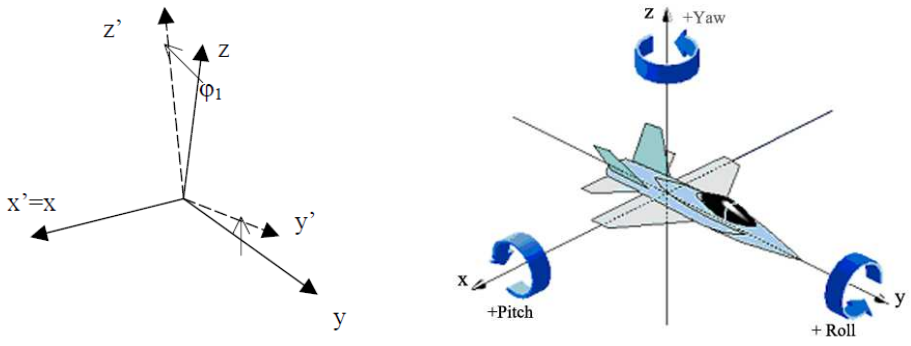

Figure 1-7. General rotation composed of three partial rotations. The first rotation according to the Bryant-Cardan convention (above). The first of the general rotations using Euler as the selection of the axes and angles of rotation (below).

For reasons of simplicity, we have presented single or combined rotations about coordinate axes, but more complicated rotational laws can be applied as we deal with rotations about arbitrary axes. Rotation and translation can also be integrated into one single motion with Chasles Theorem. Chasles Theorem states that "the general motion in three-dimensional space is helical motion", or "the basic type of motion adapted to describe any change of location and orientation in three-dimensional space is helical motion". The relevant axis of rotation is designated the "helical axis". Chasles Theorem is also known as the "helical axis" theorem.

In many cases in biomechanics the problem is not in describing the motion of a body in a laboratory coordinate system but in describing the relative motion of two bodies. One example of such relative motion is that of the shank relative to the motion of the thigh. If one succeeds in fixing a "measurement coordinate system" on the thigh, the motion of the shank would then be observed in the coordinate system of the thigh and interpreted according to one of the above conventions (Euler's angles etc.).

2.4 Kinetics of joints

The study of the forces that bring about the movements discussed above is called kinetics. Because kinetics provides insights into the cause of the observed motion, it is essential to the proper interpretation of human movement processes. Forces and loads are not visually observable; they must be either measured with instrumentation or calculated from kinematics data. Kinetic quantities studied include such parameters as the forces produced by muscles; reaction loads between body parts as well as their interactions with external surfaces; the load transmitted through the joints; the power transferred between body segments; and the mechanical energy of body segments. Inherent to such studies are the functional demands imposed on the body. The structure and stability of each extremity and its joints reflect different systems and functional demands.

The kinetics deal with the effects of forces on the motion of a body. When the motion is known, the problem is then to find the force system acting on the body. There are joint forces and joint moments. With all the kinematic quantities known, it

is possible to find the joint forces and moments from the resulting force system that acts on each element. This is done by solving a system of simultaneous equations at successive time intervals. Since muscles are an unknown force system, the resolved muscle force and the real joint force are treated as totally unknown joint forces in the analysis. The three equations of motion for linear motions are

$$\sum F = ma_x \quad \sum F = ma_y \quad \sum F = ma_z$$

The three equations of motion for rotation are

$$\sum M_x = I_{xx}a_x - (I_{yy} - I_{zz})\omega_y\omega_z - I_{xy}(\alpha_y - \omega_x\omega_z) - I_{yz}(\omega_y^2 - \omega_z^2) - I_{xx}(\alpha_z + \omega_x\omega_y)$$

$$\sum M_y = I_{yy}a_y - (I_{zz} - I_{xx})\omega_z\omega_x - I_{yz}(\alpha_z - \omega_y\omega_x) - I_{xx}(\omega_z^2 - \omega_x^2) - I_{xy}(\alpha_x + \omega_y\omega_z)$$

$$\sum M_z = I_{zz}a_z - (I_{xx} - I_{yy})\omega_x\omega_y - I_{zx}(\alpha_x - \omega_z\omega_y) - I_{xy}(\omega_x^2 - \omega_y^2) - I_{yz}(\alpha_y + \omega_z\omega_x)$$

where M is the moment, I is the mass moment of inertia, α the angular acceleration, and ω is the angular velocity. The moment equations can be simplified if the axes of the reference frames coincide with the principal axes, with the origin at the center of gravity. These equations, called

Euler equations, are

$$\sum M_x = I_x a_x - (I_y - I_z)\omega_y\omega_z \quad \sum M_y = I_y a_y - (I_z - I_x)\omega_z\omega_x \quad \sum M_z = I_z a_z - (I_x - I_y)\omega_x\omega_y$$

Continuity conditions are derived based on the fact that equal and opposite forces and momentsoccur at the joint between the two segments.

The anthropometric data for the mass, the center of gravity, the moment of inertia, and so on for the different parts of the human body are available in the literature [9, 10].

Reference

(1) Kempson GE, Spivey CJ, Swanson SA, Freeman MA. Patterns of cartilage stiffness on normal and degenerate human femoral heads. J Biomech 1971; Dec;4(6):597-609.

(2) Johnston RC, Smidt GL. Hip motion measurements for selected activities of daily living. Clin Orthop Relat Res 1970; Sep-Oct;72:205-15

(3) Winter DA. Motor Control of Human Gait - A Multitask Movement. IEEE EMBS 10th Annual Conference. New Orleans: IEEE Press, 1988.

(4) Andriacchi TP, Mikosz RP, Hampton SJ, Galante JO. Model studies of the stiffness characteristics of the human knee joint. J Biomech 1983;16:23-9.

(5) Bringmann C, Eckstein F, Bonel H, Englmeier KH, Reiser M, Graichen H. A new in vivo

(6) Wittenburg J. Dynamics of Systems of Rigid Bodies. Stuttgart, Germany: B.G. Teubner, 1977.

(7) Woltring HJ. Planar control in multi-camera calibration for 3-D gait studies. J Biomech 1980;13:39-48.

(8) Woltring HJ. Representation and calculation of 3-D joint movement. Human Movement Science 1991;10:603-616.

(9) Dempster WT. Space Requirements of the Seated Operator. Wright Patterson Air Force Base, OH, 1955.

(10) Drillis R, Contini R, Bluestein M. Body Segment Parameters; a Survey of Measurement Techniques. Artif Limbs 1964;25:44-66.

Chapter 3

Method for Segment Orientation analysis Using Triaxial Accelerometers

3.1 Introduction

In the medical field, there is a need for small ambulatory sensor systems for measuring the kinematics of body segments. It is essential to detect the motion of certain segment of lower limbs in biomechanical applications, especially in human gait analysis. Current methods for ambulatory measurement of body segment orientation have limitations in terms of volume, price and accuracy. Optical motion analysis systems are precise but expensive and lab-limited. With the development of inertial sensors, many wearable sensor systems composed of accelerometers and/or gyroscopes were developed and many novel approaches for gait analysis using inertial sensors were proposed [1-4]. Kinematics data for gait analysis such as knee joint angles, thigh and shank orientations were obtained [5-8]. A wearable sensor system comprised of accelerometers and gyroscopes is a new direction for gait analysis, which has come into its own [9-10].

However, when accelerometers were used to measure the accelerations of human lower limb segments, the measured signal along each sensitive axis was a resultant acceleration composed of gravitational, translational and rotational accelerations and noise, which cannot be separated. Hence, the actual resultant acceleration could not be simply integrated as angular acceleration alone to predict the rotational angular velocity and displacement for segmental orientation, since it was composed of translational and gravitational acceleration components and noise at any time when the subject moved at any speed, which would lead in integral errors. If the angular displacement of the rotational segment is calculated using the equation $\theta=(180/\pi)\arcsin(a_z/g)$, where az is the measured vertical acceleration, the measured subject must remain still, or the linear acceleration component must be neglected. Else

if rotational angles were estimated by numerical integration of the angle velocities measured by a gyroscope on the thigh, there must be integration drift caused by noise in the angular velocity signal. In addition, offset of the gyroscope had to be continuously recalibrated and orientation of the gyroscope had to be continuously corrected [11].

In this chapter, a novel and simple method for estimating the orientations of human body segments was discussed. It can be used for ambulatory estimation of real time orientation of certain lower limb segment with fewer types and numbers of sensors and without integration of accelerations or angular velocities. Simulations of the method were expatiated and results of the simulations were discussed. Then a prototype of a wearable sensor system composed of two coaxially placed triaxial accelerometers and one piece of MCU was developed. The prototype was attached to a board with one freedom of rotation and a thigh of a volunteer to capture the 3D accelerations of the board and the thigh. Then, the angular displacements of the board and the thigh were calculated with the measured accelerations. Compared with the results obtained from the prototype and the high accuracy camera system, the method could be used in the gait analysis.

3.2 Materials and methods

When a triaxial accelerometer is attached on a rigid body segment at a known position **r** in segment-fixed coordinate system, the measured acceleration **a** is shown as follow:

$$\mathbf{a} = \mathbf{R} \cdot (\mathbf{g} + \mathbf{A}) + \dot{\boldsymbol{\omega}} \times \mathbf{r} + \boldsymbol{\omega} \times (\boldsymbol{\omega} \times \mathbf{r}) \qquad (3\text{-}1)$$

where **R** is the attitude matrix of the body segment with respect to ground, **A** is the acceleration of the origin of the segment-fixed coordinate system with respect to ground, $\mathbf{g} = (0, 0, -g)^T$ is the gravitational field, and $\boldsymbol{\omega}$ is the angular velocity of the rigid body, expressed in the segment -fixed coordinate system.

Actually, the gravitational acceleration, inertial acceleration due to translation and rotation and noise cannot be separated out of the measured signal. When we wanted to estimate rotational angles of a rigid body using only the readings of

accelerometers, a double-sensor difference based algorithm was developed and expatiated in 2D coordinate system. Then it was used to evaluate orientation angles of lower limb segments in 3D space.

3.2.1 Double-sensor difference based algorithm for analyzing the orientation of a rotational rigid body in 2D frame

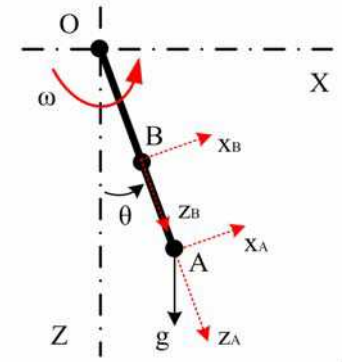

Fig.3-1 Rotation of a rigid body in 2D coordinate frame

To analyze the rotation of a rigid segment in 2D coordinate frame, three reference coordinate systems are introduced: one global reference frame *XOZ* is defined at the rotation joint of the segment, another two sensor-fixed coordinate frames x_AAz_A and x_BBz_B are defined at the position A and B on the segment with the z_A and z_B axes along the rigid segment, as Fig. 3-1 shows. When the rotation joint is fixed in the global frame, the relationship between accelerations and angular displacements at positions A and B are given by the following equations:

$$a_{Ax} = \ddot{x}_A - g\sin\theta = r_A\ddot{\theta} - g\sin\theta \tag{3-2}$$

$$a_{Az} = \ddot{z}_A + g\cos\theta = -r_A\dot{\theta}^2 + g\cos\theta \tag{3-3}$$

$$a_{Bx} = \ddot{x}_B - g\sin\theta = r_B\ddot{\theta} - g\sin\theta \tag{3-4}$$

$$a_{Bz} = \ddot{z}_B + g\cos\theta = -r_B\dot{\theta}^2 + g\cos\theta \tag{3-5}$$

where (a_{Ax} a_{Az}) and (a_{Bx}, a_{Bz}) are the accelerations in corresponding directions of the sensor fixed frame x_AAz_A and x_ABz_A, (x_A,z_A) and (x_B,z_B) are the coordinates at position A and B in the global frame, and θ is the rotational angular displacement of the rigid segment in the global frame *XOZ*.

Based on Eq. (3-2)·r_B- Eq. (3-4)·r_A and Eq. (3-)·r_B- Eq. (3-5)·r_A, the angular displacement equations are obtained:

$$\theta = \sin^{-1}\left(\frac{a_{Ax}r_B - a_{Bx}r_A}{g(r_A - r_B)}\right) \quad \text{or} \quad \theta = \cos^{-1}\left(\frac{a_{Az}r_B - a_{Bz}r_A}{g(r_B - r_A)}\right) \tag{3-6}$$

Based on Eq. (3-2)- Eq. (3-4) and Eq. (3-3)- Eq. (3-5), the angular velocity and acceleration of the rigid segment are calculated as follows:

$$\dot{\theta}^2 = \frac{a_{Az} - a_{Bz}}{r_B - r_A} \tag{3-7}$$

$$\ddot{\theta} = \frac{a_{Ax} - a_{Bx}}{r_A - r_B} \tag{3-8}$$

where r_A, r_B could be measured from the rotation joint to the positions A and B, and $a_{Ax}, a_{Bx}, a_{Az}, a_{Bz}$ could be measured with accelerometers.

3.2.2 Analysis of the orientation of a rotational rigid body in 3D frame

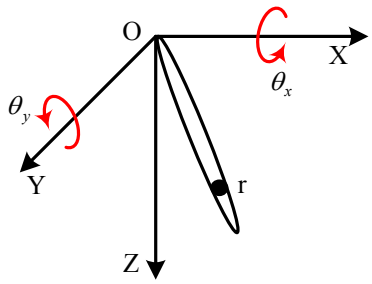

Fig. 3-2 Rotation of a rigid body in *X*-*Y*-*Z* reference frame

First, a rigid body is supposed to rotate in the global coordinate system (*O*-*XYZ*) in 3D space, as Fig. 3-2 shows. θ_y,and θ_x are the rotation angles about the Y and X axis, and **r** is the vector from origin to arbitrary position on the rigid body in the global coordinate system. The rotation acceleration of the rigid body can be obtained without considering acceleration of gravity:

$$\mathbf{a}_r = \ddot{\mathbf{r}} = \begin{bmatrix} \ddot{\mathbf{x}} \\ \ddot{\mathbf{y}} \\ \ddot{\mathbf{z}} \end{bmatrix} = \begin{bmatrix} r\ddot{\theta}_y \\ r\ddot{\theta}_x \\ -r\dot{\theta}_x^{\,2} - r\dot{\theta}_y^{\,2} \end{bmatrix} \tag{3-9}$$

Then, if only the acceleration of gravity is considered, and the rigid body rotates about *Y* axis at first, and then about *X* axis, the gravitational acceleration components

about each sensitive axis are shown as follows:

$$\mathbf{a}_g = \begin{bmatrix} a_{gx} \\ a_{gy} \\ a_{gz} \end{bmatrix} = \begin{bmatrix} 1 & 0 & 0 \\ 0 & \cos\theta_x & \sin\theta_x \\ 0 & -\sin\theta_x & \cos\theta_x \end{bmatrix} \begin{bmatrix} \cos\theta_y & 0 & -\sin\theta_y \\ 0 & 1 & 0 \\ \sin\theta_y & 0 & \cos\theta_y \end{bmatrix} \mathbf{g} = \begin{bmatrix} -g\sin\theta_y \\ g\sin\theta_x\cos\theta_y \\ g\cos\theta_x\cos\theta_y \end{bmatrix} \quad (3\text{-}10)$$

In fact, the actual acceleration is a composition including both of the gravitational and rotational accelerations, which can be obtained as follow without considering noise:

$$\mathbf{a} = \mathbf{a}_r + \mathbf{a}_g = \begin{bmatrix} r\ddot{\theta}_y \\ r\ddot{\theta}_x \\ -r\dot{\theta}_x^{\,2} - r\dot{\theta}_y^{\,2} \end{bmatrix} + \begin{bmatrix} -g\sin\theta_y \\ g\sin\theta_x\cos\theta_y \\ g\cos\theta_x\cos\theta_y \end{bmatrix} = \begin{bmatrix} r\ddot{\theta}_y - g\sin\theta_y \\ r\ddot{\theta}_x + g\sin\theta_x\cos\theta_y \\ -r\dot{\theta}_x^{\,2} - r\dot{\theta}_y^{\,2} + g\cos\theta_x\cos\theta_y \end{bmatrix} \quad (3\text{-}11)$$

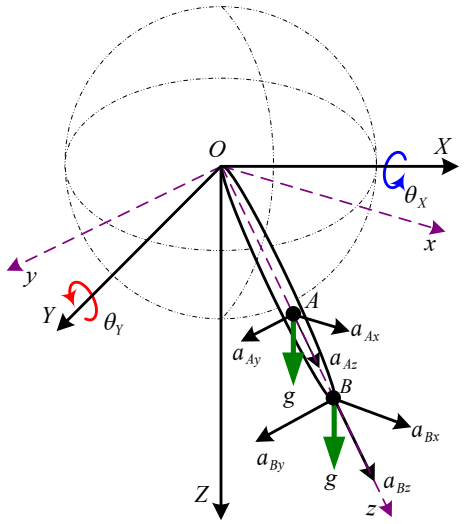

Fig. 3 Rotation of a rigid body with two triaxial accelerometers in 3D reference frame

Based on Eq. (3-11), accelerations in each direction on a rigid body are known when it rotates in 3D reference frame. Then, how to estimate the orientation of the rigid body is the keystone. Suppose there was a rigid body with two triaxial accelerometers placed in 3D frame as Fig. 3-3 shows. The two triaxial accelerometers were fixed coaxially at positions A and B on the rigid body, and the corresponding axes of the two accelerometers were in the same direction, then two groups of signals $\boldsymbol{a_A}$, $\boldsymbol{a_B}$ could be obtained as follows:

$$\mathbf{a}_A = \begin{bmatrix} a_{Ax} \\ a_{Ay} \\ a_{Az} \end{bmatrix} = \begin{bmatrix} r_A\ddot{\theta}_y - g\sin\theta_y \\ r_A\ddot{\theta}_x + g\sin\theta_x\cos\theta_y \\ -r_A\dot{\theta}_x^{\,2} - r_A\dot{\theta}_y^{\,2} + g\cos\theta_x\cos\theta_y \end{bmatrix} \quad (3\text{-}12)$$

$$\mathbf{a}_B = \begin{bmatrix} a_{Bx} \\ a_{By} \\ a_{Bz} \end{bmatrix} = \begin{bmatrix} r_B\ddot{\theta}_y - g\sin\theta_y \\ r_B\ddot{\theta}_x + g\sin\theta_x\cos\theta_y \\ -r_B\dot{\theta}_x^{\,2} - r_B\dot{\theta}_y^{\,2} + g\cos\theta_x\cos\theta_y \end{bmatrix} \tag{3-13}$$

where $\boldsymbol{a_A}$, $\boldsymbol{a_B}$ are the actual accelerations measured by the two triaxial accelerometers at positions **A** and **B**. Then the following equation could be obtained with the rotational radiuses ($\mathbf{r}_A$, $\mathbf{r}_B$) and the measured accelerations:

$$\mathbf{a}_A \cdot \mathrm{r}_B - \mathbf{a}_B \cdot \mathrm{r}_A = \left[\dot{\boldsymbol{\omega}} \times \mathbf{r}_A + \boldsymbol{\omega} \times (\boldsymbol{\omega} \times \mathbf{r}_A) + \mathbf{R} \cdot \mathbf{g}\right] \cdot r_B - \left[\dot{\boldsymbol{\omega}} \times \mathbf{r}_A + \boldsymbol{\omega} \times (\boldsymbol{\omega} \times \mathbf{r}_A) + \mathbf{R} \cdot \mathbf{g}\right] \cdot r_A \tag{3-14}$$

Then the angular displacements θ_y, and θ_x about the Y and X axes were calculated from Eq.(3-14) and shown as follows.

$$\theta_y = \cos^{-1}\left(\frac{\pm\sqrt{(a_{Ay}r_B - a_{By}r_A)^2 + (a_{Az}r_B - a_{Bz}r_A)^2}}{g(r_A - r_B)}\right) \tag{3-15}$$

$$\theta_y = \sin^{-1}\left(\frac{a_{Ax}r_B - a_{Bx}r_A}{g(r_A - r_B)}\right) \tag{3-16}$$

$$\theta_x = \cos^{-1}\left(\frac{a_{Az}r_B - a_{Bz}r_A}{g(r_A - r_B)\cos\theta_y}\right) \tag{3-17}$$

$$\theta_x = \sin^{-1}\left(\frac{a_{Ay}r_B - a_{By}r_A}{g(r_A - r_B)\cos\theta_y}\right) \tag{3-18}$$

3.2.3. Simulation and analysis

As expatiated in the method, it was theoretically feasible to measure the segmental orientation. As Eq.(3-6) shows, rotational angular displacements of a rigid segment in the global frame can be calculated with two inverse trigonometric functions. In order to show the accuracy of both the functions in indifferent conditions and select a low-error function to calculate the angular displacement of the rotational segment, simulations with different parameters in the equations were presented. In the simulations, a_{Ax}, a_{Az}, a_{Bx}, a_{Bz} were given signals, as shown in Fig. 3-4(a), the period was 2/3 second, r_A=10cm, r_B=15cm.

Random noise of less than 5% of the given acceleration amplitude was added to the given acceleration. In Fig. 3-4(b), the curves show the angular displacement θ calculated by arcsine and arccosine functions with random noise. The percentage

errors calculated by the two inverse trigonometric functions are shown in Fig. 3-4(c). When the absolute value of the angle displacement was close to 0°, the errors calculated by arccosine were much greater than those calculated by arcsine, due to the fact that the linearity of arccosine was worse than arcsine and the noise was amplified by arccosine. The condition was opposite when the absolute value of the angular displacement was close to 90°.

Consequently, in order to achieve higher precision of the calculated angle from -90° to 90°, a switching method was used when the rotational angular displacement was calculated off-line after each experiment. The inverse trigonometric function (either arcsine or arccosine) that resulted in smaller errors was selected to calculate the rotational angles. As is shown in Fig. 3-4(c), the percentage errors of the angles calculated by arcsine and arccosine fluctuate according to the value of the angle. The value of the percentage error at the crossing points of the two curves is the smallest amplitude value of the fluctuating percentage errors. At these points, the percentage error is 4.35% and the absolute value of the angle is 34.02°. Therefore, 34.02° is the absolute value for switching the calculation function between arcsine and arccosine. When a rigid segment swings about the fixed local frame origin, arcsine was selected to calculate the rotational angular displacement when the absolute value of the rotational angle was less than 34.02°, otherwise by arccosine.

When the absolute value of the rotational angular displacement of a rigid segment was more than 45°, as the simulation data in Fig.3-4(c) shows, the precision of the calculated angular displacement by arcsine was no more than 5.6%. Therefore, the equation described with arcsine functions can be used to calculate the rotational angle for the orientation of a segment when the rotation angle is less than 45°.

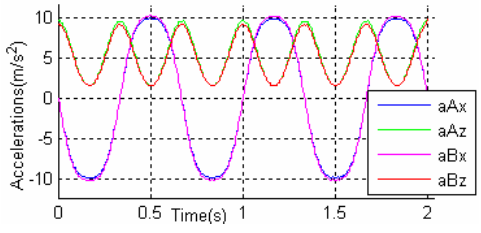

a. Given accelerations of each axis in local frame on positions A and B

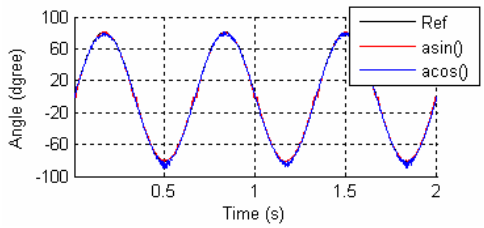

b. Rotation angles calculated from given accelerations using arcsine and arccosine

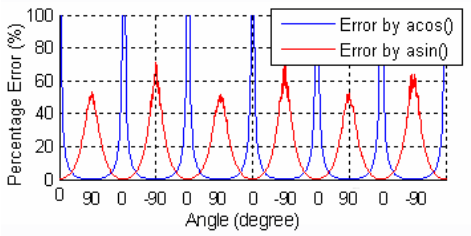

c. Percentage errors of the angles calculated by arcsine and arccosine using given accelerations with random noise

Fig. 3-4 Simulation results using given signals (accelerations) in the reference frame

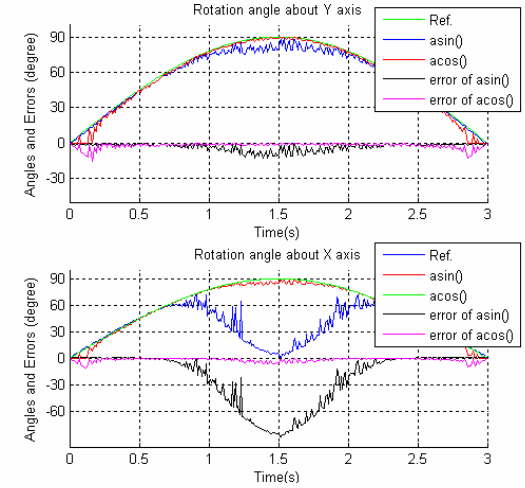

Fig. 3-5 The calculated rotation angles θ_y, θ_x with noises in half a motion circle (0-90°)

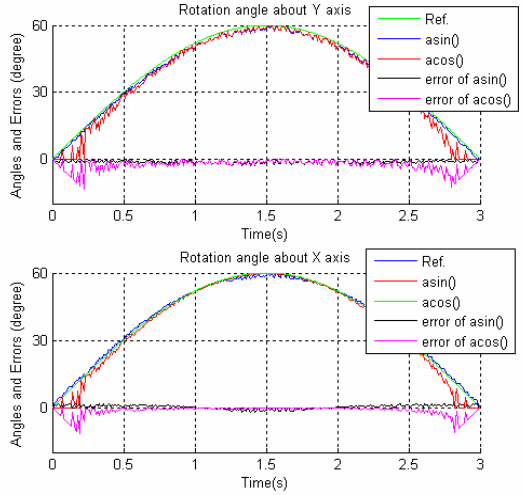

Fig. 3-6 the calculated rotation angles θ_y, θ_x with noises in half a motion circle (0-60°)

Then, simulation for evaluating the double-sensor difference based algorithm for

lower limb orientation analysis in 3D frame was done. As Eqs.(3-15)~(3-18) show, angular displacements in two directions can be obtained on the basis of a series of accelerations. In the simulation, a_{Ax}, a_{Ay}, a_{Az}, a_{Bx}, a_{By}, a_{Bz} were given signals, r_A, r_B were constant.

In Fig.3-5, the curves show the rotation angle θ_y, θ_x calculated by the functions of arcsine and arccosine in half a motion cycle, and there are random noises acting on accelerations about each axis. As the curves of the errors show, when the angle displacement is close to 0°, errors of the calculated result by arccosine are much greater than those calculated by arcsine, and when the angle displacement is close to 90°, the errors obtained from arcsine are much greater than those calculated by arccosine. Because the linearity of arcsine is much better than arccosine when the angle is close to 0°, which is in direct contrast to the situation when the angle is close to 90°. Additionally, the curve of θ_x fluctuates more intensively than the curve of θ_y when the absolute value of the angle displacement is close to 90°. The reason is that Eqs.(3-17) and (3-18) for calculating θ_x contain $cos\theta_y$ in the denominators which had some errors already when noise was added. That is to say, the calculated result of θ_x included the errors from θ_y, and it had been magnified. Particularly when the rotation angle is 90°, the error is infinite. In order to show this problem clearly, random noise with bigger amplitude was used in the simulation. Then, Fig.3-6 shows the calculated angles about Y and X axes using given accelerations when rotation angles are less than 60°. As the error curves show, the calculated results by arcsine are much better than those calculated by arccosine. Therefore, in order to gain a higher precision of angle placement when the rotation angles about Y and X axes are less than 60°, the equations expressed by arcsine are used. Fig.3-7 shows the calculated rotation angles θ_y, θ_x using arcsine in 20 seconds.

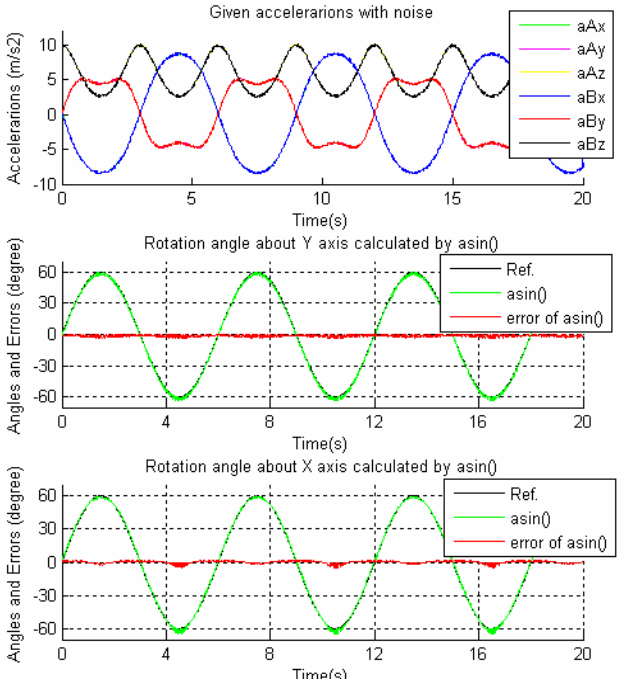

Fig. 3-7 Given accelerations and the corresponding angle of θ_y, θ_x with noises

3.2.4. Experiment

In order to evaluate the algorithm in a simple condition, a device composed out of two triaxial accelerometers (MM-2860), a carbon composition potentiometer (RV30YN20S-B504) and a rotationable board was developed as shown in Fig.3-8. In this experiment, PCI-6071E DAQ device was used to capture the analogue signal and send it to a PC after being transformed into a digital signal. The two triaxial accelerometers attached to the board were used to measure accelerations for the calculation of the rotation angle. The potentiometer was fixed in the rotation axis of the rotationable board to measure the rotational angle as reference.

In order to test the method for lower limb segment orientation, especially its feasibility in gait analysis, an elementary wearable sensor system composed of two triaxial accelerometers (MM-2860) and one MCU (H8/3694) was developed. Fig.3-9 shows the experiment with the sensor system on the thigh. Three marks were attached on the thigh. A high-accuracy camera system was used to track the trajectories of the three marks and show the orientation angle of the thigh as reference. In this experiment, a simple situation was assumed that is the thigh rotated at the original place.

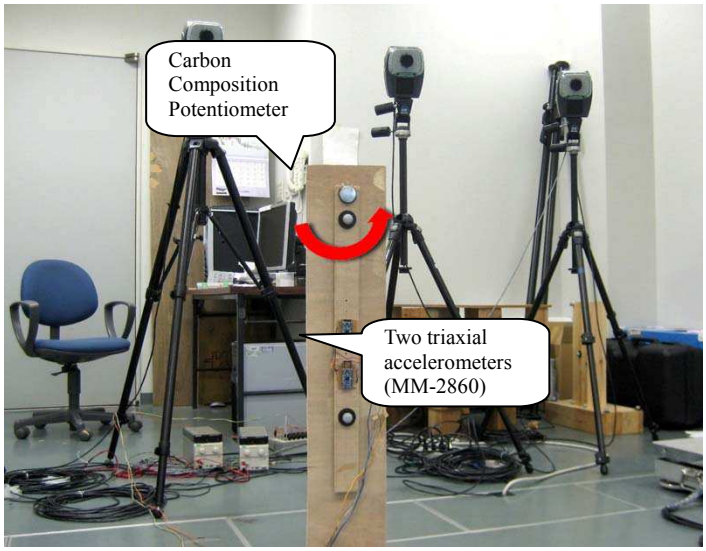

Fig.3-8 A simple device for estimating the rotation angles in a 2D frame using two accelerometers

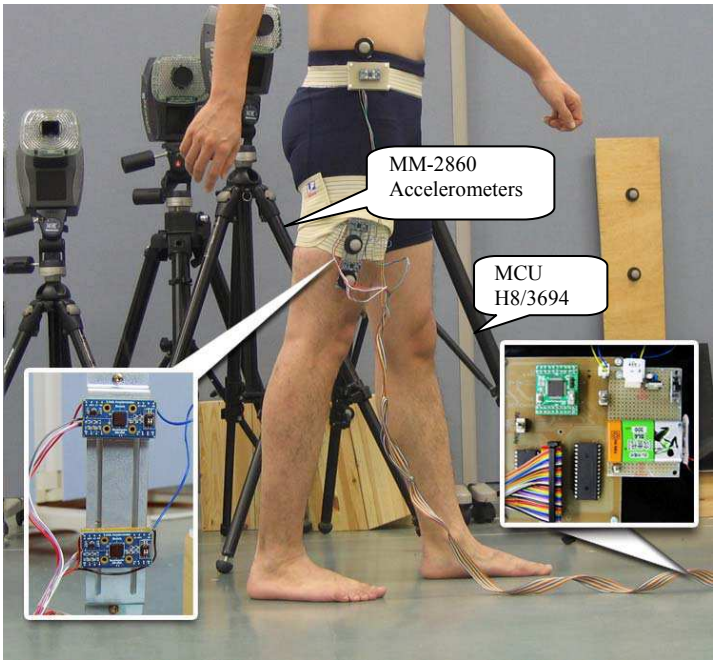

Fig.3-9 Experiment for the lower limb orientation using the developed wearable system

3.3 Results

To recognize the orientation of human body segment, the way that the angle displacement changes about each axis is most important. As shown by the first chart in Fig.3-10 and Fig.3-11, a_{Ax}, a_{Ay}, a_{Az}, a_{Bx}, a_{By}, a_{Bz} are the accelerations about each sensitive axis measured by the accelerometers, which are used to calculate angular displacement. The data obtained from the sensors was voltage signal. It was translated into actual accelerations for calculations. In Fig.3-10, the calculated rotation angle of

the board is compared with the angle measured by the potentiometer. Fig.3-11 shows the accelerations measured by the wearable sensor system, the calculated angles θ_y, θ_x and the referenced angles from the high-accuracy camera system.

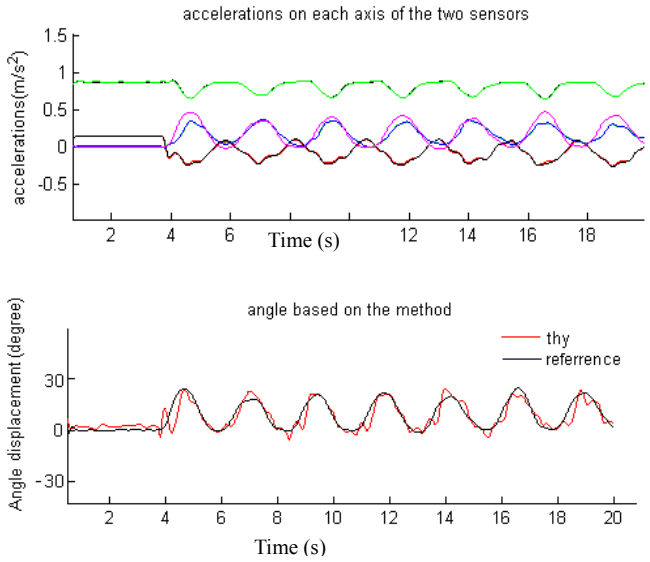

Fig.3-10 Experiment data from the simple device

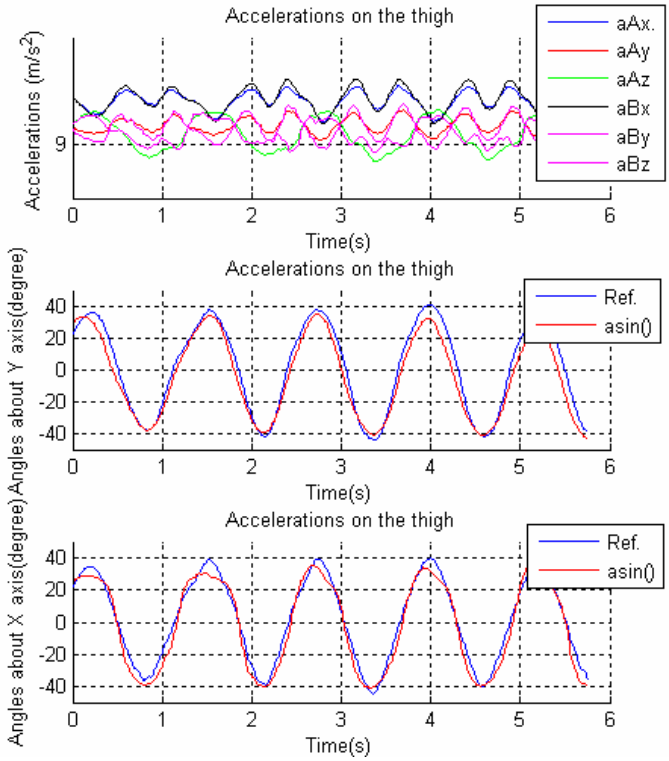

Fig.3-11 Experiment data from the prototype of the wearable sensor system

3.4 Discussion

It is obvious that there are errors between the calculated angles and the

referenced angles, especially the angle θ_x about X axis in Fig.3-11. There are some reasons for this. First, in the experiment, the axes of the two sensors cannot be coaxially placed exactly as described in the theory. Second, it is hard to firmly fix the device on the thigh as on a rigid body, because the muscle and skin of the lower limb must be moving with the motion of the body segments. What's more, as shown in the equations for calculating the rotation angles, the difference between r_A and r_B is in the denominator of each equation, therefore a small error of (r_B-r_A) must cause a large error in the calculated angles. And in §3.2.3, it has been discussed that the error of θ_x contains the errors of θ_y, so that it must be less accurate than θ_y, which is why the curve of the calculated angle had a bad tracking of the referenced angle in the third chart of Fig.3-11.

Additionally, r_A and r_B are the distances from each accelerometer to the rotation joint, which depend on the positions where the sensors are fixed. However, in each experiment, the acceleration signals and the distance are measured quantities that must contain noise. And the scale of r_A, r_B also affects the precision of the calculated result of the angle displacement θ_y, θ_x, especially when the prototype is attached on the lower limb, so the measurement precision of the measured distances r_A and r_B is important.

Since human motion contains substantial translation and rotation, the motion of a lower limb segment cannot be perfectly modeled as a simple rotation of a rigid model but contains movement with the trunk. In addition, when two triaxial accelerometers were fixed on the thigh, if each two corresponding axes of the two sensors were not in exactly the same orientation, there was also some misreading of the accelerations for the calculation of the rotation angles. Therefore, we will present our research work on how to apply the double-sensor difference based algorithm to estimate the actual human motions when subjects walk with translation and rotation of the thigh in another paper.

Consequently, although the prototype was only tested in ideal conditions in the lab, and it was only for qualitative analysis of the human segment orientation but not quantitative analysis, the double-sensor difference based algorithm is original for

qualitative analysis of lower limb segmental orientation in 2 directions (about the Y and X axis). We are currently working to enlarge the investigable moving range of the body segments and the precision of the device when it is used for estimating actual human motions. Additionally, with the continuous decrease in costs and miniaturization of inertial sensors, we are working toward realization of sensor assemblies in a single chip to measure two groups of accelerations for a lightweight and portable wearable sensor system, and then promote it to clinical applications in daily life for patients or medical personnel.

3.5 Conclusion

A novel approach for real time recording of human body segment orientation was presented and discussed. Based on the simulation analysis and the experiment results, it can be found that there is a clear relationship between the measured accelerations and the calculated angles using two coaxially placed triaxial accelerometers on the thigh. Using only triaxial accelerometers, without integration, the orientation angles of the lower limb segment can be obtained in the gravitational field. Compared with the referenced angles obtained from the high-accuracy camera system, the novel method is available to measure orientation angles of the lower limb for human gait analysis. Using simple calculation and fewer types and quantities of sensors, the method is useful for developing a wearable sensor system for studying the human gait of patients or healthy persons during routine daily life.

References

(1) Boonstra MC, van der Slikke RM, Keijsers NL, van Lummel RC,Waal Malefijt MC, Verdonschot N., The accuracy of measuring the kinematics of rising from a chair with accelerometers and gyroscopes, *Journal of Biomechanics*, Vol.39, No.2(2006), pp. 354-358.

(2) Agnes Zijlstra, Jon H.M. Goosen, Cees C.P.M. Verheyen, Wiebren Zijlstra, A body-fixed-sensor based analysis of compensatory trunk movements during unconstrained walking, *Gait & Posture*, Vol.27, No.2(2008), pp. 164–167.

(3) Turcot, K., Aissaoui, R., Boivin, K., Pelletier, M., Hagemeister, N., De Guise, J.A., New accelerometric method to Discriminate between asymptomatic subjects and patients with medial knee osteoarthritis during 3-D gait, *IEEE Transactions on Biomedical Engineering*, Vol.55, No.4(2008), pp. 1415-1422.

(4) Liu Kun, Liu Tao, Shibata Kyoko, Inoue Yoshio, Zheng Rencheng, Novel approach to ambulatory

(5) Kavanagh, J.J., Menz, H.B., Accelerometry: A technique for quantify movement patterns during walking, *Gait and Posture*, Vol.28, No.1 (2008), pp. 1-15.

(6) Williamson, R., Andrews, B.J., Detecting absolute human knee angle and angular velocity using accelerometers and rate gyroscopes, *Medical and Biological Engineering and Computing*, Vol.39, No.3(2001), pp. 294-302.

(7) Kun Liu, Tao Liu, Shibata, K., Inoue, Y., Rencheng Zheng, Novel approach for lower limb segment orientation in gait analysis using triaxial accelerometers, *Proceedings of IEEE/ASME International Conference on Advanced Intelligent Mechatronics*, No. 4601709 (2008-7), pp.488-492.

(8) N.Hagemeister, G.Parent, M.Van de Putte, N.St-Onge, N.Duval, J.de Guise, A reproducible method for studying three-dimensional knee kinematics, *Journal of Biomechanics*, Vol.38, No.9(2005), pp. 1926-1931.

(9) Findlow, J. Goulermas, C. Nester, D. Howard, L. Kenney, Predicting lower limb joint kinematics using wearable motion sensors, *Gait & Posture*, Vol.28, No.1(2008), pp. 120-126.

(10) J. Kavanagh, S. Morrison, D. James, R. Barrett, Reliability of segmental accelerations measured using a new wireless gait analysis system, *Journal of Biomechanics*, Vol.39, No.15(2006), pp. 2863-2872.

(11) H. J. Luinge, P. H. Veltink, Measuring orientation of human body segments using miniature gyroscopes and accelerometers, *Medical and Biological Engineering and Computing*, Vol.43(2005), pp. 273–282.

Chapter 4

Approach to Ambulatory Assessment of Human Segmental Orientation on a Wearable Sensor System

4.1 Introduction

In the medical field, parameters of human motion, especially the orientations of lower limb segments, are very important for clinicians to determine suitable treatments for patients [(1) (2)]. Gait analysis has become an effective tool for quantifying surgical intervention effects and evaluating patients' conditions [(3)]. Therefore, it is essential to detect the orientations of lower limb segments in biomechanical applications. And various kinematic sensor techniques and sensor-based wearable systems have been developed for studying gait analysis [(4)-(8)].

As far as the measurement of certain lower limb segment orientation is concerned, joint angle has been estimated using accelerometers and/or gyroscopes [(9) (10)]. In chapter 3, we have discussed the disadvantage of estimating rotation angles by numerical integration of the angular velocities or accelerations measured by a gyroscope or accelerometer. The offset of the gyroscope had to be continuously recalibrated and orientation of the gyroscope had to be continuously corrected Hooman et al. [(11)] presented a method to solve the contradiction, obtaining the angular displacement with both accelerometer and gyroscope, and switching between the two sensors according to the wave frequency of the body segment. However, it proved difficult to achieve an accurate switching frequency. Karol et al. [(12)] presented a methodology for joint angle measurement, but it combined three kinds of sensors (gyroscope, accelerometer and magnetometer) and the study was limited to a static system (no global rotational or linear acceleration existed). Bogert et al. [(13)] presented a method for inverse dynamic analysis in three dimensions using only accelerometers mounted on the upper body. He just presented the equations for calculating the total resultant force and moment on a body segment but not solve the equation for

segmental orientation.

Therefore, in this chapter, the algorithm that uses only data from accelerometers attached to the subject in order to measure lower limb orientation and other gait parameters was discussed. The proposed double sensor deference based algorithm is capable of measuring the rotation of a body segment about two local axes when the volunteers walk in straight line. It does not use gyroscope data, therefore, it does not contain the gyroscope integration errors reported by others.

Actually, the gravitational acceleration and inertial acceleration due to translation and rotation and noise cannot be separated out of the measured signal [(14)]. When a triaxial accelerometer is attached to a rigid body segment at a known position **r** in a segment-fixed coordinate system, the measured acceleration **a** is shown as follows:

$$\mathbf{a} = \mathbf{R} \cdot (\mathbf{g} + \mathbf{a}_0) + \dot{\boldsymbol{\omega}} \times \mathbf{r} + \boldsymbol{\omega} \times (\boldsymbol{\omega} \times \mathbf{r}) \qquad (4\text{-}1)$$

where **R** is the attitude matrix of the body segment with respect to the ground, $\mathbf{a}_0$ is the acceleration of the origin of the segment coordinate system with respect to ground, $\mathbf{g} = (0, 0, -g)^T$ is the gravitational field, and $\boldsymbol{\omega}$ is the angular velocity of the rigid body, expressed in the body-fixed coordinate system. Additionally, when the sensors are attached to the lower limb, the skin motion artifact due to impact loading and muscle activation can readily contaminate signals. The measurement of body segment orientation from only accelerometer data therefore requires the assumptions explained below and the equations developed in the following section.

It was amused that the lower limb segments were rigid segments and the subjects walked in a straight forward way with very little trunk sway, skin artifacts and no significant internal/external rotation of the leg. When two accelerometers are attached at two different positions with each corresponding axis in the same directions, the gravitational acceleration, translational acceleration, skin motion artifact and other noise acting on the two sensors should be the same except the rotational acceleration. To exploit the difference between the rotational accelerations, a new and simple method based on a double-sensor difference based algorithm was expatiated to estimate the rotational angles of lower limb segment in two directions for the

segmental orientation in 3D space. To validate the method, a wearable sensor system based only on triaxial accelerometers was developed and tested on human segments and a mechanical arm.

4.2. Methods and Materials

4.2.1 Calculation of the under limb segmental orientation

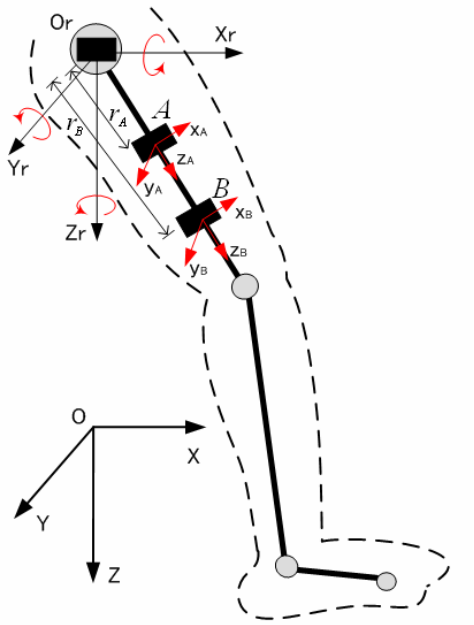

Fig. 4-1 Schematic of the lower limb with accelerometers during ordinary steps

To identify the human segmental orientation in the body fixed local coordinate system, the rotational angles of the right thigh were measured as an example, i.e., the relative attitude of the thigh compared with the pelvis in 3D space was analyzed by considering the hip joint as a ball joint, which permits rotations in three angular directions (flexion/extension, abduction/adduction and thigh inernal/external rotation directions).

The following systems of coordinates are introduced to explain the flexion/extension and abduction/adduction hip joint rotational angles as shown in Fig.4-1:

1, O-XYZ is global frame with the axes X, Y, and Z pointing forward, outward and downward.

2, O_r-$X_rY_rZ_r$ is body fixed local frame with the origin O_r at the hip joint. Suppose it

maintains constant orientation in 3D space with the axes parallel to the axes of the global system. In the joint rotation convention for a hip joint [15], Y_r axis describes the flexion-extension motion. X_r axis is used to measure abduction and adduction.

3, A-$x_A y_A z_A$ and B-$x_B y_B z_B$ are the sensor coordinate systems for the two accelerometers which are attached to the thigh at position A and B. The z_A axis is the long axis of the thigh segment (along the femur); the x_A axis is perpendicular to the z_A axis in the sagittal plane of the femur; the y_A axis is orthogonal to both axis x_A and z_A. The axes in o_B-$x_B y_B z_B$ have the same orientation with the axes in o_A-$x_A y_A z_A$ correspondingly

When the subjects perform straight-line walking trials, the origin O_r (the hip joint) of the local coordinate system is not fixed in the global frame. In this paper, only the translational acceleration on the hip joint was considered. The actual resultant acceleration ($\mathbf{a}_A$) at point ***A*** on the thigh can be measured by an accelerometer and be formulated as follows:

$$\mathbf{a}_A = \dot{\boldsymbol{\omega}} \times \mathbf{r}_A + \boldsymbol{\omega} \times (\boldsymbol{\omega} \times \mathbf{r}_A) + \mathbf{R}_{\theta_{Z_r}} \cdot \mathbf{R}_{\theta_{X_r}} \cdot \mathbf{R}_{\theta_{Y_r}} \cdot (\mathbf{g} + \mathbf{a}_{O_r}) \quad (4\text{-}2)$$

where $\mathbf{r}_A$ is the position vector of point ***A*** in the local coordination system, $\mathbf{a}_{Or}$ is the translational acceleration of the hip joint in the global coordinate system, $(\mathbf{g} + \mathbf{a}_{O_r})$ is the actual acceleration at the hip joint which will be denoted by $\mathbf{A}_{Or}$ in the following equations. θ_{Y_r} is the flexion-extension angle (pitch angle) about the Y_r axis; θ_{X_r} is the abduction-adduction angle (yaw angle) about the X_r axis; θ_{Z_r} is the internal-external rotational angle about Z_r axis. $\mathbf{R}_{\theta_{Z_r}}$, $\mathbf{R}_{\theta_{Y_r}}$ and $\mathbf{R}_{\theta_{X_r}}$ are rotation matrices.

As Fig.4-1 shows, two triaxial accelerometers were fixed at two positions ***A*** and ***B*** on the thigh with corresponding axes in the same directions, therefore, two sets of accelerations $\mathbf{a}_A$ and $\mathbf{a}_B$ at positions ***A*** and ***B*** were measured. Then the following equation could be obtained with the rotational radiuses ($\mathbf{r}_A$ and $\mathbf{r}_B$) and the measured accelerations:

$$\begin{aligned}&\mathbf{a}_A \cdot r_B - \mathbf{a}_B \cdot r_A \\ &= \left[\dot{\boldsymbol{\omega}} \times \mathbf{r}_A + \boldsymbol{\omega} \times (\boldsymbol{\omega} \times \mathbf{r}_A) + \mathbf{R}_{\theta_{Z_r}} \cdot \mathbf{R}_{\theta_{X_r}} \cdot \mathbf{R}_{\theta_{Y_r}} \cdot \mathbf{A}_{O_r}\right] \cdot r_B \\ &\quad - \left[\dot{\boldsymbol{\omega}} \times \mathbf{r}_B + \boldsymbol{\omega} \times (\boldsymbol{\omega} \times \mathbf{r}_B) + \mathbf{R}_{\theta_{Z_r}} \cdot \mathbf{R}_{\theta_{X_r}} \cdot \mathbf{R}_{\theta_{Y_r}} \cdot \mathbf{A}_{O_r}\right] \cdot r_A\end{aligned} \quad (4\text{-}3)$$

According to the method used to calculate the angular displacement in Eq. (3-6), the angular displacements about the X_r, Y_r and Z_r axes in the local frame were calculated from Eq. (4-3). To simplify the calculation, the subject was assumed to walk in a straight forward way without considering the trunk sway, skin artifacts and internal/external rotation of the leg. Only the flexion-extension angle θ_{Y_r} and abduction-adduction angle θ_{X_r} were used to describe the orientation of the thigh in the local coordinate frame, and the equations for calculating the angles were shown as follows:

$$\theta_x = \sin^{-1}\left(\frac{r_B a_{Ay} - r_A a_{By}}{(r_B - r_A)\sqrt{A_{O_r y}{}^2 + A_{O_r z}{}^2}}\right) - \sin^{-1}\left(\frac{A_{O_r y}}{\sqrt{A_{O_r y}{}^2 + A_{O_r z}{}^2}}\right) \quad (4\text{-}4)$$

$$\theta_y = \sin^{-1}\left(\frac{r_B a_{Ax} - r_A a_{Bx}}{(r_B - r_A)\sqrt{A_{O_r x}{}^2 + A_{O_r y}{}^2 + A_{O_r z}{}^2 - \left(\frac{r_B a_{Ay} - r_A a_{By}}{r_B - r_A}\right)}}\right) - \sin^{-1}\left(\frac{A_{O_r x}}{\sqrt{A_{O_r x}{}^2 + A_{O_r y}{}^2 + A_{O_r z}{}^2 - \left(\frac{r_B a_{Ay} - r_A a_{By}}{r_B - r_A}\right)}}\right) \quad (4\text{-}5)$$

where $(A_{O_r x}, A_{O_r y}, A_{O_r z})$ is the measured translational acceleration of the local frame origin (hip joint) in the global frame.

As were shown in Eqs. (4-4) and (4-5), it was obvious that rotation angles of the thigh in flexion/extension, abduction/adduction directions of the local coordinate system can be obtained using only three actual accelerations ($\mathbf{A}_{Or}$, $\mathbf{a}_A$ and $\mathbf{a}_B$) at three points (the hip joint and two arbitrary points on the thigh), which can be measured only with accelerometers instead of a combination of accelerometers, gyroscopes and other kinds of sensors.

4.2.2 Experiment design

In the first experiment, to test the method in a simplified situation, a 2 DOF mechanical arm was assembled out of rigid segments and encoders, and the rigid arm was driven by hand to sway with a fixed pivot point. As Fig.4-2 showed, on the joint

of the mechanical device, there were two incremental shaft encoders (RS-32-0/1000ER.11KB) from Hengstler, which were fixed along X_r and Y_r axes in the local frame. The rotational angles of the rigid arm about the two axes were measured by the encoders with a definition of 1000 pulses per minute (0.36° per pulse). To test the accelerations of the rotational arm, two triaxial accelerometer based chips, which were the same as the ones used in the second experiment, were fixed on the rigid segment.

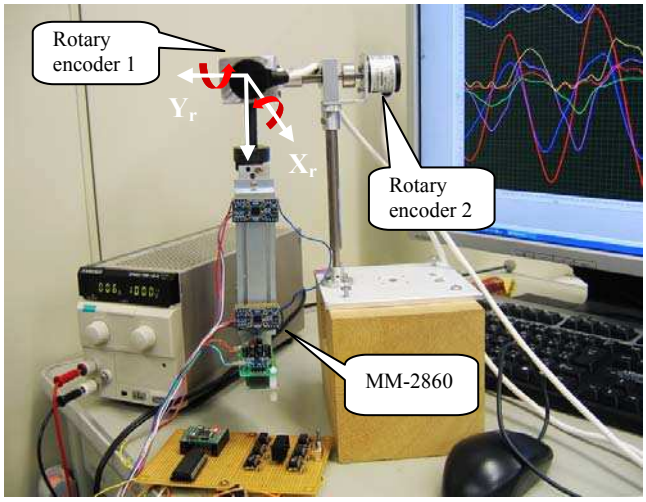

Fig.4-2 Reference mechanical system assembled out of encoders, mechanical arms, and the wearable sensor system including two accelerometers and one single-chip microcomputer (H8-3694F).

In the second experiment, a wearable sensor system only based on triaxial accelerations was developed and tested for the thigh orientation in the segment fixed local coordinate system.. Three triaxial accelerometer based chips (MM-2860 Sunhayato, Japan) and one MCU (H8/3694, from Renesas Technology Corp.) were used in the system as Fig.4-3 shows. The MCU was used to capture accelerations from the triaxial accelerometers, store data in the EEPROM real time and communicate with a PC after each test.

Since it was hard to fix the accelerometer on the hip joint exactly, and the hip joint moved at the same speed as the trunk, the first accelerometer for measuring the translational accelerations of the local frame origin was fixed above the hip joint, on the waist, with an elastic strap, where more stable accelerations could be captured than on the hip joint. To prevent gravity being erroneously recorded as acceleration in the horizontal plane and ensure the measured accelerations coincided with the

directions of idealized translational accelerations as the method described, the accelerometer must be kept upright on the waist. Therefore, a flat aluminum sheet was placed inside the elastic strap on the waist, and the accelerometer was fixed on it. During the initial calibration, the aluminum sheet with the accelerometer was optimally adjusted to coincide with the sagittal plane of the thigh and the z axis of the accelerometer was upright.

In order to capture the accelerations at two points on the thigh, two MM-2860 chips were fixed on a non-reflective L-shaped aluminum sheet with the three pairs of corresponding axes in the same directions; the distance between them was 50mm. Simultaneously, three retro-reflective marks were fixed on the two endpoints and the corner of the L-shaped aluminum sheet. In the initial installation of the wearable sensor system before each test, to calibrate the orientation of the two accelerometers to the orientation of the thigh segment, the edge with the two MM-2860 of the L-shaped sheet was fixed on the right thigh with an elastic strap to coincide with the line which connected the hip joint and the knee joint. The distance (r_A) from the hip joint to the first accelerometer on the thigh was measured with a ruler in each trial.

In the experiment, eight subjects (6 males, 2 females, Age: 25±3 years, Height: 170±5cm, mass: 60±11kg) with no history of musculoskeletal pathology and injury were requested to perform 3 straight-line walking trials at self-selected slow, normal and fast walking speeds. Three groups of 3D accelerations at the three points were obtained from the wearable sensor system during each motion test. Simultaneously, a commercial optical motion analysis system, NAC Hi-Dcam II Digital High Speed Camera Systems (NAC image technology. Japan), was used to track and measure the 3D trajectories of the retro-reflective markers, with sampling frequency of 100 Hz and calibration error 0.22% for capturing the trajectory of an ambulatory subject. Then the referenced angular displacements of the thigh in X_r and Y_r directions were obtained from the camera system by analyzing the motion parameters of the markers.

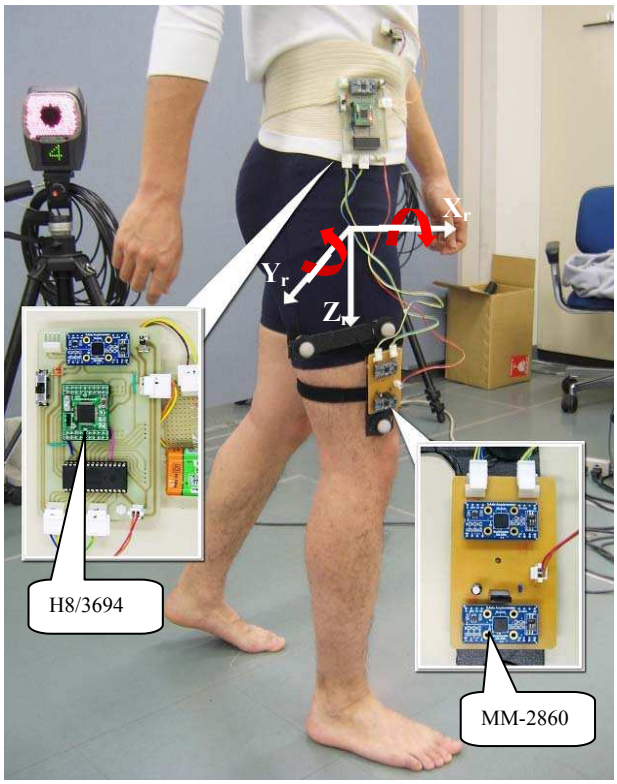

Fig.4-3 Thigh movement analysis with the developed device

4.3. Results

All signals captured in the experiment were off-line processed by Matlab. A low-pass filter with a cut-off frequency of 20 Hz was used to remove noise from all the initial data. Fig.4-4 and Fig.4-5 show the calculated (red dotted line) and referenced (blue real line) angular displacements about X_r and Y_r axes from the developed device and the encoders in the mechanical system at high (mean velocity=85deg./s) and low (mean velocity=55deg./s) angular velocities respectively. The distances from the accelerometers to the local frame origin were 10cm and 19cm respectively. The curves in Fig.4-6 and Fig.4-7 show the calculated (red dotted line) and the referenced (blue real line) angular displacements of the thigh about X_r and Y_r axes at a self-selected slow and fast speed.

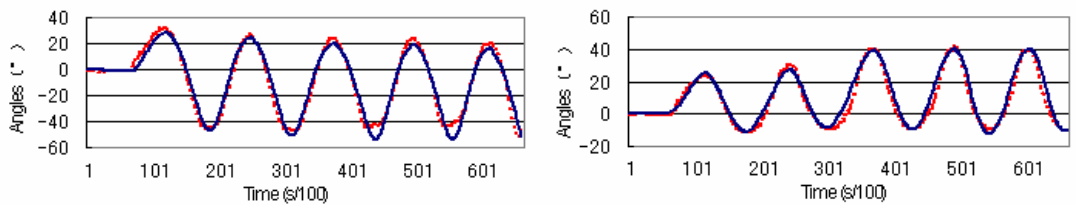

Fig.4-4 The calculated (red dotted line) and referenced (blue real line) angular displacements about the X_r and Y_r axes when the mechanical arm swung at a higher speed.

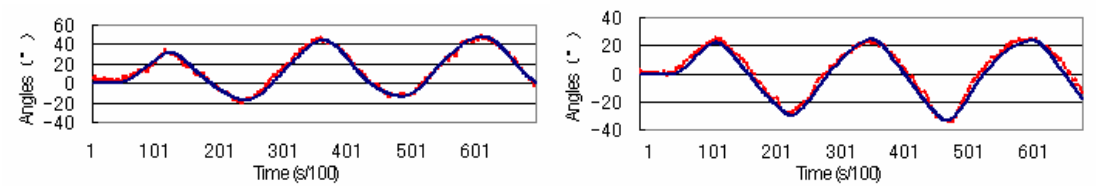

Fig.4-5 The calculated (red dotted line) and referenced (blue real line) angular displacements about the X_r and Y_r axes when the mechanical arm swung at a lower speed.

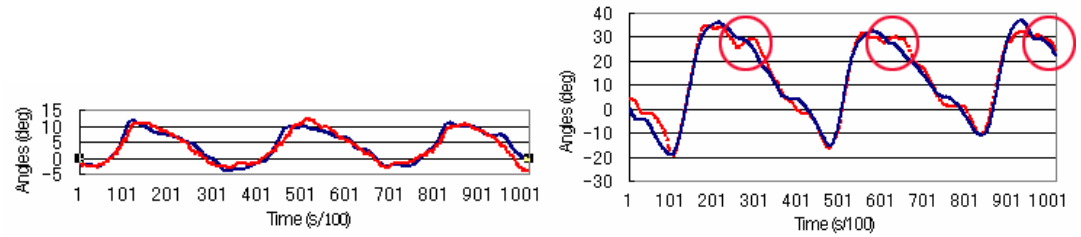

Fig.4-6 The Calculated (red dotted line) and referenced (blue real line) angular displacements about X_r and Y_r axes at the self-selected slow speed

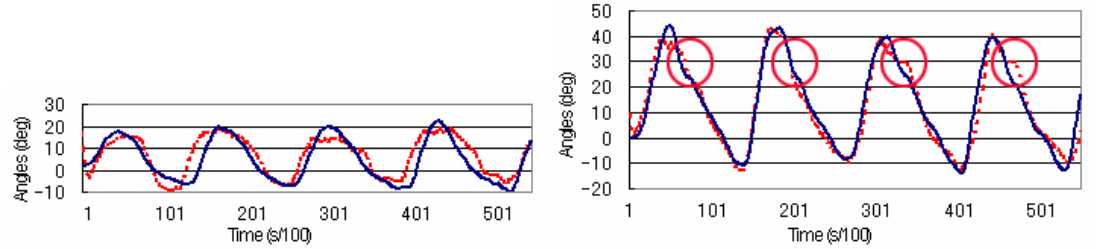

Fig.4-7 The calculated (red dotted line) and referenced (blue real line) angular displacements about the X_r and Y_r axes at the self-selected high speed

4.4. Discussion

All the related parameters between the referenced and calculated angular displacements in the X_r and Y_r directions of each case are shown in Table 1-4, where RMS was the root of the mean of the square differences, R was the correlation coefficient, r_A and r_B were the rotation radiuses from each triaxial accelerometer to the rotational origin, e_{max} was the maximum error, ROM was the range of the motion of the rigid body in each direction.

Table 4-1, Result of comparing angular displacement around X_r axis between the referenced mechanical system and the two triaxial accelerometers based measuring system.

θ_x	r_A(cm)	r_B(cm)	e%	$RMS_{\theta x}$(°)	$R_{\theta x}$	ROM(°)	e_{max}(°)
Slow	10	19	0.304%	0.8239	0.9981	40	1.71
	14	19	0.626%	0.9642	0.9967	40	2.26
	17	19	0.834%	1.2759	0.9934	40	3.85
Fast	10	19	0.395%	1.0460	0.9972	40	2.27
	14	19	1.432%	1.1643	0.9956	40	3.91
	17	19	2.085%	1.5236	0.9917	40	4.73

Table 4-2, Result of comparing angular displacement around Y_r axis between the referenced mechanical system and the two triaxial accelerometers based measuring system.

θ_y	r_A(cm)	r_B(cm)	e%	$RMS_{\theta y}$(°)	$R_{\theta y}$	ROM(°)	e_{max}(°)
Slow	10	19	0.793%	0.8105	0.9988	40	1.83
	14	19	1.011%	0.8760	0.9976	40	2.89
	17	19	1.380%	1.0148	0.9955	40	3.61
Fast	10	19	0.936%	1.2543	0.9980	40	2.37
	14	19	1.078%	1.3546	0.9968	40	3.74
	17	19	1.577%	1.6668	0.9946	40	5.35

As Table 4-1 and Table 4-2 showed, when r_A and r_B were the same but rotational velocities of the mechanical arm were different, higher rotational velocities resulted in greater e_{max}, RMS and lower correlation coefficient. When the rotational velocities were the same but r_A and r_B were different, greater difference between r_A and r_B resulted in smaller e_{max}, RMS and a higher correlation coefficient. It proved that the precision of the calculated angular displacements depended on the distance between the two accelerometers and the rotational velocity of the rigid arm. Therefore, in order to obtain a more precise angular displacement and velocities, it was better to increase the distance between two accelerometers and decrease the rotating velocity of the mechanical arm.

When the wearable sensor system was tested on the thigh, the distance (r_A) from the hip joint to the first accelerometer on the thigh depended on where it was fixed in each test. The range of the measured distance was 200±50mm.

As Table 4-3 and Table 4-4 showed, the e_{max} and RMS of the calculated angular displacements of the thigh were much greater than those of the mechanical system, because it was more difficult to firmly fix the wearable sensor system on the thigh than on a rigid body without any relative motion. Especially at high speed, the skin motion artifact due to impact loading and muscle activation added noise to the accelerations. Also, the third accelerometer, for measuring the accelerations of the local frame origin, could not be fixed on the hip joint exactly as in the design. As walking speed increased, the non-translation acceleration of the local frame origin also increased, leading to greater error, especially when the accelerometer on the waist was not exactly upright. Also the gravitational acceleration contaminated the

measured acceleration on each axis, which was assumed in the upright, forward and outward directions. Obviously, to get a more precise translational acceleration of the hip joint, the method of fixing the accelerometer should be improved. Additionally, since the mechanical system was a 2 DOF rigid arm without internal/external rotation (no roll angle) when it was driven to sway, the calculation equations shown by Eq.(4-4) and Eq.(4-5) are more accurate for measuring the orientation of the 2 DOF rotational segment without considering roll angle. When the orientation angles of the thigh were calculated, disregarding the trunk sway, the gravity in the local horizontal plane of the trunk fixed accelerometer and internal/external rotation of the leg which existed exactly, was bound to induce errors.

Table 4-3 Gait velocity conditions (mean±SD) and corresponding average result of comparing angular displacements around X_r axis (yaw angle) between the referenced camera system and the developed wearable sensor system.

Walking speed(m/s)	$RMS_{\theta y}$	$R_{\theta y}$	ROM(°)	e_{max}(°)
Slow (1.05±0.15)	2.4469	0.9321	30°	4.57
Preferred (1.40±0.15)	3.5379	0.8956	30°	6.21
Fast(1.90±0.25)	4.1135	0.8113	30°	9.53

Table 4-4 Gait velocity conditions (mean±SD) and corresponding average result of comparing angular displacements around Y_r axis (pitch angle) between the referenced camera system and the developed wearable sensor system.

Walking speed(m/s)	$RMS_{\theta y}$	$R_{\theta y}$	ROM(°)	e_{max}(°)
Slow (1.05±0.15)	3.0403	0.9619	40°	4.69
Preferred (1.40±0.15)	4.1278	0.9371	40°	5.91
Fast(1.90±0.25)	4.9031	0.9039	45°	8.87

When the subject performed the three walking trials at three different speeds, at the terminal swing of each stride, the limb began to actively decelerate, and the yaw and pitch angular displacement of the thigh gradually reached a maximum [(16)]. When the body moved forward continuously, the hip joint also moved forward. The rotational angular displacement of the thigh in the local frame decreased before the foot touched the floor. At the same time, the body weight was transferred to this limb, then the reaction force between the foot and the floor increased immediately, and subsequently the acceleration in the radial direction rose steeply. Therefore the difference between the experimental results and the results for the reference system was greater than in other phasic actions of the stride, and the e_{max} happened in this phase of a whole gait

generally, as shown in the circled parts in Fig.4-6 and Fig.4-7.

As the subjects were healthy young males and females with normal gait, the results should not be generalized to the case of patients, where systematic errors and measuring errors respectively due to axis misalignment and complexity of the case of patient gait are likely to be more significant. Therefore, more studies are necessary to determine reliability and validity in more diverse groups, especially in clinical populations. Further study is needed to identify the type and duration of activities.

4.5. Conclusion

The experiment result showes that the double-sensor difference based algorithm is feasible for ambulatory measurement of body segmental orientation in two directions of the segment fixed local coordinate system in 3D space in the gravitational field. It also suggest that using simple calculations without integration error and only using accelerometers, the rotational angles of a rotational rigid body or a human segment can be achieved. The original methodology and device presented here would be useful in the gait analysis field, since they provide simple, rapid and objective information to the researcher or clinician about the orientation of the lower limb segment in 3D space.

In addition, as the two accelerometers on the thigh were fixed on the same board, the difference between external disturbances acting on them was small, so the error in the calculated angular displacement was small (RMS 2.4 degrees to 4.9 degrees, Table 3 and 4). Therefore, it is feasible to integrate the two triaxial accelerometers on one micro-electronic chip to create a new model of sensor that can measure angular displacement of a body segment in tandem with another accelerometer on the rotational joint. it would be practicable to perform human gait analysis using only triaxial accelerometers in the course of the daily activities of patients requiring mobility evaluation.

References

(1) Findlow, A., Goulermas, J.Y., Nester, C., Howard, D., Kenney, L.P.J., 2008. Predicting lower limb joint kinematics using wearable motion sensors. Gait and Posture 28(1), 120-126.

(2) Favre, J., Jolles, B.M., Aissaoui, R., Aminian, K., 2008. Ambulatory measurement of 3D knee joint angle. Journal of Biomechanics 41(5), 1029-1035.

(3) Aminian K., C. Trevisan, B. Najafi, H. Dejnabadi, C. Frigo, E. Pavan, A. Telonio, F. Cerati, E. C. Marinoni, P. Robert, and P.-F. Leyvraz, 2004. Evaluation of an ambulatory system for gait analysis in hip osteoarthritis and after total hip replacement. Gait and Posture 20(1), 102-107.

(4) Ruth E. Mayagoitiaa, Anand V. Neneb, Peter H. Veltinkc, 2002. Accelerometer and rate gyroscope measurement of kinematics:an inexpensive alternative to optical motion analysis systems. Journal of Biomechanics 35(4), 537-542.

(5) Turcot, K., Aissaoui, R., Boivin, K., Pelletier, M., Hagemeister, N., De Guise, J.A., 2008. New accelerometric method to Discriminate between asymptomatic subjects and patients with medial knee osteoarthritis during 3-D gait. IEEE Transactions on Biomedical Engineering 55(4), 1415-1422.

(6) Kavanagh, J.J., Menz, H.B., 2008. Accelerometry: A technique for quantify movement patterns during walking. Gait and Posture 28(1), 1-15.

(7) Nyan, M.N., Tay, F.E.H., Seah, K.H.W., Sitoh, Y.Y., 2006. Classification of gait patterns in the time-frequency domain. Journal of Biomechanics 39(14), 2647-2656.

(8) Kun Liu, Tao Liu, Shibata, K., Inoue, Y., Rencheng Zheng, 2008. Novel approach for lower limb segment orientation in gait analysis using triaxial accelerometers. IEEE/ASME International Conference on Advanced Intelligent Mechatronics 2008, 488-492.

(9) Mehmet Engin, Alparslan Demirel, Erkan Zeki Engin, Musa Fedakar, 2005. Recent developments and trends in biomedical sensors. Measurement 37, 173–188.

(10) Daniel Roetenberg, Per J. Slycke, and Peter H., 2007. Ambulatory Position and Orientation Tracking Fusing Magnetic and Inertial Sensing. IEEE Transactions on Biomedical Engineering 54(3), 883-890.

(11) Hooman Dejnabadi, B. M. Jolles, and K. Aminian, 2005. A new approach to accurate measurement of uniaxial joint angles based on a combination of accelerometers and gyroscopes. IEEE Transactions on Biomedical Engineering 52(8), 1478-1484.

(12) Karol J. O'Donovan, Roman Kamnik, Derek T. O'Keeffe, Gerard M. Lyons, 2007. An inertial and magnetic sensor based technique for joint angle measurement. Journal of Biomechanics 40(12), 2604-2611.

(13) Bogert van den, A. J., Read, L., & Nigg, B. M., 1996. A method for inverse dynamic analysis using accelerometery. Journal of Biomechanics 29(7), 949-954.

(14) Nicola Hagemeister, Gerald Parent, Maxime Van de Putte, 2005. A reproducible method for studying three-dimensional knee kinematics. Journal of Biomechanics 38(9), 1926-1931.

(15) Vladimir M. Zatsiorsky, 1998. Kinematics of human motion, 90-103

(16) Jessica Rose, James G. Gamble, 2006. Human Walking. by LIPPINCOTT WILLIAMS & WILKINS 3rd Edition, 111-114.

.

Chapter 5

Estimation of Lower Limb Gait Posture using Accelerometers and Gyroscopes

5.1 Introduction

Ambulatory assessment of gait posture is a promising clinical tool to diagnose walking disabilities. Especially the three-dimensional (3D) quantitative information for the lower limb gait posture is essential for the clinical evaluation and therapeutic treatment comparisons in the orthopedic and rehabilitation fields [(1)]. Common methods for gait posture analysis include using cameras to track the position of body-mounted reflective markers, from which the motion information on hip and knee joints and lower limb segments can be derived, and then the lower limb posture can be estimated. Posture and motion estimation using video or image data to extract parameters of human body model are actively studied [(2) (3)], and human joint motion for sports and medical purposes are discussed [(4)].

However, since the camera-based system is space-consuming, expensive and complex, it restricts the user to the constrained environment where the cameras are installed and therefore not applicable for the out-lab ambulatory measurement of under limb posture in the ordinary life. Recently, small inertial sensors combining accelerometers, gyroscopes and magnetometers were developed and appeared to be promising for measuring human movement. Various alternative methods using inertial sensors were available for assessing 3D gait posture [(5) (6)]. And many ambulatory systems for various clinical applications have been developed to monitor physical activities [(7-9)], for example, ambulatory systems for the quantitative and qualitative analysis of gait and posture in chronic pain patients treated [(10)] or for the joint angle measurement [(11)].

A method to estimate the hip and knee joint angles and positions for the 3D lower limb posture using the gravitational acceleration along the anterior axis of the segment was proposed [(12)], however, the result was insensitive to the complex geomagnetic

field distortions, and the application was limited to movement such as walking, running, or ascent and descent of stairs. Another method for gait posture estimation using wearable acceleration and gyro sensors was present [13], the result showed that it was better for qualitative analysis than quantitative analysis, but the work conducted experiments at fairly low velocity (88 steps/min). Dejnabadi et al. [14] proposed a method to estimate sagittal kinematics of lower limbs orientation using body-fixed physical and virtual sensors, but there was no detailed application for the lower limb posture analysis. In addition, the physical sensors were attached on the frontal side of the thigh and shank, which resulted to a complicated algorithm to calculate the knee joint FE angles.

Therefore, there is a need for a system that should be accurate, ambulatory, and easy to use in routine practice, and could visually and quantitatively confirm the lower limb posture. The aim of our work is to propose a practical approach and develop an ambulatory system to analyze lower limb gait posture under normal life conditions, without using gravitational acceleration and integration of angular velocity. The posture detection allows the assessment of the hip joint and the knee joint kinematics, the joint angles, positions and other temporal gait parameters (i.e. swing and stance).

In the former chapters, novel approach to ambulatory assessment of lower limb segmental orientation on a wearable sensor system [15], in which only one kind of sensor (accelerometer) was used and only arithmetic was adopted without integration. However, there was no further discussion for a gait posture analysis but only for the segmental orientation estimation. As a further research of former work, the accelerations and angular velocities exerted on the lower limb segments were used to estimate the hip and knee joint angles, and the knee joint and ankle joint positions. The hip joint angles for the thigh orientation were estimated using double-sensor difference based algorithm, and the knee joint rotational angle in the sagittal plane was calculated with virtual-sensor difference based algorithm, then the lower limb posture was shown in the 3D coordinate frame. In order to insure a reliable estimation of the lower limb posture, it was amused that the lower limb segments were rigid segments and the subjects walked in a straight forward way with very little trunk

sway, skin artifacts and no significant IE rotation of the thigh and shank.

5.2. Materials and methods

5.2.1 Virtual-sensor difference based algorithm for the calculation of knee joint angle

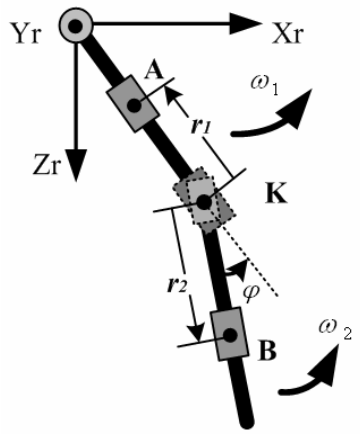

Fig.5-1 Virtual-sensor difference based method to calculate the knee joint angle in the sagittal plane. Two physical sensors were attached on the thigh and shank

Dejnabadi et al.[(14)] proposed a method to estimate sagittal kinematics of lower limbs orientation using body-fixed physical and virtual sensors, but there was no further application for the lower limb posture analysis. Besides, in their method, the physical sensors were attached on the frontal side of the thigh and shank, which resulted to a complicated algorithm to calculate the knee joint FE angles. In this section, we proposed a simplified algorithm by attaching the physical sensors on the lateral surface of the thigh and shank segments. The main strategy for analyzing the knee joint angle between femur and tibia in the sagittal plane is to split the knee joint motion into linear translational motion of the knee joint and the rotational angular motion of the two segments about the knee joint. As Fig.5-1 shows, physical sensors are fixed at position **A** and **B** on the two linked segments and two virtual sensors are implanted at point ***K***. The rotational acceleration at position ***A*** on the segment ***AK*** is

$$\ddot{\mathbf{r}}_1 = \dot{\boldsymbol{\omega}}_1 \times \mathbf{r}_1 + \boldsymbol{\omega}_1 \times (\boldsymbol{\omega}_1 \times \mathbf{r}_1) \tag{5-1}$$

and the acceleration $\mathbf{a_{k1}}$ at position ***K*** can be expressed using the following equation

$$\mathbf{a}_{K1} = \mathbf{a}_A + \ddot{\mathbf{r}}_1 = \mathbf{a}_A + \dot{\boldsymbol{\omega}}_1 \times \mathbf{r}_1 + \boldsymbol{\omega}_1 \times (\boldsymbol{\omega}_1 \times \mathbf{r}_1) \tag{5-2}$$

Then the acceleration $\mathbf{a_{k2}}$ at position **K** can be expressed as follow if it calculated

from the accelerations on the segment ***KB***.

$$\mathbf{a}_{\mathrm{K2}} = \mathbf{a}_{\mathrm{B}} + \ddot{\mathbf{r}}_2 = \mathbf{a}_{\mathrm{B}} + \dot{\boldsymbol{\omega}}_2 \times \mathbf{r}_2 + \boldsymbol{\omega}_2 \times \left(\boldsymbol{\omega}_2 \times \mathbf{r}_2\right) \tag{5-3}$$

where $\mathbf{a_A}$ and $\mathbf{a_B}$ are the measured accelerations by the physical sensors at position ***A*** and ***B***, $\mathbf{a_{k1}}$ and $\mathbf{a_{k2}}$ represent the accelerations measured by the two virtual sensors at position ***K***.

The FE angle of the knee joint in the sagittal plane can be measured by the angle φ between the femur and tibia (i.e., the rotational angle φ between the two virtual sensors). Since one point should physically have a unique acceleration, the two virtual sensors on the knee joint must have equal accelerations in the same coordinate frame. Then the correction for coordinate frames rotation by angle φ should be considered and the relationship between the accelerations of the two virtual sensors in the sagittal plane is:

$$\mathbf{a}_{\mathrm{K1}} = \mathbf{R}_{\varphi}\mathbf{a}_{\mathrm{K2}} \tag{5-4}$$

where $\mathbf{R}_{\varphi}$ is the rotation matrix. In the sagittal plane, the equation can be simplified,

$$\begin{bmatrix} a_{x_A} - r_1\omega_1^2 \\ a_{y_A} + r_1\dot{\omega}_1 \end{bmatrix} = R_{\varphi}\begin{bmatrix} a_{x_B} - r_2\omega_2^2 \\ a_{y_B} + r_2\dot{\omega}_2 \end{bmatrix} \tag{5-5}$$

and the rotational angle can be expressed as follow

$$\varphi = \tan^{-1}\left(\frac{a_{x_{K2}}}{a_{y_{K2}}}\right) - \tan^{-1}\left(\frac{a_{x_{K1}}}{a_{y_{K1}}}\right) = \tan^{-1}\left(\frac{a_{y_B} + r_2\dot{\omega}_2}{a_{x_B} - r_2\omega_2^2}\right) - \tan^{-1}\left(\frac{a_{y_A} + r_1\dot{\omega}_1}{a_{x_A} - r_1\omega_1^2}\right) \tag{5-6}$$

5.2.2 Gait posture analysis of the lower limb

In this part, to estimate the lower limb posture in the local coordinate system using the presented methods, a system is structured as Fig.5-2 shows. To calculate the hip joint flexion-extension and AA angles and the knee joint trajectory using the double physical-sensor difference based algorithm, three physical sensors are in a group to measure accelerations and angular velocities. A physical sensor is fixed on the hip joint without rotation but translation only, and another two physical sensors with each corresponding axes in the same direction are attached on the thigh. Then to calculate the knee joint angle in sagittal plane and the ankle joint trajectory using the

virtual-sensor difference based algorithm, two physical sensors are in a group to measure accelerations and angular velocities, which are attached near the knee joint on the thigh and shank. Table 5-1 shows the detailed terms used in the equations.

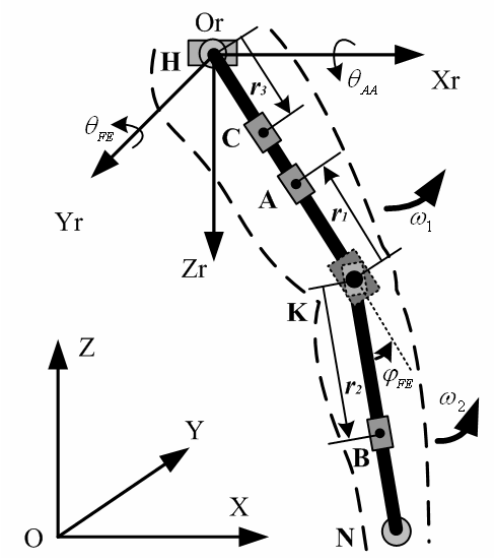

Fig.5-2 Lower limb model with sensors to estimate the joint rotations and positions

Table 5-1 List of the terms used in Fig.5-2

Terms	Description
O-ZYZ	Global coordinate system
O_r-$Z_rY_rZ_r$	Local coordinate system on the hip joint for the orientations of the lower limb segments (joint rotations) and the trajectories of the lower limb joints (joint positions)
θ_{AA}	Abduction/adduction angle of the thigh in the local coordinate system
θ_{FE}	Flexion-extension angle of the thigh in the local coordinate system
φ_{FE}	Flexion-extension angle of the knee joint in the sagittal plane
r_3	Distance from hip joint to the physical sensor C on the thigh
r_1	Distance from the virtual sensor in the knee joint to the physical sensor A on the thigh
r_2	Distance from the virtual sensor in the knee joint to the physical sensor B on the shank

Then, to visually confirm the posture of the lower limb during walking, the positions of the hip joint, knee joint and ankle joint in the local coordinate system *Or-XrYrZr* are calculated using the hip and knee joint angles and the segment lengths. The origin of the local coordinate system *Or(0,0,0)* was at the hip joint, then the coordinates for estimating the motions of knee and ankle joints were obtained with the following equations [12].

$$\mathbf{H}(x,y,z) = \begin{pmatrix} 0 & 0 & 0 \end{pmatrix} \tag{5-7}$$

$$\mathbf{K}(x,y,z) = \left(\mathbf{R}_{\theta_{AA}} \mathbf{R}_{\theta_{FE}} \begin{pmatrix} 0 \\ 0 \\ L_{thigh} \end{pmatrix} \right)^{\mathrm{T}} \tag{5-8}$$

$$\mathbf{N}(x,y,z)=\left(\mathbf{R}_{\theta_{\mathrm{AA}}}\mathbf{R}_{\theta_{\mathrm{FE}}}\begin{pmatrix}0\\0\\L_{thigh}\end{pmatrix}\right)^{\mathrm{T}}+\left(\mathbf{R}_{\theta_{AA}}\mathbf{R}_{\theta_{FE}}\mathbf{R}_{\varphi_{FE}}\begin{pmatrix}0\\0\\L_{shank}\end{pmatrix}\right)^{\mathrm{T}} \tag{5-9}$$

where L_{thigh} is the distance between the hip and knee joints, L_{shank} is the distance between the knee and ankle joints, $\mathbf{R}_{\theta_{AA}}$, $\mathbf{R}_{\theta_{FE}}$ and $\mathbf{R}_{\varphi_{FE}}$ are rotation matrices

5.3 Experiment using the developed wearable sensor system

In order to evaluate the presented approach, a wearable sensor system was developed. The system was mainly comprised out of one piece of MCU (H8/3694, from Renesas Technology Corp.), one triaxial accelerometer-based chip (MM-2860), and three analog inertial sensors named MAG^3 (MEMSense, MAG10-1200S050) which could provide triaxial analog outputs of acceleration, rate of turn and magnetic field data. Fig.5-3 shows the procedure of the experiment, and Fig.5-4 gives the configuration of the developed wearable sensor system. The two MAG^{3}s are integrated on a piece of electric circuit board and fixed on the thigh with corresponding axes in the same direction and a distance of 60mm between each other. A third MAG^3 is attached on the shank. To prevent the skin motion artifact from adding noise to the measured accelerations and angular velocities, the sensors on the thigh and shank were fixed on one of the two step slides of a stainless steel telescopic slide rails. The length of the slide rail can be adjusted according to the length of the thigh or shank of different subjects. To prevent gravity being erroneously recorded as acceleration in the horizontal plane and ensure the measured accelerations coincided with the directions of idealized translational accelerations, the MM-2860 was fixed on a flat aluminum sheet, and then was attached on the hip joint. During the initial calibration, the aluminum sheet with the accelerometer was optimally adjusted to coincide with the sagittal plane of the thigh and the z axis of the accelerometer was upright. To ensure the thigh only perform FE and AA rotations without IE rotation as supposed in the method, the slide rail and the flat aluminum sheet were connected with an universal joint. And the slide rails on the thigh and shank were connected by a bearing to make sure only FE rotation in the knee joint. The slide rails were attached

on the lateral surface of the lower limb with elastic straps, coincided with the lines which connected the hip joint and knee joint, the knee joint and ankle joint. The recorded accelerations and angular velocities about y-axis indicated anterior-posterior motion, about x-axis indicated lateral motion, and about z-axis indicated vertical motion in the sensor coordination system on the thigh and shank.

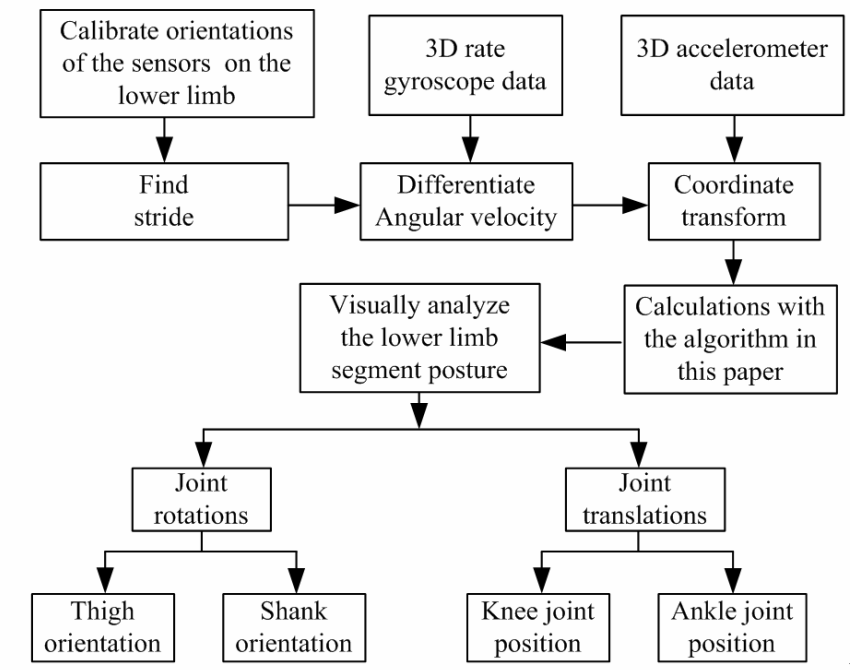

Fig.5-3 Schematic representation of the algorithm for deriving 3D thigh and shank orientations and the knee joint and ankle joint translations during gait on the basis of 3D inertial sensor signals.

In the experiment, five subjects (4 males, 1 females, Age: 25±3 years, Height: 170±5cm, mass: 60±11kg) with no history of musculoskeletal pathology and injury were requested to perform 3 straight-line walking trials at self-selected walking speeds in each trial. Four groups of accelerations were simultaneously obtained from the wearable sensor system and a commercial optical motion analysis system, NAC Hi-Dcam II Digital High Speed Camera Systems (NAC image technology. Japan). The sampling frequency of the camera system is 100 Hz, and the average calibration error was 0.014% for capturing stationary subject and 0.21% for capturing dynamic subject.

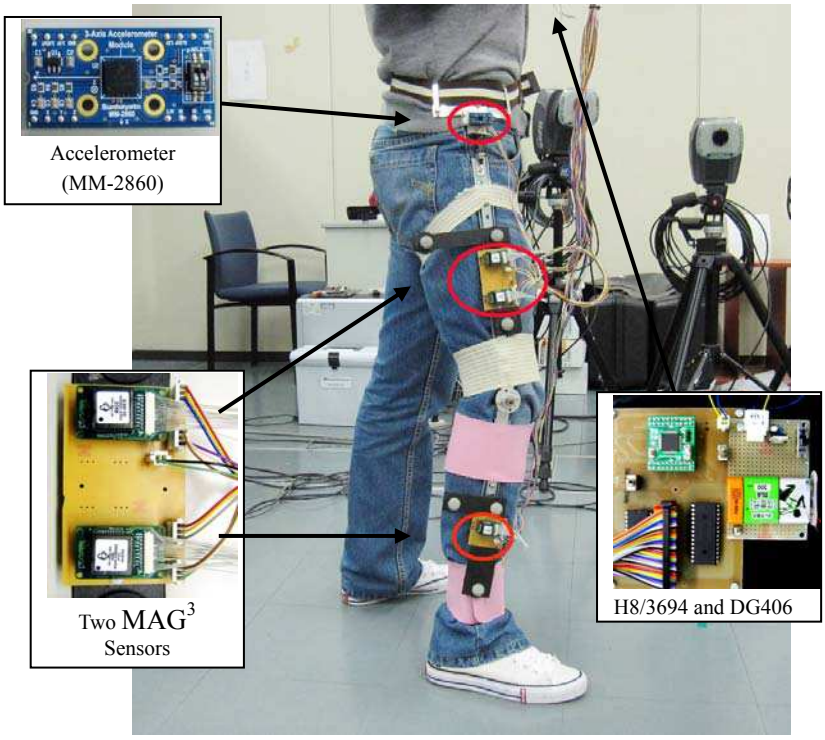

Fig.5-4 Experiment with the wearable sensor system in the working space of the optical motion system

5.4 Results

All the readings of the sensors were recorded in the MCU real time and sent to PC off-line after each test, and the signals captured in the experiment were off-line processed. The sampling frequency was 100 Hz and the A/D had a 12-bit resolution. The calculated rotation angles of the hip and knee joints were compared with the reference angles obtained from the camera system. Fig.5-5 shows the compared result of the estimation for the FE and the AA angles of the hip joint, the FE angle of the knee joint in three trials by three subjects at self-selected speeds, and the analysis result is shown in Table 5-2. Fig.5-6 shows trajectories of the knee and ankle joint in 3D coordination systems. Fig. 5-7 gives the continuous stick figures of the lower limb in one gait circle for visual confirmation of the human gait posture.

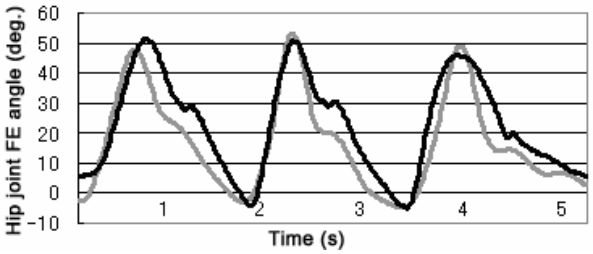

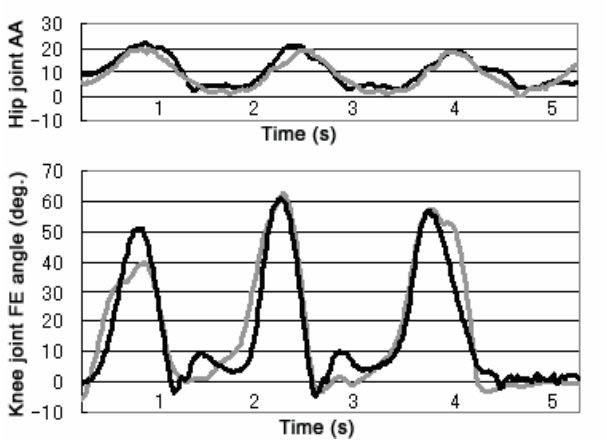

a, Subject 1

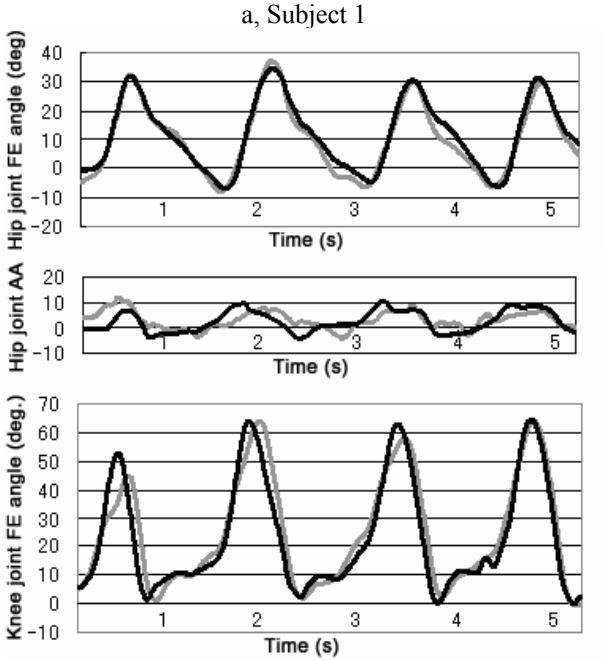

b, Subject 2

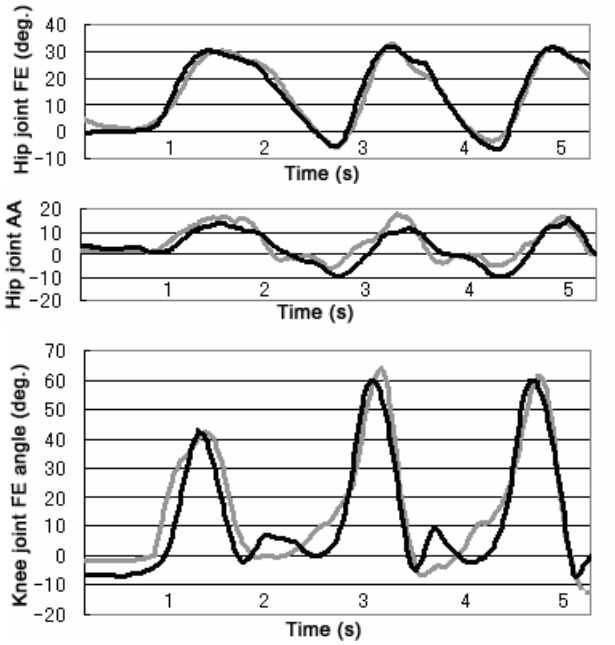

c, Subject 3

Fig.5-5. The FE and AA angles of the hip joint and the FE angle of the knee joint in three trials by three

different subjects at self-selected speeds. The dark black line was the referenced angle measured by the camera system and the light gray line was the calculated angle using measured signals measured by the developed wearable system

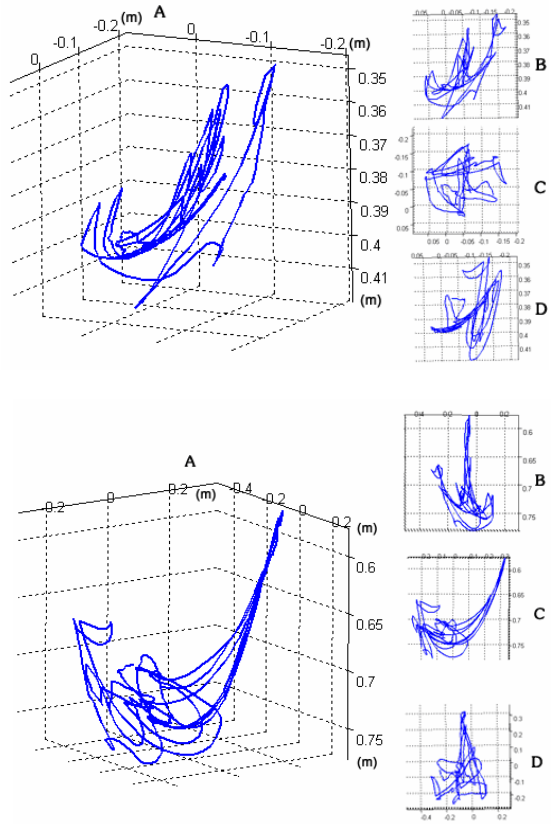

Fig.5-6 To visually estimate the lower limb gait posture using the data obtained by the developed wearable system, the calculated trajectories of the knee and ankle joints in the 3D local coordinate system (*Or-XrYrZr*) were showed on the left side marked as **A** in each picture. On the right side, the three smaller pictures marked as **B**, **C** and **D** were the detail information of the joint trajectory in the sagittal, transverse and frontal plane.

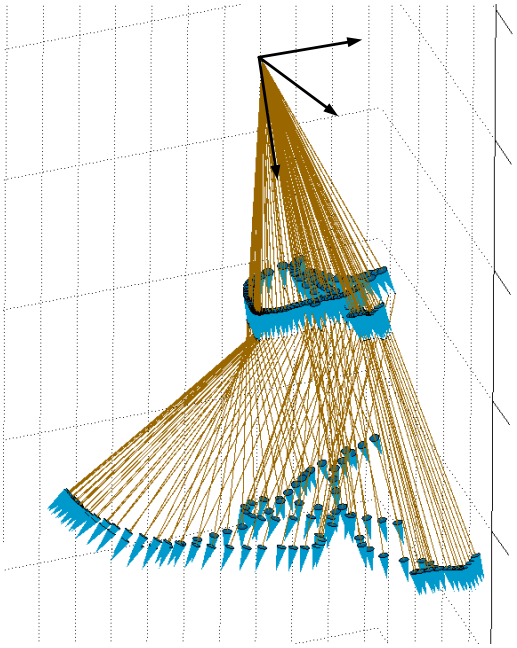

Fig.5-7 One gait circle shown by continuous stick figures to estimate the human gait posture. The blue arrows represent the knee joint and ankle joint.

Table 5-2 Analysis result of the rotation angles of the hip and knee joints which were obtained from the referenced system and the wearable sensor system. The value of each parameter is an average of three trials when each subject walked at three self-selected speeds. At the bottom of the table, the overall average of each parameter in five trials was given.

Subject	hip joint FE angle			hip joint AA angle			knee joint FE angle		
	$RMS_{\theta FE}$	$R_{\theta FE}$	e_{max}	$RMS_{\theta FE}$	$R_{\theta FE}$	e_{max}	$RMS_{\theta FE}$	$R_{\theta FE}$	e_{max}
1	4.01	0.93	6.13	3.51	0.94	4.51	5.32	0.93	10.57
2	3.28	0.94	6.53	3.78	0.95	3.94	4.31	0.95	6.21
3	3.64	0.95	5.77	4.34	0.92	5.43	5.89	0.91	8.53
4	5.33	0.89	10.12	4.93	0.9	6.75	6.69	0.88	10.42
5	4.15	0.92	7.84	4.75	0.93	5.72	4.25	0.92	7.73
Average	4.08	0.93	7.28	4.19	0.93	5.27	5.29	0.92	8.69

5.5 Discussion

Since the trajectories of the knee and ankle joints were calculated from the three joint angles, the analysis result of the joint trajectories were not shown here but only the analysis result of the joint angles. From the analysis result shown in Table 5-2, the presented method showed a strong correlation with the camera system data and involved significantly less calculation than reported in the Ref. (13). One limitation was the assumption of no rotation of the trunk but only straight forward translation in the walking direction, therefore, the method introduced here can be based on the assumption that the accelerations measured on the hip joint only included translational and gravitational accelerations without rotational accelerations. The method was suitable for various velocities of walking in the sagittal plane, no matter whether the anterior/posterior acceleration of the trunk increased or not. It was an improvement of the method in the Ref. (12), which neglected any anterior/posterior accelerations and only conducted experiments at fairly low velocity (88 steps/min). Maybe that was why the result in this paper was better than that Takeda et al. presented.

In addition, since there must be skin motion artifact due to impact loading and muscle activation, the attachment of any kind of wearable sensor on the lower limb segments could induce error. Especially during the swing phase and at the time the foot contacted the floor when the volunteer was walking at a high speed, the sensors on the slide rails must have relative motion with the thigh and shank, which would contaminate the measured accelerations and angular velocities, thus reduced error to the calculated result.

Besides, the increase of non-translational acceleration of the trunk along with the increase of the walking speed also contaminated the accelerations measured by the accelerometer on the hip. Furthermore, in the initial calibration, since the accelerometer on the hip cannot be placed exactly in the upright, forward and outward directions as assumed, the gravitational acceleration also contaminated the measured accelerations about each axis. Therefore the measured acceleration of the hip joint, assumed as translational acceleration only and used for the calculation in the algorithm, must induce error to the result.

To control these problems, rigorous initial calibration process and predefined motions were conducted in each trial. After the sensor system worn on the lower limb, all the sensors were aligned upright in the sagittal plane. Although with the limitations detailed here, the work here shows that the wearable sensor system can provide quantitative analysis of the lower limb gait posture with high accuracy, which was expressed by joint angles for lower limb segment orientations and joint trajectories for lower limb joint positions. To provide more detail information for the gait posture analysis, further research is under working to develop a method for calculating the IE rotation of the hip joints and more rotations of the knee joint.

5.6 Conclusion

The combination of physical-sensor difference based algorithm and virtual-sensor difference based algorithm was original and created for the analysis of lower limb posture. There was no integration of angular acceleration or angular velocity in the method. The developed wearable sensor system was suitable for estimating the absolute hip joint FE and AA angles and knee joint FE angle in the local coordinate system, and the joint trajectories for the 3D lower limb posture analysis. It was reliable and convenient to do ambulatory, visual and quantitative estimation of lower limb gait, therefore it can be used as a substitute for the camera system to analyze gait posture of patients or health persons in the daily life. The method can be easily popularized to estimate the posture of other segments such as upper limb or mechanical arms.

References

(1) de Asla RJ, Kozanek M., Wan L., Rubash HE., Li G., Six DOF in vivo kinematics of the ankle joint complex: application of a combined dualorthogonal fluoroscopic and magnetic resonance imaging technique, *Journal of Orthopaedic Research*, Vol.24, No.5(2006), pp.1019–1027.

(2) Iwasawa, S., Ebihara, K., Ohya, J., Morishima, S., Real-Time Estimation of Human Body Posture from Monocular Thermal Images. *IEEE Computer Society Conference on Computer Vision and Pattern Recognition*, (1997), pp. 15-20.

(3) Takahashi, K., Sakaguchi, T., Ohya, J., Real-time estimation of human body postures using Kalman filter. *8th IEEE International Workshop on Robot and Human Interaction,* (1999), pp.189-194.

(4) Ahn Ryul Choi, Yong Hoon Rim, A position based kinematic method for the analysis of human gait, *Journal of Mechanical Science and Technology*, Vol.19, No.10 (2005), pp.1919-1931.

(5) Christine Azevedo, et al., Rehabilitation of Functional Posture and Walking-Coordination of Healthy and Impaired Limbs, *Journal of Automatic Control*, No.15(2005), pp. 11-14.

(6) Gallagher, A., Matsuoka, Y., Wei-Tech Ang, An efficient real-time human posture tracking algorithm using low-cost inertial and magnetic sensors, *International Conference on Intelligent Robots and Systems (IROS 04)*, (2004), pp. 2967-2972.

(7) Pages, G., Ramdani, N., Fraisse, P., Guiraud, D., Upper body posture estimation for standing function restoration, *IEEE International Conference on Robotics and Automation (ICRA 07)*, 2007, pp. 3742-3747.

(8) Plamondon A., Delisle A., Larue C., et al., Evaluation of a hybrid system for three-dimensional measurement of trunk posture in motion, *Applied Ergonomics*, Vol.38, No.6(2007), pp. 697-712.

(9) Salarian, A., Russmann, H., Wider, C. et al., Quantification of tremor and bradykinesia in Parkinson's disease using a novel ambulatory monitoring system. *IEEE Transactions on Biomedical Engineering*, Vol.54, No. 2(2007), pp. 313-322.

(10) Paraschiv-Ionescu A., Buchser E. E., Rutschmann B., Najafi B., Aminian K., Ambulatory system for the quantitative and qualitative analysis of gait and posture in chronic pain patients treated with spinal cord stimulation, *Gait & Posture*, Vol.20, No. 2(2004), pp. 113-125.

(11) Karol J. O'Donovan, Roman Kamnik, Derek T. O'Keeffe, Gerard M. Lyons, An inertial and magnetic sensor based technique for joint angle measurement, *Journal of Biomechanics*, Vol.40, No.12(2007), pp. 2604-2611.

(12) Takeda Ryo, Tadano Shigeru, Todoh Masahiro, Morikawa Manabu, Nakayasu Minoru, Yoshinari Satoshi, Gait posture estimation using wearable acceleration and gyro sensors, *Journal of Biomechanics*, Vol.42, No.15 (2009), pp.2486-2494.

(13) Takeda Ryo, Tadano Shigeru, Todoh Masahiro, Morikawa Manabu, Nakayasu Minoru, Yoshinari Satoshi, Gait analysis using gravitational acceleration measured by wearable sensors, *Journal of Biomechanics*, Vol.42, No.3 (2009), pp. 223-233.

(14) Dejnabadi H., Jolles B. M., and Aminian K., A new approach to accurate measurement of uniaxial joint angles based on a combination of accelerometers and gyroscopes, *IEEE Transactions on Biomedical Engineering*, Vol.52, No.8 (2005), pp. 1478-1484.

(15) Liu Kun, Liu Tao, Shibata Kyoko, Inoue Yoshio, Zheng Rencheng, Novel approach to ambulatory assessment of human segmental orientation on a wearable sensor system, *Journal of Biomechanics*, Vol.42, No.16 (2009), pp. 2747-2752.

Chapter 6

Visual and quantitative estimation of lower limb 3D gait posture using accelerometers and magnetometers

6.1 Introduction

Ambulatory estimation of lower limb posture is very important in the diagnosis of patients with stroke, Parkinson or knee osteoarthritis disease [(1) (2)], and useful to evaluate the rehabilitation of patients. Based on the kinematic and kinetic data of the lower limb, proper treatment for the patients can be chosen by the clinicians [(3)]. A complete understanding of joint kinematics is the key point for the lower limb posture analysis. In the lab, the typical system for gait analysis is the optical motion system for kinematic data combined with force platforms for kinetic data [(4)]. However, since the system is space-consuming and expensive, it is not applicable for the out-lab ambulatory estimation of lower limb posture in the daily life.

With the development of more and more advanced inertial sensors, many algorithms for calculating the parameters of human kinematics were put into practice, and more and more wearable sensor systems based on inertial sensors were developed for gait analysis and clinical application [(5) ~ (7)], kinematics data for gait analysis such as knee joint angles, thigh and shank orientations were obtained [(8) ~ (10)].

In the diagnosis of joint disorders resulting from injury or disease, in the quantitative assessment of treatment, and in the general study of locomotion, the 3D knee joint kinematics and the thigh and shank orientation are crucial. J. Faver et al. [(11) (12)] developed an ambulatory system to measure the 3D knee angles by filtering and integrating the gyroscope signals from the thigh and shank, the f/e and a/a rotational angles were obtained. However, the data derived by integration of angular acceleration or angular velocity was distorted by offset and angle drift, and a proper calibration was not given. H. Dejnabadi et al. [(4) (15)] gave a new approach to estimate sagittal kinematics of lower limbs without accumulation of errors. Virtual accelerometers were fixed in the knee joint center and ankle to measure the joint

rotational angles using external skin-mounted accelerometer and gyroscope, but only the f/e joint angle in the sagittal plane was estimated. K. O'Donovan [13] presented a technique which used a combination of rate gyroscope, accelerometer and magnetometer to measure 3D inter-segment joint angles, but the investigation of the performance of the technique was limited to a static system, and there was no evaluation for dynamic system. R. Takeda [14] proposed a novel method for measuring human gait posture using tri-axial accelerometers and gyroscopes, in which the optimization algorithm used for estimating gravitational acceleration gave an optimal lower limb gait posture. However, since the algorithm involved searching for large number of combinations, it was not suitable for small computing devices.

In the previous chapters, the method was only evaluated in a restrained condition that the lower limb segments were assumed to be rigid segments and the subjects walked in a straight forward way with very little trunk sway, skin artifacts and no significant i/e rotation of the leg, thus not a true 3D analysis of the joint kinematics. For a further application of the double-sensor difference based algorithm to estimate 3D lower limb joint kinematics in anatomical coordinate system, in this chapter, an original approach based on accelerometers and magnetometers for ambulatory estimation and analysis of 3D knee joint kinematics was presented. The f/e angle, a/a angles and i/e rotation angles in the anatomical joint coordinate system were estimated. A wearable sensor system composed of two MAG^{3}s (inertial measurement unit composed out of an accelerometer, a magnetometers and a gyroscope) and two MM2860s (accelerometer) was developed, and then tested on the lower limb. Then, the method was used to visually and quantitatively confirm the 3D lower limb posture in the geomagnetic field. The hip joint angles were estimated using a physical-sensor difference based algorithm, and the knee joint angles were calculated using a virtual-sensor difference based algorithm, and then the stick figures for visual confirmation of the 3D human gait posture were shown.

6.2 Method

6.2.1 Estimation of the hip joint angles using physical-sensor difference based

algorithm

Since the acceleration measured on a body segment comprises gravitational acceleration, translational acceleration and rotational acceleration, the signal can not be separated and a resultant signal is composed of the three components. When two accelerometers are attached at two different positions with each corresponding axis in the same direction, the gravitational acceleration, translational acceleration, skin motion artifact and other noise acting on the two sensors should be the same except the rotational acceleration. To exploit the difference between the rotational accelerations, a physical-sensor difference based algorithm to estimate the joint rotation angles for the segmental orientation in 3D space was developed.

As Fig. 6-1 shows, there are two accelerometers on a board. The equivalent acceleration measured by the accelerometer including the gravitational component is shown by

$$\mathbf{a}_{ij} = \mathbf{g} - \ddot{\mathbf{R}}_{i0} - \mathbf{r}_{ij}\dot{\boldsymbol{\omega}}_i - \mathbf{r}_{ij}\boldsymbol{\omega}_i \times \boldsymbol{\omega}_i \tag{6-1}$$

where $\mathbf{a}_{ij}$ is equivalent acceleration at point P_{ij}, i is segment index, j is point index (j=0: origin of segment), $\mathbf{g}$ is gravitational acceleration, $\mathbf{R}_{ij}$ is the position of point P_{ij} relative to the global coordinate system (O-XYZ).

Then we can get

$$\mathbf{a}_{i0} = \mathbf{g} - \ddot{\mathbf{R}}_{i0} \tag{6-2}$$

$$\mathbf{a}_{i1} = \mathbf{g} - \ddot{\mathbf{R}}_{i0} - \mathbf{r}_{i1}\dot{\boldsymbol{\omega}}_i - \mathbf{r}_{i1}\boldsymbol{\omega}_i \times \boldsymbol{\omega}_i \tag{6-3}$$

$$\mathbf{a}_{i2} = \mathbf{g} - \ddot{\mathbf{R}}_{i0} - \mathbf{r}_{i2}\dot{\boldsymbol{\omega}}_i - \mathbf{r}_{i2}\boldsymbol{\omega}_i \times \boldsymbol{\omega}_i \tag{6-4}$$

At the two positions on the board where the two accelerometers are fixed, if the rotational radiuses about the origin O_r of the local coordination system (Or-$XrYrZr$) is measured as r_1 and r_2, the vector of acceleration at the rotation joint can be obtained from Eq.2-Eq.4 regarded as measuring by a virtual accelerometer,

$$\mathbf{a}_{i0} = \frac{\mathbf{r}_{i2}\mathbf{a}_{i1} - \mathbf{r}_{i1}\mathbf{a}_{i2}}{\mathbf{r}_{i2} - \mathbf{r}_{i1}} \tag{6-5}$$

Then, to obtain the joint rotation angles, an accelerometer was fixed on the hip with

the x and y axes in the sagittal plane of the thigh and z axis in upright direction as Fig.1 shows. Since one point should physically have the same acceleration at the same position, the acceleration measured by the accelerometer and the equivalent acceleration calculated by the physical-sensor difference algorithm should represent the same acceleration vector. The difference between the two accelerations represents the difference between the coordinate systems of the physical and virtual accelerometers. Only the FE angle θ_{FE} and AA angle θ_{AA} about the *Yr*, *Xr* axes in the local frame (*Or-XrYrZr*) is considered here, the two angles can be calculated as the Eqs. (6-6) and (6-7) show, which are used to describe the orientation of the thigh in the local coordinate frame and shown as follow.

$$\theta_{AA} = \sin^{-1}\left(\frac{r_B a_{Ay} - r_A a_{By}}{(r_B - r_A)\sqrt{A_{O_r y}{}^2 + A_{O_r z}{}^2}}\right) - \sin^{-1}\left(\frac{A_{O_r y}}{\sqrt{A_{O_r y}{}^2 + A_{O_r z}{}^2}}\right) \tag{6-6}$$

$$\theta_{FE} = \sin^{-1}\left(\frac{r_B a_{Ax} - r_A a_{Bx}}{(r_B - r_A)\sqrt{A_{O_r x}{}^2 + A_{O_r y}{}^2 + A_{O_r z}{}^2 - \left(\frac{r_B a_{Ay} - r_A a_{By}}{r_B - r_A}\right)}}\right) \tag{6-7}$$

Here ($A_{O_r x}$, $A_{O_r y}$, $A_{O_r z}$) is the measured acceleration of the local frame origin (hip joint) when the segment translates in the global frame, (a_{Ax}, a_{Ay}, a_{Az}) and (a_{Bx}, a_{By}, a_{Bz}) are the accelerations measured at positions **A** and **B**, r_A and r_B are the distances from the rotational joint to the positions **A** and **B** on the segment.

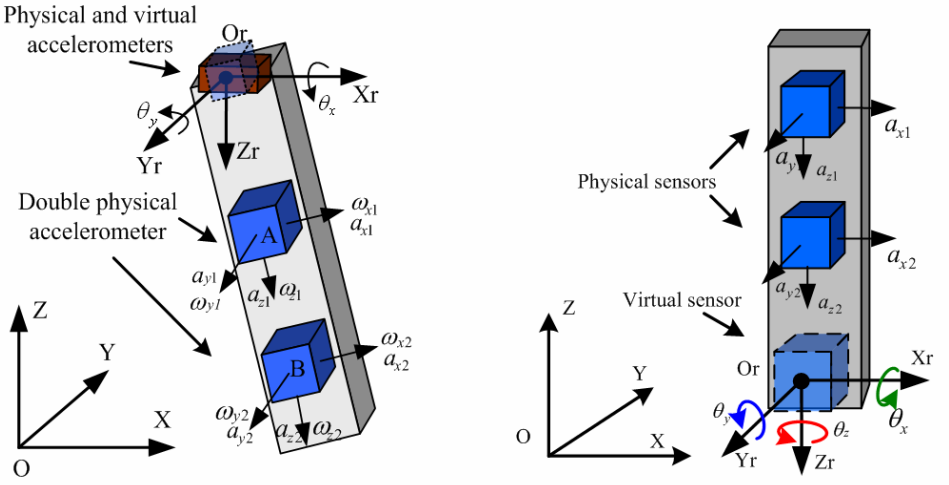

Fig. 6-1 Schematic diagram for the double-sensor difference based algorithm to calculate the orientation angles of a segment in the local coordinate system

6.2.2 Calculation of the knee joint angles using the virtual-sensor difference based algorithm

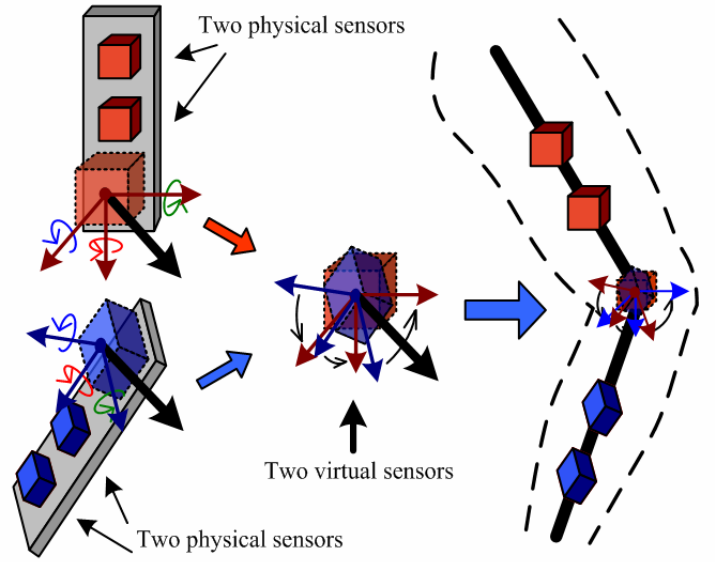

Fig. 6-2 Virtual-sensor difference based method to calculate the knee joint angles in 3D space. Two groups of physical sensors (in blue and red) were attached on the thigh and shank

Dejnabadi et al. proposed a method to estimate sagittal kinematics of lower limbs orientation using body-fixed physical and virtual sensors [(4)], but it was a 2D analysis and there was no further application for the lower limb posture analysis. In this section, we proposed an algorithm based on the diffe250

rence between two virtual sensors to estimate the knee joint kinematics.

At the knee joint, there are three rotational angles in three directions: the FE angle, AA angle and IE rotation angle. To analyze the knee joint rotation angles, an algorithm based on the difference between double virtual sensors in the knee joint, named virtual-sensor difference based algorithm, was present here. As the left picture in Fig. 6-2 shows, the lower limb segments, the thigh and shank, are supposed to be rigid segments. Two physical sensors and a virtual sensor in red are fixed on the upper segment (thigh), and another two physical sensors and a virtual sensor in blue are attached on the lower segment (shank). The corresponding axes of the physical sensors and the virtual sensor in the same group are in the same direction. Then the accelerations of the two virtual sensors can be calculated from the accelerations

measured by both physical sensors in each group respectively using the physical-sensor difference based algorithm.

As we know, when a multi-segment rigid body connected with a three degree of freedom (DOF) ball and socket joint is moving in space, one point should physically have a unique acceleration. Therefore, the two virtual sensors in the knee joint must have equal accelerations in the same coordinate frame. The two virtual sensors attached in different orientations would measure two groups of accelerations. The difference between the acceleration vectors represents the difference of orientations between the two segments which can illustrate the rotation angles of the knee joint. The relationship of accelerations measured by the two virtual sensors is:

$$\mathbf{A_t} = \mathbf{R}\mathbf{A_s} \tag{6-8}$$

where $\mathbf{R}$ is the rotation matrix between the two virtual sensors, which is also between the thigh and shank. It can be expressed with the FE angle φ_{FE}, AA angle φ_{AA} and IE rotation angle φ_{IE} as follow,

$$\mathbf{R} = \mathbf{R}_{\theta_z}\mathbf{R}_{\theta_x}\mathbf{R}_{\theta_y} = \begin{bmatrix} \cos\varphi_{IE} & \sin\varphi_{IE} & 0 \\ -\sin\varphi_{IE} & \cos\varphi_{IE} & 0 \\ 0 & 0 & 1 \end{bmatrix}\begin{bmatrix} 1 & 0 & 0 \\ 0 & \cos\varphi_{AA} & \sin\varphi_{AA} \\ 0 & -\sin\varphi_{AA} & \cos\varphi_{AA} \end{bmatrix}\begin{bmatrix} \cos\varphi_{FE} & 0 & -\sin\varphi_{FE} \\ 0 & 1 & 0 \\ \sin\varphi_{FE} & 0 & \cos\varphi_{FE} \end{bmatrix} \tag{6-9}$$

To calculate the joint angles, another two magnetometers are used to measure the magnetic field data attached on the thigh and shank, with the corresponding axes in the same directions as those of the accelerometers on the thigh and shank respectively. In the same way as where calculating the navigation angles from accelerations using the virtual accelerometers in the knee joint, two virtual magnetometers attached with different orientations in the knee joint should physically have unique magnetic field data. The difference between the vectors of magnetic field data represents the difference of orientations between the two magnetometers, which also illustrate the knee joint angles. The relationship of the measured magnetic field data is:

$$\mathbf{M_t} = \mathbf{R}\mathbf{M_s} \tag{6-10}$$

Based on physical-sensor difference based algorithm and virtual-sensor difference based algorithm, the knee joint angles can be calculated from Eqs. (6-8)~ (6-10).

6.2.3 Definition of anatomical coordinate system for lower limb motion analysis

As introduced in Chapter 2, a ball and socket joint permits rotations in three angular directions and translations in three directions. To explain the joint rotation and translation, a joint coordinate system based on segment-fixed coordinate systems was given as shown in Fig.6-3.

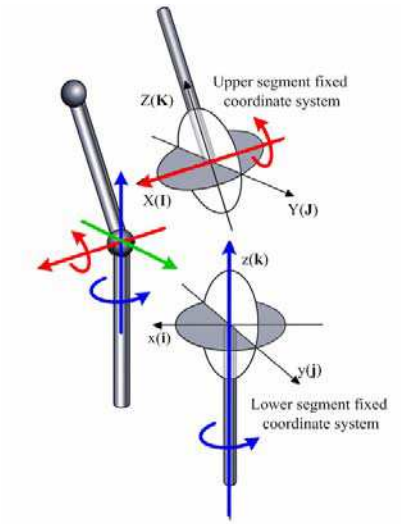

Fig.6-3 Cartesian coordinate system were defined in each rigid body segment. Capitalized letters *X,Y,Z* denoted the upper segment axes with **I, J, K** as the respective base vectors, while lower case letters *x,y,z* denoted the lower segment system axes with **i, j, k** as their respective base vectors. For both segments, the z axis was positive to the upward, the y axis was positive anteriorly, and the x axis is positive to the right.

Then the coordinate system was applies to the hip joint and knee joint to define the hip joint and knee joint coordinate systems for the lower limb posture analysis.

The key stone to ambulatory analysis the lower limb posture was to obtain the rotations and translations of both hip joint and knee joint. The rotation angles of the hip joint included the flexion-extension angle, abduction-adduction angle, and femoral inernal-external rotation angle, which were used to indicate the orientation of the thigh in the anterior- posterior and medial- lateral directions, and the rotation of the thigh about the femur-fixed longitude axis. The translations of the hip joint include medial-lateral, proximal-distal and anterior-posterior translations which were used to indicate the position of the lower limb in the global coordinate system. Correspondingly, the rotation of the knee joint were also comprised of the flexion-extension angle, abduction-adduction angle, and tibia inernal-external rotation angle, which were used to indicate the relative positions of the thigh and shank in

three directions, and to explicate the posture of the lower limb. The translations of the knee joint in the three directions were used to indicate the knee joint position in the global coordinate system.

To analysis the joint kinematics, coordinate system for the joints must be constructed. The anatomical landmarks on the bones, lower limb segments fixed coordinate systems and anatomical joint coordinate system for the knee joint kinematic analysis are defined in Fig.6-4 and indicated in Table 6-1~Table 6-3.

1, first, a Cartesian coordinate system (CCS) is established for each of the two adjacent body segments. The axes in these CCSs are defined based on bony landmarks, and follow the ISB general recommendations [22]. The common origin of both axis systems is the point of reference for the linear translation occurring in the joint, at its initial neutral position.

2, secondly, the JCS is established based on the two adjacent CCSs. Two of the JCS axes are body fixed, and one is ‘‘floating’’. Capitalized letters *X,Y,Z* was used to denote the femoral Cartesian coordinate system axes with **I, J, K** as the respective base vector, and lower case letters *x,y,z* was used with **i, j, k** as their respective base vectors for the tibial Cartesian coordinate system.

3, lastly, the joint motion, including three rotational and three translational components, is defined based on the JCS.

One clinical motion of interest was the internal-external rotation of the tibia about its mechanical axis which passes the midway between the two intercondylar eminences proximally and through the centre of the ankle distally, and was lablled as the ***z*** axis. Then the **j** direction was taken oriented anteriorly in the sagittal plane of the tibia and was identified as the tibial ***y*** axis. In the femur, the body fixed axis was chosen so that rotations about it correspond to the clinical motion of flexion-extension The relative joint rotations between the bones are shown in the Fig, 6-4. Flexion-extension occurs about the femoral fixed axis, abduction-adduction motion occurs about the floating axis, and the tibial inernal-external rotation is about the tibial fixed axis,

Table 6-1 Anatomical landmarks on the bones

HCR	hip center of rotation

SIS	anterior superior iliac spine
PSIS	posterior superior iliac spine
MFE	medial femoral epicondyle
LFE	lateral femoral epicondyle
MM	Tip of the medial malleolus
LM	Tip of the lateral malleolus
MTC	The most medial point on the border of the medial tibial condyle
LTC	The most lateral point on the border of the lateral tibial condyle
IM	The inter-malleolar point located midway between MM and LM
IC	The inter-condylar point located midway between the MC and LC

Table 6-2 Lower limb segment fixed coordinate system.

Pelvic coordinate system ($O\text{-}X_pY_pZ_p$)	
Origin	The origin coincident with the hip center of rotation
X_p axis	The line parallel to a line connecting the right and left ASISs, and pointing to the right.
Y_p axis	The line parallel to a line lying in the plane defined by the two ASISs and the midpoint of the two PSISs, orthogonal to the X-axis, and pointing anteriorly.
Z_p axis	The line perpendicular to both X and Z, pointing cranially
Femur fixed coordinate system ($O\text{-}X_fY_fZ_f$)	
Origin	The origin coincident with the right (or left) hip center of rotation, coincident with that of the pelvic coordinate system (O) in the neutral configuration.
Z_f axis	The line joining the midpoint between the MFE and LFE and the origin, and pointing cranially
X_f axis	The line perpendicular to the z-axis, lying in the plane defined by the origin and the two FEs, pointing to the right
Y_f axis	The line perpendicular to both x- and z-axis, pointing anteriorly
Tibia/fibula coordinate system ($O\text{-}X_tY_tZ_t$)	
Origin	The origin coincident with IM
Z_t axis	The line connecting IM and IC, and pointing cranially
X_t axis	The line perpendicular to Z axis in the frontal plane of the tibia/fibula (the plane containing points IM, MC and LC), and pointing to the right
Y_t axis	The common line perpendicular to X and Z axis

Table 6-3 Joint coordinate system for the hip joint and knee joint

Hip joint coordinate system		
$\mathbf{e_{h1}}$	Rotation (α):	The axis fixed to the pelvis and coincident with the X_p-axis of the pelvic coordinate system
	Displacement (q_1):	flexion or extension. medial-lateral translation.
$\mathbf{e_{h3}}$	Rotation (γ):	The axis fixed to the femur and coincident with the Z_f-axis of the right (or left) femur coordinate system
	Displacement (q_3):	internal or external rotation. proximo-distal translation.
$\mathbf{e_{h2}}$	Rotation (β):	The floating axis, the common axis perpendicular to $\mathbf{e_{h1}}$ and $\mathbf{e_{h3}}$.
	Displacement (q_2):	adduction or abduction. antero-posterior translation.
Knee joint coordinate system		
$\mathbf{e_{k1}}$	Rotation (a):	The axis fixed to the femur and coincident with the X_f-axis of the femoral coordinate syste
	Displacement (q1):	flexion or extension medial-lateral translation
$\mathbf{e_{k3}}$	Rotation (g):	The axis fixed to the tibia and coincident with the Z_t-axis of the right (or

	Displacement (q3):	left) tibia/fibula coordinate system. internal or external rotation. proximo-distal translation.
$\mathbf{e_{k2}}$	Rotation (b): Displacement (q2):	The floating axis, the common axis perpendicular to $\mathbf{e_{k1}}$ and $\mathbf{e_{k3}}$. adduction or abduction antero-posterior translation

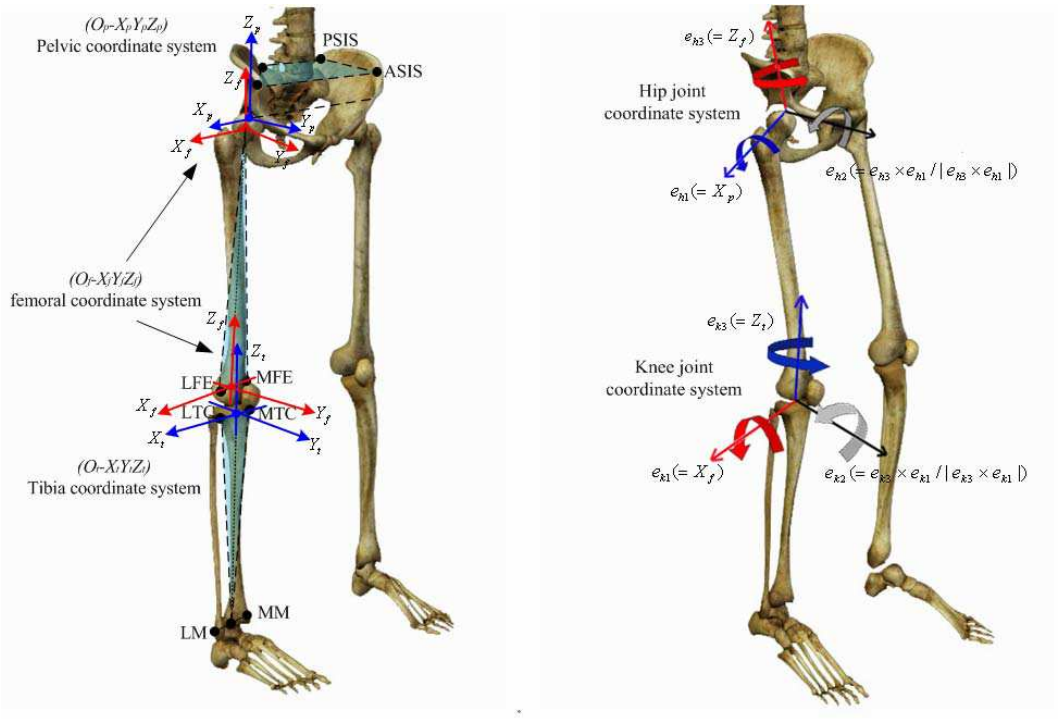

Fig.6-4 Description of coordinate system for the kinematic analysis of the lower limb segments

6.2.4 3D Knee joint kinematics in Anatomical coordinate system

To analyze knee joint kinematics in the anatomical coordinate system, the final step of data analysis is to translate the navigation angles into knee joint angles in the anatomical knee joint coordinate system, the f/e angle, a/a angle and i/e rotation angle, which were quantified by Good et al. [(16)] and have been widely used to analyze kinematics of lower limb joint motion. Suppose three unit vectors, $\mathbf{A_{Xt}}$, $\mathbf{A_{Yt}}$, $\mathbf{A_{Zt}}$, are obtained from the measured signals about each axis in the tibia/fibula coordinate system (O_t-$X_tY_tZ_t$), then another three unit vectors, $\mathbf{B_{Xf}}$, $\mathbf{B_{Yf}}$, $\mathbf{B_{Zf}}$, in the femur fixed coordinate system (O_f-$X_fY_fZ_f$) are calculated using the rotation matrix $\mathbf{R}$ expressed with navigation angles,

$$\begin{cases} \mathbf{B_{X_f}} = \mathbf{R}\mathbf{A_{X_t}} \\ \mathbf{B_{Y_f}} = \mathbf{R}\mathbf{A_{Y_t}} \\ \mathbf{B_{Z_f}} = \mathbf{R}\mathbf{A_{Z_t}} \end{cases} \tag{6-8}$$

Finally, the floating axis, the f/e angle $\theta_{f/e}$, a/a angle $\theta_{a/a}$ and i/e rotation angle $\theta_{i/e}$ of the knee joint in the anatomical knee joint coordinate system can be calculated as follows,

$$\mathbf{e}_{k2} = \frac{\mathbf{A}_{Z_t} \times \mathbf{B}_{X_f}}{|\mathbf{A}_{Z_t} \times \mathbf{B}_{X_f}|} \tag{6-9}$$

$$\theta_{f/e} = -\sin^{-1}\left(\frac{\mathbf{e}_{k2} \cdot \mathbf{B}_{Z_t}}{|\mathbf{e}_{k2}||\mathbf{B}_{Z_t}|}\right) \tag{6-10}$$

$$\theta_{a/a} = \cos^{-1}\left(\frac{\mathbf{B}_{X_f} \cdot \mathbf{A}_{Z_t}}{|\mathbf{B}_{X_f}||\mathbf{A}_{Z_t}|}\right) - \frac{\pi}{2} \tag{6-11}$$

$$\theta_{i/e} = -\sin^{-1}\left(\frac{\mathbf{e}_{k2} \cdot \mathbf{A}_{X_t}}{|\mathbf{e}_{k2}||\mathbf{A}_{X_t}|}\right) \tag{6-12}$$

In order to evaluate the presented approach for knee joint kinematics in the anatomical coordinate system, a wearable sensor system was developed. As shown in Fig.6-5, in the wearable sensor system, each group of sensors on the thigh or shank contained one piece of MM-2860 and one piece of MAG^3, and every two corresponding axes of the sensors in the same group were in the same direction. The two MM-2860s attached at positions **A** and **D** on the thigh and shank were used to measure accelerations, and the two MAG^{3}s fixed at positions **B** and **C** were used to capture accelerations and magnetic field data simultaneously. The four groups of accelerations measured by MM-2860s and MAG^{3}s were used to calculate two groups of accelerations in the knee joint using the physical-sensor difference based algorithm, which were regarded as readings of two virtual sensors, and then were used to calculate the navigation angles using the virtual-sensor difference based method in Eq.6-8. The two groups of magnetic field data captured by the two MAG^{3}s were also used to calculate the navigation angles using the virtual-sensor difference based method in Eq.6-10. The recorded accelerations about Y_t axis and Y_s axis indicated the anterior-posterior motion, about X_t axis and X_s axis indicated vertical motion along the lower limb segments, and about Z_t axis and Z_s axis indicated the lateral motion in the sensor coordination system on the thigh and shank.

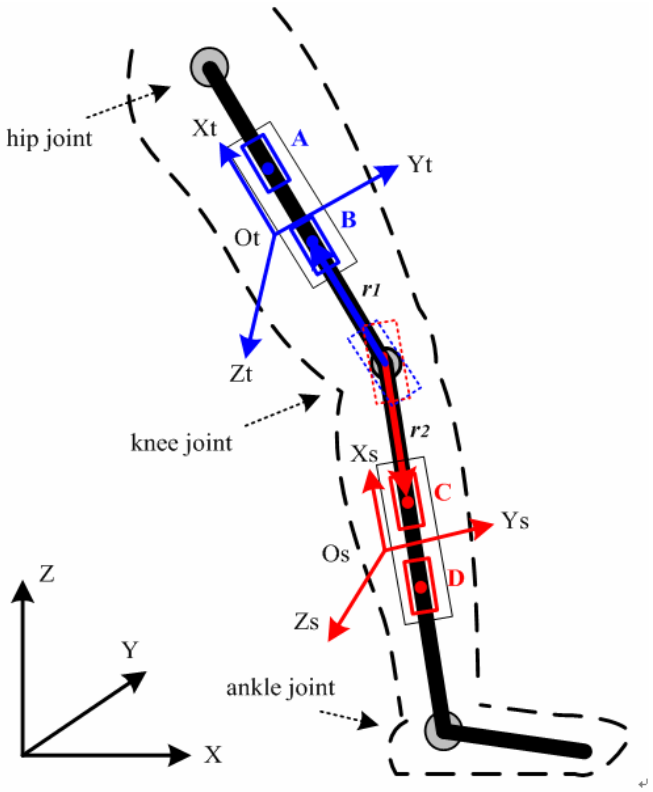

Fig.6-5. Illustration for the installation of the sensors on the lower limb to calculate the knee joint angles

Table 6-4 List of the terms used in Fig.6-5

O-ZYZ	Global coordinate system
O_t-$Z_tY_tZ_t$	Sensor coordinate system on the thigh
O_s-$Z_sY_sZ_s$	Sensor coordinate system on the shank
r_1	Distance from knee joint to the physical sensor B on the thigh
r_2	Distance from knee joint to the physical sensor C on the shank

6.2.5 3D Gait posture analysis of the lower limb

In this part, to estimate the lower limb posture in the local coordinate system using the presented methods, a prototype is structured as Fig.6-6 shows. To calculate the hip joint FE and AA angles using the physical-sensor difference based algorithm, an accelerometer is fixed on the hip as mentioned in part 2.1, and another two accelerometers are attached at positions A and B on the thigh with corresponding axes in the same directions. To calculate the knee joint angles using the virtual-sensor difference based algorithm, another two accelerometers are attached at positions C and D on the shank with corresponding axes in the same directions, and two magnetometers are fixed at positions B and C with each axis coinciding with the corresponding axis of the accelerometers at B and C.

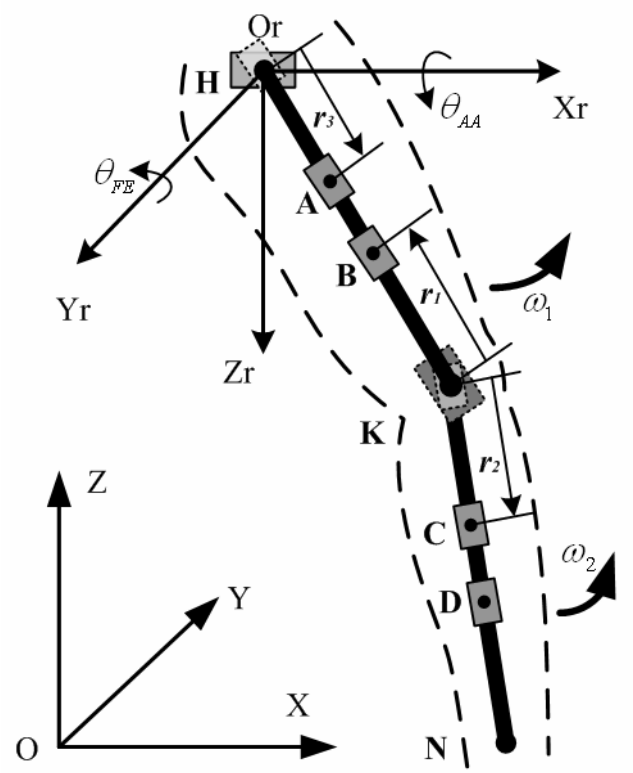

Fig.6-6 Lower limb model with sensors to estimate joint rotations and positions for gait posture analysis.

Then, to visually confirm the posture of the lower limb during walking, the positions of the hip joint, knee joint and ankle joint in the local coordinate system *Or-XrYrZr* are calculated using the joint angles and the segment lengths. The origin of the local coordinate system *Or(0,0,0)* was at the hip joint, then the trajectories for estimating the motions of knee and ankle joints were obtained with the following equations [(17)].

$$\mathbf{H}(x, y, z) = \begin{pmatrix} 0 & 0 & 0 \end{pmatrix} \tag{6-13}$$

$$\mathbf{K}(x, y, z) = \left(\mathbf{R}_{\theta_{AA}} \mathbf{R}_{\theta_{FE}} \begin{pmatrix} 0 \\ 0 \\ L_{thigh} \end{pmatrix} \right)^{\mathrm{T}} \tag{6-14}$$

$$\mathbf{N}(x, y, z) = \left(\mathbf{R}_{\theta_{\mathrm{AA}}} \mathbf{R}_{\theta_{\mathrm{FE}}} \begin{pmatrix} 0 \\ 0 \\ L_{thigh} \end{pmatrix} \right)^{\mathrm{T}} + \left(\mathbf{R}_{\theta_{AA}} \mathbf{R}_{\theta_{FE}} \mathbf{R}_{\varphi_{IE}} \mathbf{R}_{\varphi_{AA}} \mathbf{R}_{\varphi_{FE}} \begin{pmatrix} 0 \\ 0 \\ L_{shank} \end{pmatrix} \right)^{\mathrm{T}} \tag{6-15}$$

where L_{thigh} is the distance between the hip and knee joints, L_{shank} is the distance between the knee and ankle joints, $\mathbf{R}_{\theta_{AA}}, \mathbf{R}_{\theta_{FE}}, \mathbf{R}_{\varphi_{IE}}, \mathbf{R}_{\varphi_{AA}}, \mathbf{R}_{\varphi_{FE}}$ are rotation matrices.

6.3 Experiments

In order to evaluate the presented method, a prototype of wearable sensor system was developed. The prototype comprised one MCU (H8/3694, from Renesas Technology Corp.), three triaxial accelerometer-based chips (MM-2860), and two analog inertial sensors named MAG^3 (MEMSense, MAG10-1200S050, analog inertial sensor consisting of a triaxial magnetometer, an accelerometer and a gyroscope). The MCU was used to capture accelerations and magnetic field data from the sensors, store data in EEPROM real time and communicate with a PC after each test. The sampling frequency was 100 Hz and the A/D had a 12-bit resolution. Fig.6-7 shows the procedure of the experiment for the knee joint kinematics analysis in Anatomical coordinate system. Fig.6-8 shows the procedure of the experiment for lower limb gait posture analysis. Fig. 6-9 shows and the developed prototype of the wearable sensor system.

At the hip joint, to prevent gravity being erroneously recorded as translational acceleration in the horizontal plane, the x and y axes of the accelerometer must be in the upright plane. Therefore, the MM-2860 on the hip was fixed on a flat aluminum sheet and optimally adjusted to coincide with the sagittal plane of the thigh, and the z axis of the accelerometer was upright. Each group of sensors on the thigh or shank contained one piece of MM-2860 and one piece of MAG^3, and the MAG^{3}s fixed at positions B and C in Fig.6-4 and Fig.6-5 were used to capture accelerations and magnetic field data simultaneously. Four groups of accelerations measured by MM-2860s and MAG^{3}s were used to calculate two groups of virtual accelerations in the knee joint using the physical-sensor difference based algorithm, and then were used to calculate the knee joint angles using the virtual-sensor difference based method. Two groups of magnetic field data captured by the two MAG^{3}s were also used to calculate the knee joint angles using the virtual-sensor difference based method. To test the prototype in ideal conditions with less noise caused by skin motion artifact due to impact loading and muscle activation, the sensors were fixed on telescopic slide rails, and the slide rails and the flat aluminum sheet on the hip were connected with ball and socket joints. In initial installation, the slide rails were

attached on the lateral surface of the lower limb with elastic straps, coinciding with the lines which connected the hip joint and the knee joint, the knee joint and ankle joint. The lengths of the slide rails were adjusted according to the lengths of the thigh and shank. The recorded accelerations about y-axis indicated anterior-posterior motion, about x-axis indicated lateral motion, and about z-axis indicated vertical motion in the sensor coordination system.

In the experiment, five subjects (4 males, 1 females, Age: 25±3 years, Height: 170±8cm, mass: 60±11kg) with no history of musculoskeletal pathology and injury were requested to perform 3 straight-line walking trials with the speeds of 1m/s, 2m/s and 3m/s on a treadmill in each trial. Simultaneously, three groups of retro-reflective marks were fixed on the hip, thigh and shank. The three marks on the hip were used to obtain trajectory of the local coordinate system, which was used as the parent coordinate system of the other two sensor coordinate systems on the thigh and shank shown by the other two groups of marks. A commercial optical motion analysis system, NAC Hi-Dcam II Digital High Speed Camera Systems (NAC image technology. Japan), was used to track the 3D trajectories of the retro-reflective markers, with sampling frequency of 100 Hz and calibration error 0.22% for capturing the trajectory of an ambulatory subject.

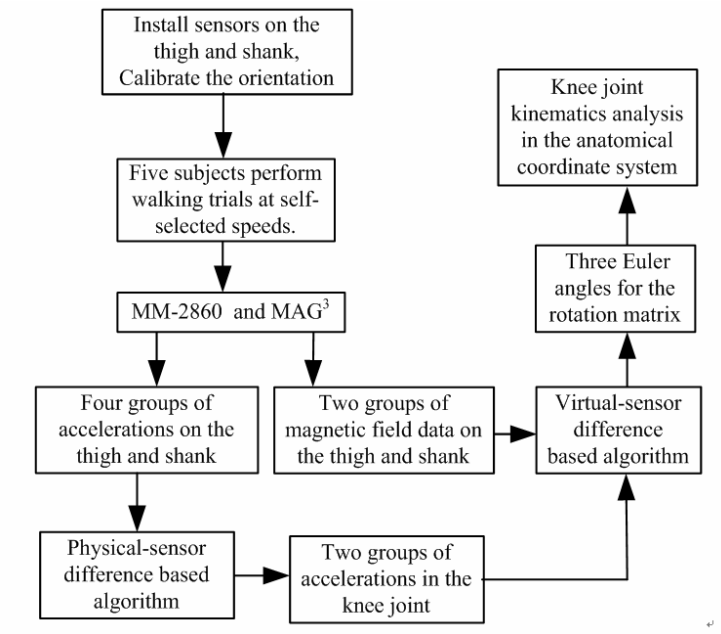

Fig.6-7. Procedure of the experiment using the developed wearable sensor system to estimate the 3D knee joint kinematics in the anatomical coordinate system.

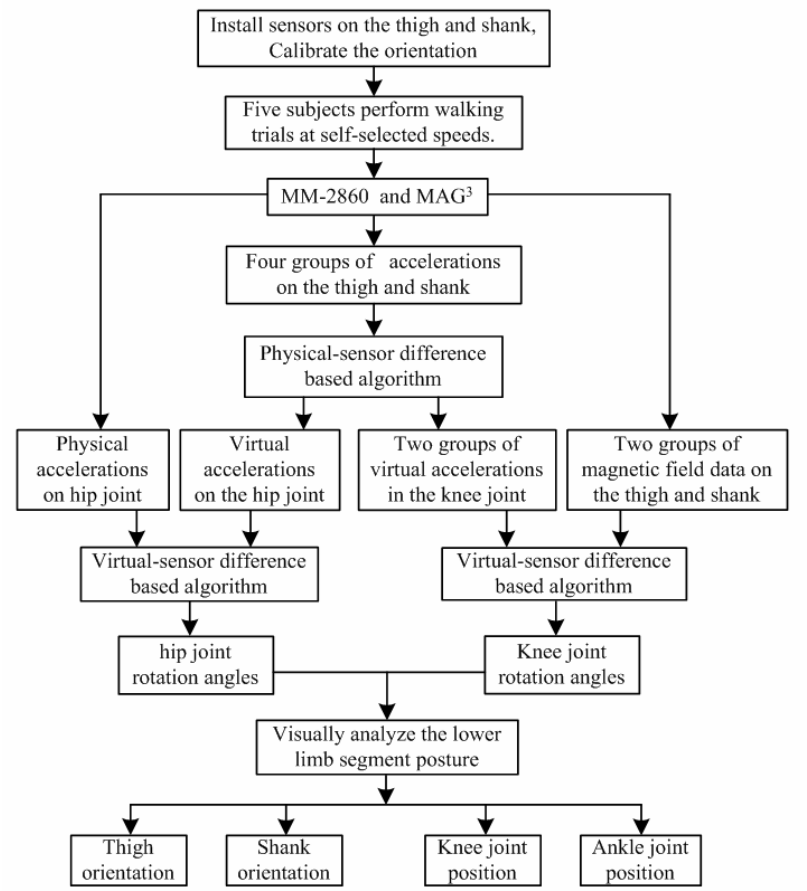

Fig.6-8 Schematic representation of the algorithm for deriving 3D thigh and shank orientations and the knee joint and ankle joint translations during gait on the basis of 3D inertial sensor signals.

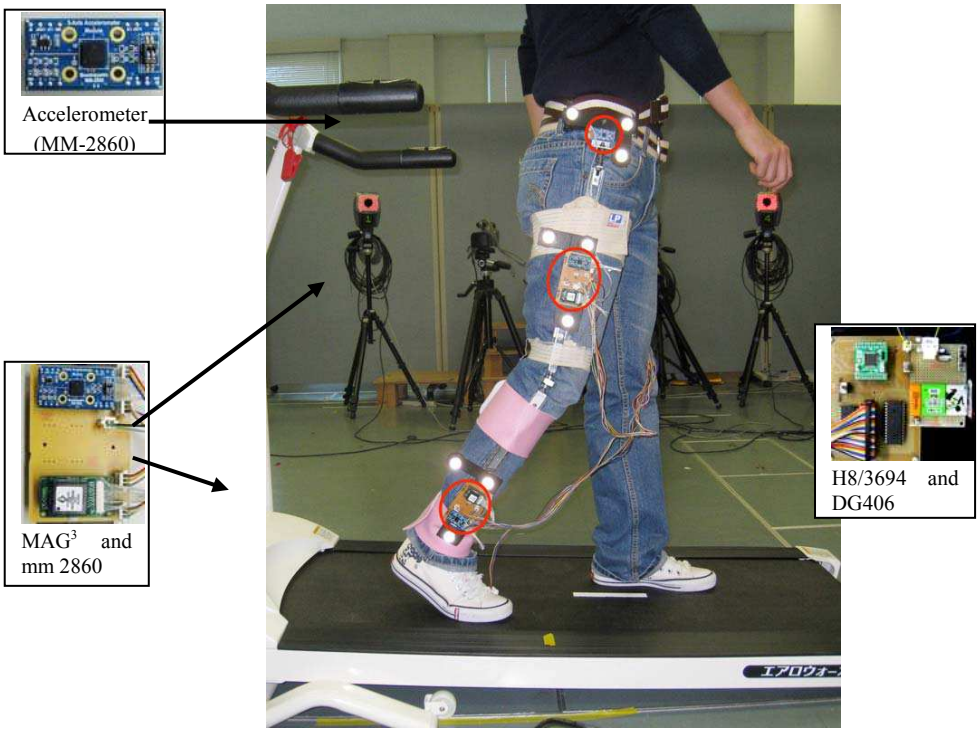

Fig.6-9 Experiment with the developed wearable sensor system in the working space of the referenced optical motion system

6.4 Results

All the readings of the sensors were recorded in the MCU real time and sent to PC off-line after each test, and the signals captured in the experiment were then processed off-line. The sampling frequency was 100 Hz and the A/D had a 12-bit resolution. The calculated angles of the hip and knee joints were compared with the reference angles obtained from the camera system.

6.4.1 Results for the knee joint 3D kinematics in Anatomical coordinate system

Two groups of accelerations in knee joint regarded as measured by virtual sensors were calculated in each trial and one group was shown in Fig.6-10. Another group of magnetic field data was shown in Fig.6-11. The knee joint rotational angles in the anatomical knee joint coordinate system were calculated and shown in Fig.6-12, compared with the angles obtained from the camera system. All the related parameters between the referenced and calculated knee joint angles used to evaluate the accuracy of the wearable sensor system compared with the referenced camera system are shown in Table 6-5, where RMS is the root of the mean of the square differences, R is the correlation coefficient, e_{max} is the maximum error.

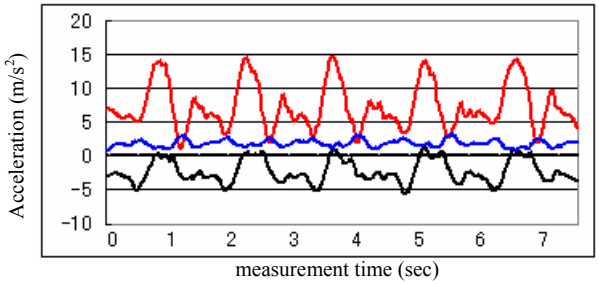

Fig.6-10 One group of accelerations in the knee joint regarded as measured by virtual accelerometers is shown. The virtual accelerations were calculated from the four groups of accelerations measured by the four physical accelerometers on the thigh and shank. The red line is the acceleration about *y* axis, black line is the acceleration about *x* axis, blue line is the acceleration about *z* axis in the sensor coordinate system

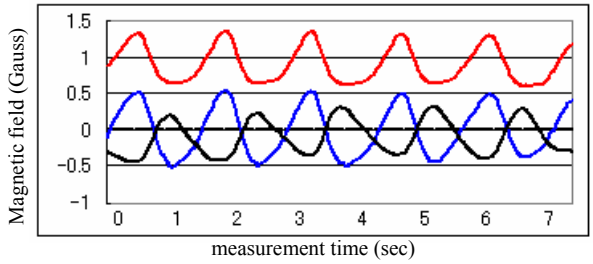

Fig.6-11 One group of magnetic field data in the knee joint regarded as measured by virtual magnetometers, which were in fact measured by two physical magnetometers on the thigh and shank. The red line is the reading about *y* axis, black line is the reading about *x* axis, blue line is the reading about *z* axis in the sensor coordinate system

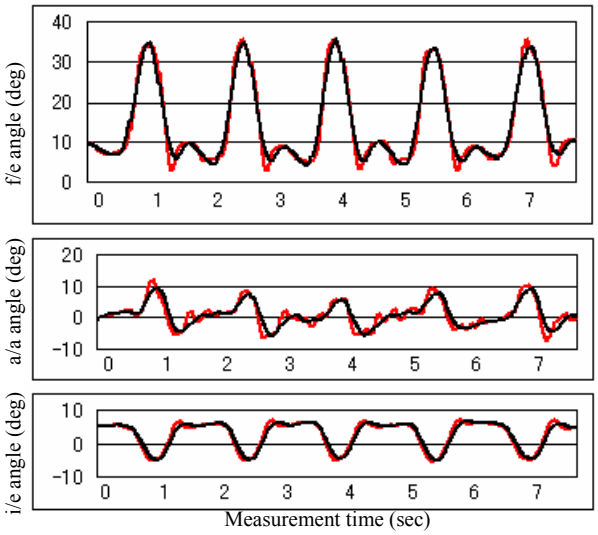

a, one result with volunteer 1

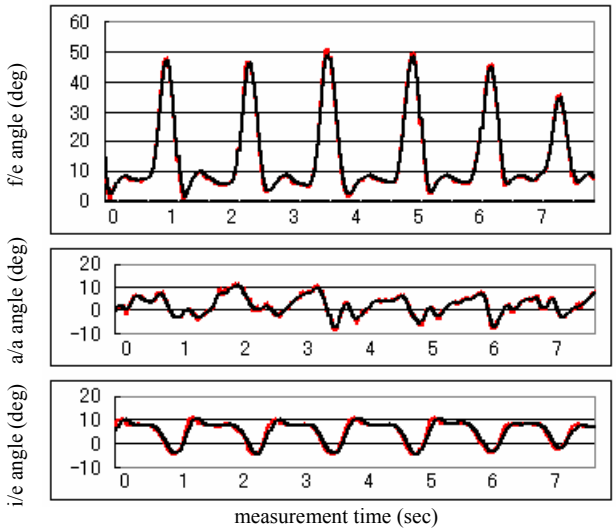

b, one result with volunteer 2

Fig.6-12 Two groups of the f/e angle, a/a angle and i/e rotation angle of the knee joint in the anatomical coordinate system. The red line correspond to the developed sensor system and the black line to the camera system

Table 6-5 Analysis results of the knee joint rotation angles in the anatomical coordinate systems which were obtained from the referenced system and the developed wearable sensor system. The value of each parameter was an average of three trials when each volunteer walked at three self-selected speeds. At the right side of the table, the overall average of each parameter with five volunteers was given.

Three angles \ Subjects		1	2	3	4	5	Average
f/e angle	RMS	2.91	1.57	2.28	2.53	3.33	2.52
	R	0.92	0.97	0.95	0.93	0.91	0.94
	e_{max}	4.13	2.53	3.23	3.62	4.37	3.58
a/a angle	RMS	2.35	1.78	1.37	3.03	2.83	2.27
	R	0.95	0.96	0.97	0.93	0.94	0.95
	e_{max}	3.51	2.94	2.13	3.86	3.55	3.20
i/e rot.	RMS	2.32	1.36	1.81	2.55	2.59	2.13
	R	0.93	0.97	0.96	0.94	0.94	0.95
	e_{max}	2.86	2.01	2.27	3.42	3.65	2.84

6.4.2 Results for 3D the lower limb gait posture analysis.

Fig.6-13 shows the compared results of the FE and AA angles of the hip joint, the FE, AA and IE angles of the knee joint in one trial. The analysis result is shown in Table 6-6 and Table 6-7. Fig.6-14 gives the continuous stick figures of the lower limb in one gait circle for visual confirmation of the human gait posture.

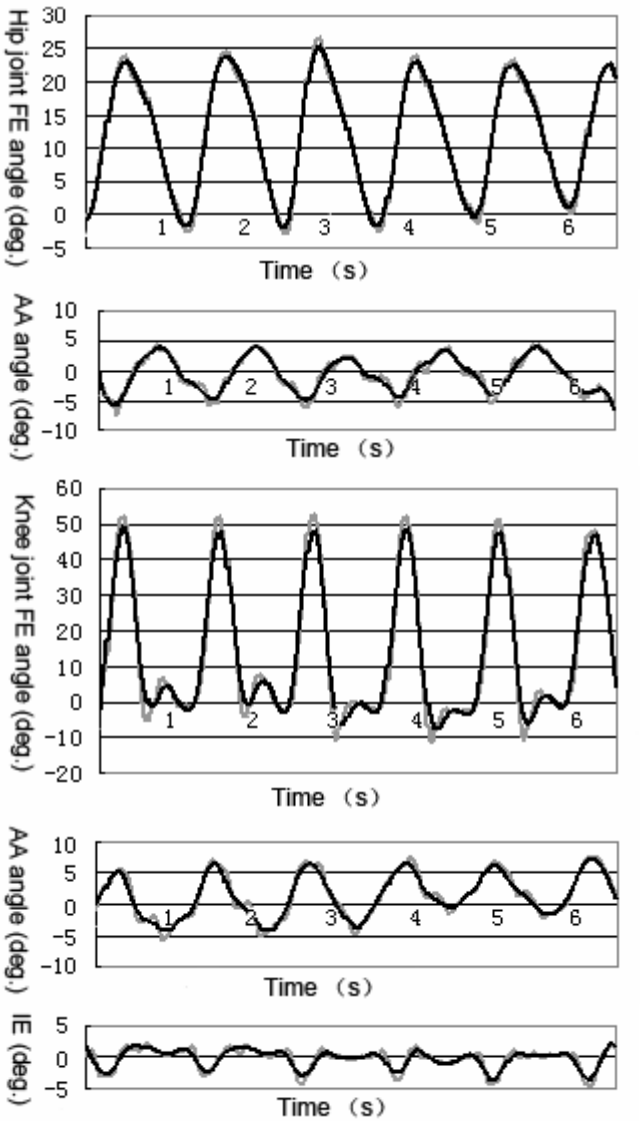

Fig.6-13. The FE and AA angles of the hip joint and the FE, AA and IE angles of the knee joint in one trial. The dark black line was the referenced angle measured by the camera system and the light gray line was the calculated angle using measured signals from the prototype.

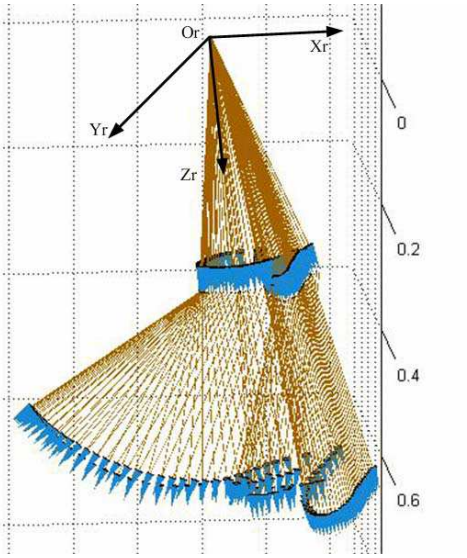

Fig.6-14 One gait circle shown by continuous stick figures for visual and quantitative confirmation of the human gait posture. The blue arrows represent the knee joint and ankle joint.

Table 6-6 Analysis result of the hip joint FE and AA angles which were obtained from the prototype and the camera system. The value of each parameter was an average of three trials when each subject walked at three different speeds on the treadmill. At the bottom of the table, the overall average of each parameter in five trials was given.

Sub.	hip joint flexion/extension angle			hip joint abduction/adduction angle		
	$RMS_{\theta F}$	$R_{\theta FE}$	e_{max}	$RMS_{\theta F}$	$R_{\theta FE}$	e_{max}
1	4.01	0.93	6.13	3.51	0.94	4.51
2	3.28	0.94	6.53	3.78	0.95	3.94
3	3.64	0.95	5.77	4.34	0.92	5.43
4	5.33	0.89	10.12	4.93	0.9	6.75
5	4.15	0.92	7.84	4.75	0.93	5.72
Av.	4.08	0.93	7.28	4.19	0.93	5.27

Table 6-7 Analysis result of the knee joint FE, AA and IE angles which were obtained from the prototype and the camera system. The value of each parameter was an average of three trials when each subject walked at three speeds on the treadmill. At the bottom of the table, the overall average of each parameter in five trials was given.

Subject	knee joint FE angle			knee joint AA angle			knee joint IE angle		
	$RMS_{\varphi FE}$	$R_{\varphi FE}$(°)	e_{max}(°)	$RMS_{\varphi AA}$(°)	$R_{\varphi AA}$(°)	e_{max}(°)	$RMS_{\varphi IE}$(°)	$R_{\varphi IE}$(°)	e_{max}(°)
1	3.23	0.95	4.73	2.74	0.95	3.53	2.57	0.94	2.73
2	2.31	0.96	3.54	1.86	0.97	2.60	1.21	0.95	1.95
3	2.89	0.95	3.71	2.03	0.95	3.11	1.53	0.95	2.61
4	3.69	0.94	4.89	2.52	0.93	3.68	2.17	0.93	2.88
5	3.25	0.95	4.52	2.13	0.95	2.79	1.96	0.95	2.52
Average	3.07	0.95	4.28	2.26	0.95	3.14	1.89	0.94	2.54

6.5 Discussion and Conclusion

As curves in Fig.6-12 and the result in Table 6-5 show, the results obtained from the wearable sensors are closed to those from the optical motion analysis system, with small RMS and large correlation coefficient. Therefore, it was feasible to use the method and the wearable sensor system to analysis the lower limb joint kinematics,

such as knee joint kinematics in this chapter. In the experiment, the gravitational acceleration, translational acceleration and noise, which were simultaneously acting on every two sensors in each sensor group, were eliminated based on the physical-sensor difference based algorithm, i.e., the accelerations of the virtual sensors in the knee joint were calculated only based on the differences between the rotational accelerations at every two positions on the thigh or shank.

Since the trajectories of the knee and ankle joints were calculated from the joint angles, only the analysis results of the joint angles were shown. From the analysis result shown in Table 6-6, the presented method showed a strong correlation with the camera system data and involved significantly less calculation than reported in the paper [18]. The method was suitable for various velocities of walking no matter whether the anterior/posterior acceleration of the trunk increased or not. It was an improvement of the method in the paper [17] which neglected any anterior/posterior accelerations and only conducted experiments at fairly low velocity (88 steps/min). Maybe that was why the result in this paper was better than that Takeda et al. presented.

Since the 1970s, the advantages and disadvantages of using kinematic sensors have been discussed by Padgaonkar [19] and Morris et al. [20]. Recently, Daniele et al. [21] demonstrated that architectures with sole accelerometers did not allow an accurate reconstruction of joint kinematics, and then gyroscopes were introduced in the algorithm in their further research. Although the insensitivity of gyroscopes improved the trajectory reconstruction, the design and the introduction of a real-time algorithm for the drift compensation was necessary. Our method was the first to consider the joint kinematics using accelerometers and magnetometers without gyroscopes. In this technique, gravitational acceleration, translational acceleration and noise, which were simultaneously acting on every two sensors in each sensor group, were eliminated based on the physical-sensor difference based algorithm, i.e., the virtual accelerations of the knee joint were calculated only based on the differences between the two rotational accelerations on the thigh or shank. There was no integration of angular acceleration or angular velocity for the calculation of the knee joint angles, therefore

the results were not distorted by offset and drift. Besides, it was more simple and practical to use virtual sensors than implant physical sensors in the knee joint to calculate the rotation angles.

However, although the sensors were fixed on rails, skin motion artifact due to impact loading and muscle activation must lead to relative motion between the rails and the lower limb segments, which would contaminate the measured rotation accelerations, and then bring errors to the calculated joint angles. Besides, since the distances from the sensors to the knee joint were just measured at the beginning of each test, unfixedness of the sensors or the rails in each trial would also bring errors to the actual distances used for the calculation of rotation angles.

In this technique, since the newly launched analog inertial sensors (MAG^3) were used in the experiment, which were capable of sensing rotation, acceleration and magnetic field about three orthogonal axes and packaged in a single SMT (0.70 × 0.70 × 0.40 inches), the prototype was miniaturized and convenient to wear for patients. Especially compared with the expense and bulk of the optoelectronic equipments, the prototype could introduce adequate and necessary quantitative analysis of joint kinematics. Another advantage of this method is that the developed device is not model-dependent, and so is practical for time-limited clinical applications with many patients, or space-unlimited continuous clinical evaluation for a patient to wear in his daily life.

Consequently, although the prototype is cumbersome and has only been tested in ideal conditions in the lab, the combination of physical-sensor difference based algorithm and virtual-sensor difference based algorithm in this paper is original for visual and quantitative analysis of 3D lower limb posture. With the continuous decrease in costs and miniaturization of inertial sensors, we are working toward realization of sensor assemblies in a single chip to measure two groups of 3D angular accelerations and one group of 3D magnetic field data simultaneously for a lightweight and portable wearable sensor system without mechanical linkage, then promote it to clinical applications in daily life for patients or medical personnel.

References

(1) K. Turcot, R.Aissaoui, K. Boivin, M.Pelletier, N.Hagemeister, De Guise, "New accelerometric method to Discriminate between asymptomatic subjects and patients with medial knee osteoarthritis during 3-D gait," IEEE Trans. Biomed. Eng., vol. 55, no. 4, pp. 1415-1422, 2008.

(2) T. Steven. Moore, G. Hamish, MacDougall, G. William. Ondo, "Ambulatory monitoring of freezing of gait in Parkinson's disease," J Neurosci. Methods, vol. 167, pp. 340-348, 2008.

(3) A. Salarian, H. Russmann, Vingerhoets, F.J.G., Burkhard, P.R., K. Aminian, "Ambulatory Monitoring of Physical Activities in Patients With Parkinsonapos's Disease," IEEE Trans. Biomed. Eng., vol. 54, no. 12, pp. 2296-2299, 2007.

(4) H. Dejnabadi, B. M. Jolles, and K. Aminian, "A new approach to accurate measurement of uniaxial joint angles based on a combination of accelerometers and gyroscopes," IEEE Trans. Biomed. Eng., vol. 52, no. 8, pp. 1478-1484, 2005.

(5) Justin J. Kavanagh, Hylton B. Menz, "Accelerometry: A technique for quantify movement patterns during walking," Gait Posture, vol. 28, pp. 1-15, 2008.

(6) R.Williamson, B.J. Andrews, "Detecting absolute human knee angle and angular velocity using accelerometers and rate gyroscopes," Med. Biol. Eng. Comput., vol. 39, no. 3, pp. 294-302, 2001.

(7) Kun Liu, Tao Liu, Kyoko Shibata, Yoshio Inoue, Rencheng Zheng, "Novel Approach to Ambulatory Assessment of Human Segmental Orientation on a Wearable Sensor System," J. Biomech., vol. 42, no. 16, pp. 2747-2752, 2009.

(8) N.Hagemeister, G.Parent, M.Van de Putte, N.St-Onge, N.Duval, J.de Guise. "A reproducible method for studying three-dimensional knee kinematics," J. Biomech., vol. 38, no. 9, pp. 1926-1931, 2005.

(9) A. Findlow, J. Goulermas, C. Nester, D. Howard, L. Kenney, "Predicting lower limb joint kinematics using wearable motion sensors," Gait Posture, vol. 28, no.1, pp. 120-126, 2008.

(10) J. Kavanagh, S. Morrison, D. James, R. Barrett, "Reliability of segmental accelerations measured using a new wireless gait analysis system," J. Biomech., vol. 39, no. 15, pp. 2863-2872, 2006.

(11) J.Favre, F.Luthi, B.M.Jolles, O.Siegrist, B.Najafi and K.Aminian, "A new ambulatory system for comparative evaluation of the three-dimensional knee kinematics, applied to anterior cruciate ligament injuries," Knee Surgery Sports Traumatology Arthroscopy, vol. 14, no. 7, pp. 592-604, 2006.

(12) J. Favre, B.M. Jolles, R. Aissaoui, K. Aminian, "Ambulatory measurement of 3D knee joint angle," J. Biomech., vol. 41, no.5, pp. 1029-1035, 2008.

(13) K. O'Donovan, R. Kamnik, D. O'Keeffe, G. Lyons, "An inertial and magnetic sensor based technique for joint angle measurement," J. Biomech., vol. 40, no.12, pp. 2604-2611, 2007.

(14) R. Takeda, S. Tadano, M. Todoh, M. Morikawa, M. Nakayasu, S. Yoshinari, "Gait analysis using gravitational acceleration measured by wearable sensors," J. Biomech., vol. 42, no.3, pp. 223-233, 2009.

(15) H. Dejnabadi, B. M. Jolles, and K. Aminian, "Estimation and visualization of sagittal kinematics of lower limbs orientation using body-fixed sensors," IEEE Trans. Biomed. Eng., vol. 53, no. 7, pp. 1385-1392, 2006.

(16) Grood ES, Suntay WJ., "A joint coordinate system for the clinical description of three-dimensional motions: application to the knee," ASME J. Biomech. Eng. vol. 105, pp. 136-144, May 1983.

(17) Takeda Ryo, Tadano Shigeru, Todoh Masahiro, Morikawa Manabu, Nakayasu Minoru, Yoshinari Satoshi, 2009b. Gait posture estimation using wearable acceleration and gyro sensors. Journal of Biomechanics 42 (15), 2486-2494.

(18) Takeda Ryo, Tadano Shigeru, Todoh Masahiro, Morikawa Manabu, Nakayasu Minoru, Yoshinari Satoshi, 2009a. Gait analysis using gravitational acceleration measured by wearable sensors.

(19) Padgaonkar A. J., K. W. Krieger, and A. I. King, “Measurement of angular acceleration of a rigid body using linear accelerometers,” ASME J. Appl. Mech., vol. 42, pp. 552-556, 1975.

(20) Morris J. R. W., “Accelerometry—A technique for the measurement of human body movements,” J. Biomech., vol. 6, pp. 729-736, 1973.

(21) D. Giansanti, V. Macellari, G. Maccioni, and A. Cappozzo, “Is it feasible to reconstruct body segment 3-D position and orientation using accelerometric data?,” IEEE Trans. Biomed. Eng., vol. 50, no. 4, Apr. 2003.

(22) Wu, G., & Cavanagh, P.R. (1995). ISB recommendations for standardization in the reporting of kinematic data. Journal of Biomechanics, 28, 1257-1261.

Chapter 7
Conclusion

Kinematics analysis of lower limb can provide a deeply and quantitatively understanding of motion mechanism and assessment of motion abilities, which is fundamental for rehabilitating and clinical applications. However, human motion data are commonly obtained by means of traditional laboratory-restricted bulky equipments, such as force plate and optical camera system. Therefore, cheaper and more comfortable human kinematic and kinetic analysis devices with compact biomedical sensor combinations are in urgent necessity for visual and quantitative gait phase analysis and human kinematics and kinetics analysis.

In this dissertation, some methods for lower limb kinematics analysis were provided, and relevant prototypes of wearable sensor systems were developed and tested for ambulatory and unobtrusive motion measurement of lower limb in daily activities instead of the traditional ones. First，a novel method using a double-sensor difference based algorithm for analyzing rigid segment rotational angles in 2 directions was presented and discussed, To verify the method qualitatively, a prototype of a wearable sensor system only using one kind of inertial sensor (accelerometer) was developed. The prototype was first test on a board which performed a one-freedom of rotation in sagital plane, then was tested on the thigh of a volunteer to obtain the pitch and yaw angles for the lower limb segment orientation when the thigh swung in the original place without translation. To promote the double-sensor difference based algorithm to analyze human segment rotational angles in two directions when the subject walked in a straight line, a wearable sensor system based only on triaxial accelerometers was developed to obtain the pitch and yaw angles of thigh segment. To evaluate the method, the system was first tested on a two degrees of freedom (DOF) mechanical arm assembled out of rigid segments and encoders. Then, to estimate the human segmental orientation, the wearable sensor system was tested on the thighs of eight volunteer subjects, who walked in a straight forward line in the work space of an optical motion analysis system at three

self-selected speeds: slow, normal and fast.

However, just the lower limb segment orientation is not enough to estimate the gait posture. To visually and quantitatively confirm lower limb posture, except the double-sensor difference based algorithm, a virtual-sensor difference based algorithm was proposed for analyzing the knee joint and hip joint angles. Using accelerometers and gyroscopes, flexion/extension (FE) and abduction/adduction (AA) hip joint angles and FE knee joint angle were estimated for orientations of the lower limb segments; knee and ankle joint trajectories were obtained with the segmental orientations and lengths for the positions of lower limb joints. As a further research of the physical-sensor difference based algorithm and virtual-sensor difference based algorithm, an original approach based on accelerometers and magnetometers for ambulatory estimation of 3D knee joint kinematics in anatomical coordinate system was presented. The FE, AA and inversion/extension (IE) rotation angles of the knee joint in the anatomical joint coordinate system were estimated. Then, to visually and quantitatively confirm the 3D lower limb posture, combine all the method above, a wearable sensor system was developed and tested on the lower limb.

Finally, some research challenges and future directions are discussed for developing a new biomechanical analysis technique.

Appendix A

Abbreviations and Symbols

A/D	Analog to digital converter.
DOF	Degree of freedom.
3D	Three dimensional
SMT	Surface Mounted Technology
DAQ	Data Acquisition
MCU	Micro control unit
MEMS	Micro-electromechanical systems.
PCB	Printed circuit board.
RMS	Root of the Mean of the Square differences
AA	Abduction/Adduction
FE	Flexion/Extension
IE	Inversion/Extension

Appendix B

Terminology in gait phase analysis

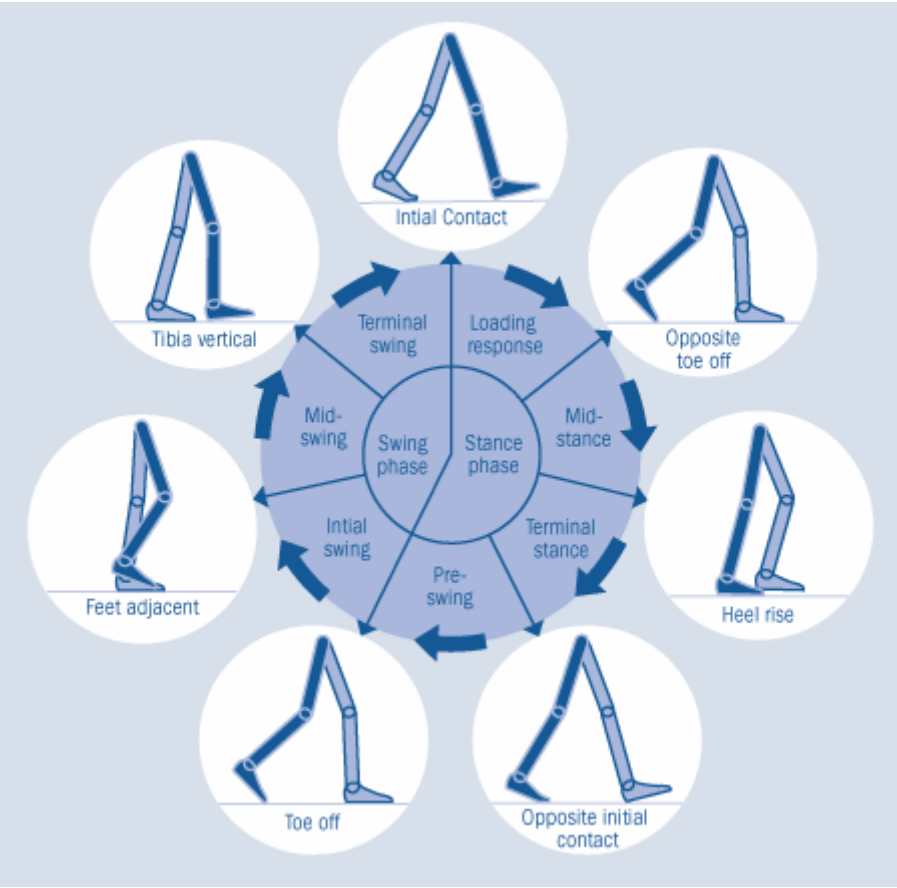

1. Initial contact: This phase includes the moment when the foot just touches the floor. The joint postures presented at this time determine the limb's loading response pattern.

2. Loading response: This is the initial double stance period. The phase begins with initial floor contact and continues until the other foot is lifted for swing. Using the heel as a rocker, the knee is flexed for shock absorption. Ankle plantar flexion limits the heel rocker by forefoot contact with floor.

3. Mid stance: This is the first half of the single limb support interval. In this phase, the limb advances over the stationary foot by ankle dorsiflexion (ankle rocker) while the knee and hip extend. It begins as the other foot is lifted and continues until body

weight is aligned over the forefoot.

4. Terminal stance: This phase complete single limb support. It begins with heel rise and continues until the other foot strikes the ground, in which the heel rise and the limb advance over the forefoot rocker. Throughout his phase body weight moves ahead of the forefoot.

5. Pre-swing: This final phase of stance is the second double stance interval in the gait cycle. It begins with initial contact of the opposite limb and end with ipsilateral toe-off. Objective of this phase is position the limb for swing.

6. Initial swing: This phase is approximately one-third of the swing period. It begins with lift of the foot from the floor and ends when the swinging foot is opposite the stance foot. In this phase, the foot is lifted and limb advanced by hip flexion and increased knee flexion.

7. Mid swing: This phase begins as the swinging limb is opposite the stance limb and ends when the swinging limb is forward and the tibia is vertical (i.e., hip and keen flexion postures are equal). The knee is allowed to extend in response to gravity while the ankle continues dorsiflexion to neural.

8. Terminal swing: This final phase of swing begins with a vertical tibia and ends when the foot strikes the floor. Limb advancement is completed as the leg (shank) moves ahead of the thigh. In this phase the limb advancement is completed by knee extension, and the hip maintains its earlier flexion, and the ankle remains dorsiflexed to neural.

Appendix C

Drawings, Schematics and PCB Layouts

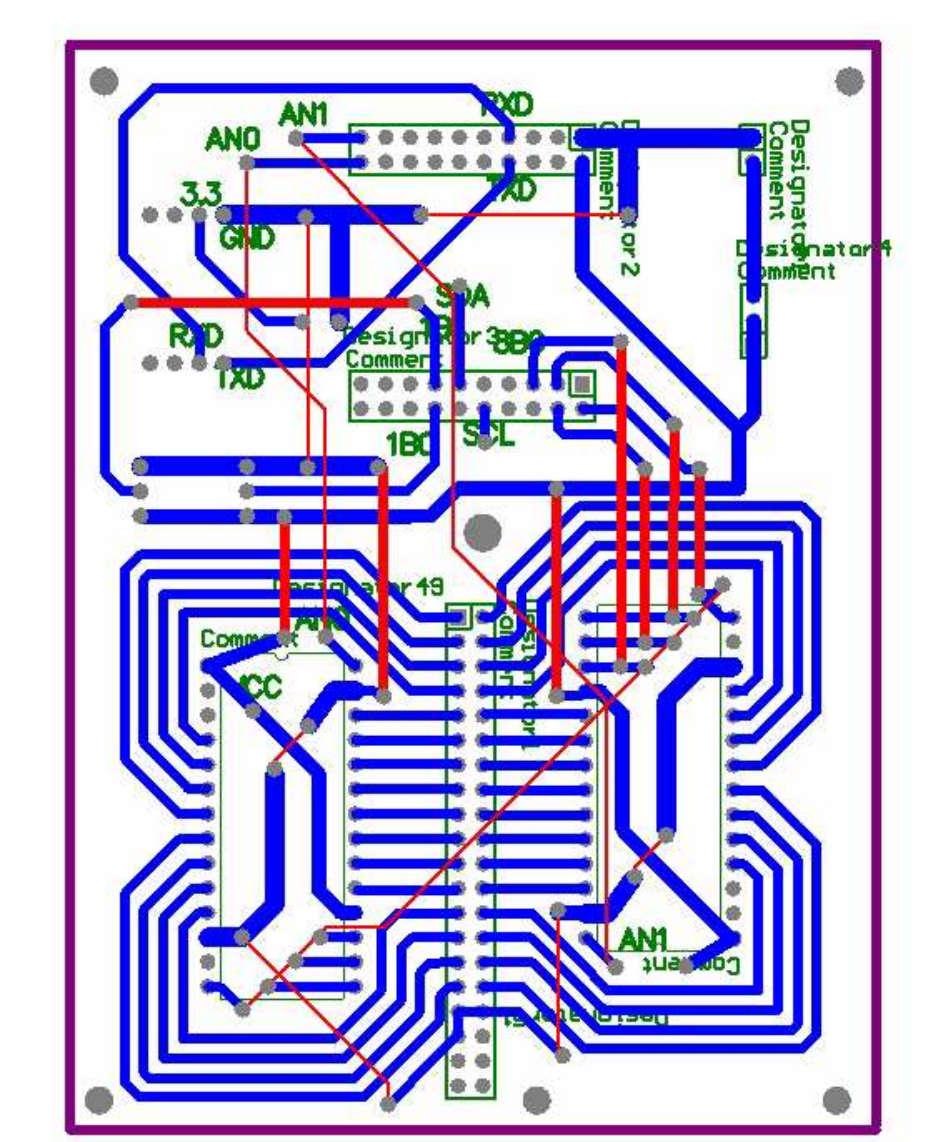

Data Acquiring and Processing electrical board (MCU) PCB

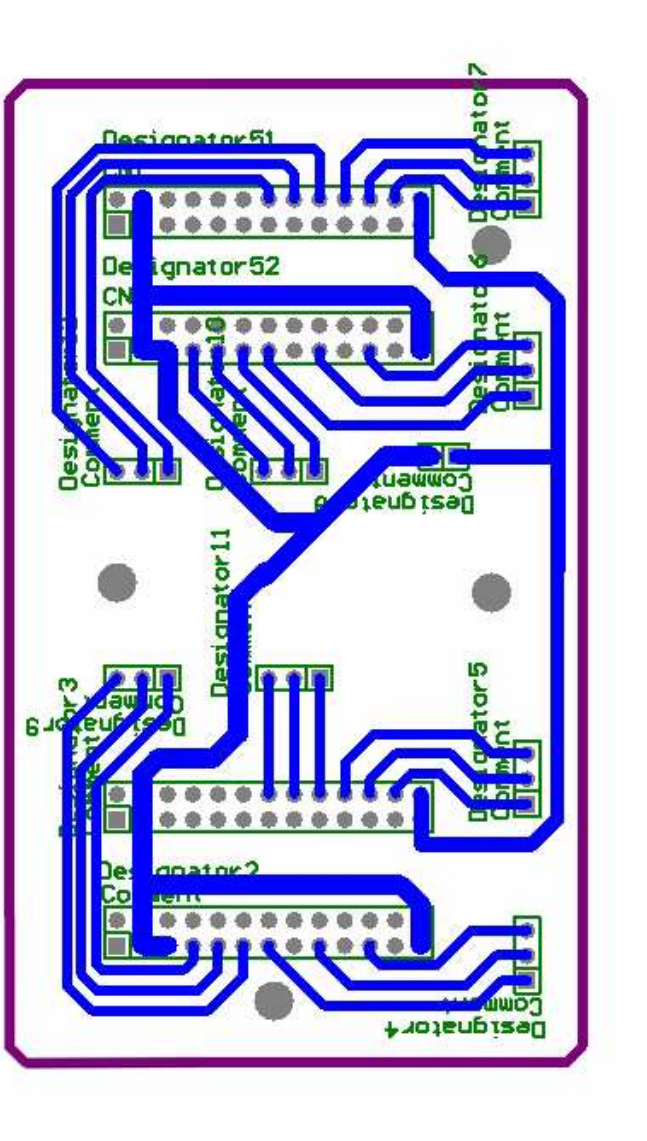

Motion sensor electrical board (accelerometer and magnetometers sensor) PCB

Appendix D

MATLAB Code (Offline analysis)

Acquiring and Processing Motion Sensor Data for Visual Analysis of Human Gait

```
mtlb = xlsread('C:\Documents and Settings\Administrator\liu51.xls')       % Load data
smtlb = sgolayfilt(mtlb,3,37);      % Apply 3rd-order filter

n=length(mtlb(:,1)')
t=0:0.01:((n-1)/100)

rA=0.23 %r3 in Fig.3 in the paper, The length from hip joint to the first sensor on the thigh
r1=0.163 % the length from the knee joint to the second sensor on the thigh
r2=0.2 % the length from the knee joint to the    sensor on the shank
g=9.8
rB=rA+0.6
i=0

x = smtlb

axA=(x(:,1)'/1023*5-2.5)/0.2*9.8
ayA=(x(:,3)'/1023*5-2.5)/0.2*9.8
azA=(x(:,5)'/1023*5-2.5)/0.2*9.8

axB=(x(:,2)'/1023*5-2.5)/0.2*9.8
ayB=(x(:,4)'/1023*5-2.5)/0.2*9.8
azB=(x(:,6)'/1023*5-2.5)/0.2*9.8

axC=(x(:,7)'/1023*5-2.5)/0.2*9.8
ayC=(x(:,9)'/1023*5-2.5)/0.2*9.8
azC=(x(:,11)'/1023*5-2.5)/0.2*9.8

wBx=(x(:,17)'/1023*5-2.5).*13.9624
wBy=(x(:,15)'/1023*5-2.5).*13.9624
wBz=(x(:,13)'/1023*5-2.5).*13.9624
```

```
wCx=(x(:,8)'/1023*5-2.5).*13.9624
wCy=(x(:,10)'/1023*5-2.5).*13.9624
wCz=(x(:,12)'/1023*5-2.5).*13.9624

Ax=(x(:,18)'/1023*5-2.45)/0.8*9.8+9.8
Ay=(x(:,16)'/1023*5-1.65)/0.8*9.8
Az=(x(:,14)'/1023*5-1.65)/0.8*9.8

for i=1:n
    if i==1
        DwBz(i)=wBz(1)
        DwCz(i)=wCz(1)
    else
    DwBz(i)=wBz(i)-wBz(i-1)
    DwCz(i)=wCz(i)-wCz(i-1)
    end
end

thx=asin((axA*rB-axB*rA)./((rB-rA).*sqrt(Az.*Az+Ax.*Ax)))-asin(Ax./sqrt(Az.*Az+Ax.*Ax))
thy=asin(Ay./sqrt(Ay.*Ay+Ax.*Ax))-asin((ayA*rB-ayB*rA)./((rB-rA).*sqrt(Ay.*Ay+Ax.*Ax)))
fai=-atan((ayC+r2*DwCz)./(axC-r2*wCz.*wCz))+atan((ayB+r1*DwBz)./(axB-r1*wBz.*wBz))

thx1=sgolayfilt(thx,3,31);
thy1=sgolayfilt(thy,3,31);
fai1=sgolayfilt(fai,3,51);

hold on
plot(t,thx.*57.325,'b')
plot(t,thy.*57.325,'r')
plot(t,fai.*57.325,'k')
plot(t,thx1.*57.325,'b')
plot(t,thy1.*57.325,'r')
plot(t,fai1.*57.325,'k')
hold off

Z_knee=[0,0,0]
Z_ankle=[0,0,0]
L_thigh=[0;0;0.4]
L_shank=[0;0;0.35]

for i=1:n
Rthx=[1,0,0;0,cos(thx(i)),sin(thx(i));0,-sin(thx(i)),cos(thx(i))];
Rthy=[cos(thy(i)),0,-sin(thy(i));0,1,0;sin(thy(i)),0,cos(thy(i))];
Rfai=[cos(fai(i)),0,-sin(fai(i));0,1,0;sin(fai(i)),0,cos(fai(i))];
```

```
P_kneejoint=Rthy*Rthx*L_thigh;
P_anklejoint=Rthy*Rthx*L_thigh+Rthy*Rthx*Rfai*L_shank;
Z_knee=[Z_knee;P_kneejoint'];
Z_ankle=[Z_ankle;P_anklejoint'];
end

D(:,1)=thx(1,:)'.*57.325
D(:,2)=thy(1,:)'.*57.325
D(:,3)=fai(1,:)'.*57.325
xlswrite('C:\Documents and Settings\Administrator\\48-.xls',D)

P(:,1)=Z_knee(:,1)
P(:,2)=Z_knee(:,2)
P(:,3)=Z_knee(:,3)
P(:,4)=Z_ankle(:,1)
P(:,5)=Z_ankle(:,2)
P(:,6)=Z_ankle(:,3)
xlswrite('C:\Documents and Settings\Administrator\48-joint persition.xls', P)
```

Acknowledgements

This thesis would not be completed without the help of many enthusiastic persons. Here, I would like to mention some of the most influential people for this thesis as well as my life.

First of all, I would like to give a big thanks to my supervisor, Prof. Yoshio Inoue, who provided me with his enthusiastic suggestions and advice to support my research works. I also have appreciated your encouragement and advice for not only this project, but also my future career that I would not have obtained anywhere except from you.

I would like to thank my vice-advisor Prof. Kyoko Shibata and Prof. Koichi OKA, who gave me so many useful suggestions and information about the project in every discussion meeting. Thank Prof. Shouyu Wang and Naoki Miura Sensei, the reviewers of my final dissertation, who give me so many advises And thank all the other members of Robotics and Dynamic Lab, who make me feel so fine and happy. Special acknowledgments to Liu tao and Zheng rencheng who brought me so many helps and smiles.

I would like to thank IRC staffs, Ban sensei, Kubo sensei, Kiyoka san, Yoshita san and my tutor Mr. Hirota, who helped me so much on Japanese study and foreign life when I just went to Japan. I will never forget their warm heart and kindness.

Thanks also to all those people helped me to correct my written English. At last, but not at least, I address my special thanks to SSP Scholarship of KUT and Kokuhi Scholarship of Japanese Government (Monbukagaku-sho) for kind supports.

List of Publications

Academic Journal Papers

(1) Kun Liu, Tao Liu, Kyoko Shibata, Yoshio Inoue, Rencheng Zheng. Novel Approach to Ambulatory Assessment of Human Segmental Orientation on a Wearable Sensor System. Journal of Biomechanics. 2009,42(16):2747-2752.

(2) Kun Liu, Yoshio Inoue, Kyoko Shibata, Analysis of Lower Limb Segment Orientation Using Triaxial Accelerometers, Journal of Biomechanical Science and Engineering. 2010, Vol.5. No.4:368-379

(3) Kun Liu, Yoshio Inoue, Kyoko Shibata, Physical-sensor and Virtual-sensor based method for Estimation of Lower Limb Gait Posture using Accelerometers and Gyroscopes, Journal of Biomechanical Science and Engineering. Accepted.

(4) Kun Liu, Yoshio Inoue, Kyoko Shibata. Ambulatory Estimation of Knee joint kinematics in Anatomical coordinate system Using Accelerometers and Magnetometers. IEEE Transaction on Biomedical Engineering. Major Revision.

(5) Kun Liu, Yoshio Inoue, Kyoko Shibata. Physical-sensor difference and virtual-sensor difference based method for visual and quantitative estimation of lower limb gait posture using wearable sensor system. Computer Methods in Biomechanics and Biomedical Engineering. Minor Revision.

International Conference Proceedings

(1) Kun Liu, Tao Liu, Kyoko Shibata, Yoshio Inoue. Novel approach for lower limb segment orientation in gait analysis using triaxial accelerometers. 2008 IEEE/ASME International Conference on Advanced Intelligent Mechatronics (AIM'08 Xin'an China), pp. 488-492.

(2) Kun Liu, Tao Liu, Kyoko Shibata, Yoshio Inoue. Ambulatory Measurement and Analysis of the Lower Limb 3D Posture Using Wearable Sensor System. 2009 IEEE International Conference on Mechatronics and Automation, (ICMA'09, Changchun China), pp. 3065-3069

(3) Kun Liu, Tao Liu, Kyoko Shibata, Yoshio Inoue. Reliability of Measuring Human Segment Three-dimensional Orientation Using Wearable Sensor System. 2009 IEEE International Conference on Control & Automation, (ICCA'09, Christchurch, New Zealand), pp. 1427-1432

(4) Kun Liu, Tao Liu, Kyoko Shibata, Yoshio Inoue. Visual Estimation of Lower Limb Motion Using Physical and Virtual Sensors. IEEE International Conference on Information and Automation (ICIA'10 Harbin China), pp. 179-184.

(5) Kun Liu, Yoshio Inoue, Kyoko Shibata. Visual and Quantitative Analysis of Lower Limb 3D Gait Posture using Accelerometers and Magnetometers 2010 IEEE International Conference on Mechatronics and Automation (ICMA'10, Xi'an China), pp. 1420-1425

(6) Kun Liu, Yoshio Inoue, Kyoko Shibata. Ambulatory estimation of 3D lower limb gait posture in anatomical coordinate frame using wearable sensor system. JSME/KSME 5th Asian Conference on Multibody Dynamics, (ACMD'10, Kyoto, Japan). Accepted